Imperial College of Science, Technology and Medicine
Department of Bioengineering

Steady Streaming as a Method for Drug Delivery to the Inner Ear

Laura Sumner

Supervised by

Dr Tobias Reichenbach

Submitted in part fulfilment of the requirements for the degree of
Doctor of Philosophy in Bioengineering of Imperial College London and
the Diploma of Imperial College, 12th February 2019

Abstract

Sensorineural hearing damage occurs when the hair cells which transduce mechanical input to electrical become damaged in the cochlea. Current drug therapies, whilst being promising in their ability to heal these cells, are limited by the inability to reliably administer them to their target sites.

This work looks at the phenomenon of steady streaming, a non-zero net motion in a fluctuating flow with non-conservative body forces, and investigates whether or not it is possible to harness the effect in order to deliver and potentially even specifically target damaged hair cells in the cochlea. Using the WKB model for the basilar membrane waves alongside experimental data to a create computational fluid dynamic simulation of the guinea pig cochlea, particle tracking was undertaken in order to find individual particle trajectories in the flows under pure tone, pitch change and multiple pitch stimulation. The steady streaming velocities and relative efficacy of the different stimuli were then determined and multiple frequency stimulation found to be superior as a method of drug transportation due to the setup of a so-called 'streaming channel' along which particles flow.

Declaration of Originality

I declare that the work which follows is entirely my own. All figures were created by myself unless stated otherwise. Any information taken from elsewhere, or work completed by others is duly referenced and acknowledged throughout.

Laura Sumner

11th February 2019

Copyright Declaration

Acknowledgements

My first, and biggest thank you goes to Tobias Reichenbach, for being a great supervisor in every way and trusting my judgement when creating this simulation and always believing that at some point I would get it to work! Also thanks to Jonathan Mestel for your very helpful inputs throughout these years.

A BIG thank you to the Reichenbach Group members past and present: Nikola, Octave, Hugo, Dr Kandy, Marina, Mikolaj, Shabnam, Anto. It has been a complete joy to have you all as my friends and I will never forget the adventures we have shared together. I hope there will be more dancing on beaches and on the edge of mountains.

Thanks to everyone involved in the CDT: shout out to Clodagh especially for being a legend and everyone in my cohort for being great friends and for helping me get through that hellish MRes year. Double thanks go to David for deciding not to go for the same project!

Next to all my friends who have made being in London the best years of my life, especially Paige, Laura and Mia. These past 4 years have been a whirlwind thanks to you. Special mention also to Davie, Marco, James, Harriet and Lev.

A very honorable and quite dramatic mention to my IB physics tutor Dave Walters for showing me the electron-positron interaction which blew my mind and basically changed the course of my life. Similarly, to Sophy, Vicky, Abi, Holli and Roshan. I have no doubt that growing up alongside such ambitious, talented and motivated women has helped me be where I am today and I thank you all for that.

Next, a huge thanks to Ian, you have encouraged and inspired me from the day we met. I would never have applied to Imperial and 100% would not be writing this thesis today without you and I thank you so much for everything you have done for me. You made me believe in myself.

A massive thank you to my family for all their support throughout my many years of study and for giving me a place to always call home in these times of upheaval and constant change. Thanks to my Dad especially for teaching me to have very high standards for myself and my work from a young age and to my Mum for having more faith in me than I sometimes have for myself. Extra thanks to

Louise and Sam for giving me a space to begin this thesis and to Andrew for all of your help in basically everything else. I won't forget it. To my baby sisters Ella and Jenny I hope this work inspires you to work hard to achieve things you never would have thought possible (even if actually reading it is very boring!).

And finally to the man who has (literally) been at my side through it all: firstly as my colleague and desk mate, then as my friend and now as my partner. Thank you for always engaging fully and sharing my frustration every time I ranted on and on about mesh and particle tracking madness and for sharing my excitement when things worked out. Antonio, you were there to see these results emerge from absolute nonsense at the beginning, and here we are now at the end.

Nomenclature

$\underline{\bar{u}}$	Time averaged velocity of particles passing through a cell in the decomposed domain.	ms^{-1}
$\underline{u}^A$	Instantaneous velocity of particles within a cell of the decomposed domain between two timesteps.	ms^{-1}
Δt	The discrete timestep for the CFD simulation	s
Δx	The discrete spatial step for the CFD simulation	m
δ	Spatial separation of resonance peaks	m
$\hat{P}$	Spatially dependant coefficient of the pressure difference between the two channels.	Pa
κ	Compressibility of the fluid	$\mathrm{m}^2\mathrm{N}^{-1}$
λ	Wavelength of the travelling waves along the basilar membrane.	m
μ_p	Friction coefficient of injected particle	
ν	Fluid kinematic viscosity	$\mathrm{m}^2\mathrm{s}^{-1}$
ω	Angular frequency of the pure-tone sound stimulation.	$^\circ$
ω_0	Resonant frequency at a certain location along the the basilar membrane	$^\circ$
ρ	Fluid density	kgm^{-3}

ρ_0	Fluid density at mean membrane displacement, x_0	kgm^{-3}
τ_{ij}^R	The Reynolds stress tensor	Nm^{-2}
$\tilde{p}^{(1)}$	Spatially dependent part of the fluid pressure field in the top channel.	Pa
$\tilde{p}^{(2)}$	Spatially dependent part of the fluid pressure field in the bottom channel.	Pa
$\tilde{U}$	Maximum fluid velocity	ms^{-1}
$\underline{u}^{(1)}$	3 Dimensional velocity vector in the top channel, $(u^{(1)}, v^{(1)}, w^{(1)})$	ms^{-1}
$\underline{u}^{(2)}$	3 Dimensional velocity vector in the bottom channel, $(u^{(2)}, v^{(2)}, w^{(2)})$	ms^{-1}
$\underline{u}_E = (u_E, v_E)$	Euler velocity	ms^{-1}
$\underline{u}_L = (u_L, v_L)$	Lagrangian velocity.	ms^{-1}
$\underline{u}_{ss} = (u_{ss}, v_{ss})$	The steady streaming velocity	ms^{-1}
ξ	Damping factor	Nsm^{-1}
A	Area of segment of basilar membrane.	m^2
a	Amplitude of the waves travelling on the basilar membrane.	m
c	Speed of compression wave through the fluid	ms^{-1}
C_o	The Courant-Friedrichs-Lewy constant	
e	Coefficient of restitution of injected particle	
F	Body force in the fluid.	N
f	Stimulation frequency	Hz
h	Height of the unrolled cochlear channel	m
$K(x)$	Stiffness of the basilar membrane.	Nm^{-1}

$k(x)$	Wave number of travelling wave along the basilar membrane.	m^{-1}
$m(x)$	Mass of the basilar membrane.	Kg
P	Pressure difference across the top and bottom channels.	Pa
p	Fluid pressure field.	Pa
p_N	Normalisation pressure (or root mean square pressure) for a specific SPL.	Pa
p_{ref}	Reference sound pressure in air: 2×10^{-5} (threshold for human hearing).	Pa
R	Ratio of log frequencies corresponding to scaled spatial separation	
R_e	Reynolds number	
R_N	Normal force exerted on a fluid element due to Reynolds stress.	N
R_T	Tangential (shear) force exerted on a fluid element due to Reynolds stress.	N
S	Strouhal number	
t	Time	s
u_{SS}^{E}	Steady streaming velocity found by Edom and Obrist.	ms^{-1}
$u_{L}^{b.l}$	Lagrangian velocity in the boundary layer	ms^{-1}
u_{L}^{B}	Lagrangian velocity in the bulk flow region	ms^{-1}
u_S	Stokes drift velocity	ms^{-1}
u_{BM}	Velocity contribution due to the 2D basilar membrane motion	ms^{-1}
V	Vertical velocity of the basilar membrane.	ms^{-1}
x	Spatial coordinate in the longitudinal direction.	m
y	Spatial coordinate in the vertical direction.	m
Z	Impedance of the basilar membrane	Nsm^{-1}

Contents

List of Tables

List of Figures

Chapter 1

Motivation for this Work

1.1 Motivation

Sensorineural hearing loss is caused by damage in the inner ear, and is one of the most common disabilities across the world [4][5]. Although research into drug therapies for various disorders in the inner ear are proving to be promising, the progress of effective therapies is stunted by the fact that the inner ear is a very complex part of the body to access and treat. Whereas most parts of the anatomy can be targeted via the cardiovascular system after oral or intravenous application of a drug, the cochlea can not. Finding a means of delivering the drugs to the desired location is therefore of the utmost importance in the field of hearing restoration and protection.

The role of the ear is to convert acoustic signals from the air into electrical signals which can be processed by the brain. Specialised hair cells are responsible for this mechanotransduction and they lie upon the Basilar Membrane (BM) inside the cochlea which is itself encased within the temporal bone: the hardest bone in the body. These hair cells can be damaged due to noise exposure or age, and once damaged cannot repair themselves in mammals, leading to sensorineural hearing loss. Treatment of these hair cells is promising, with new therapies such as gene therapy able to restore their function [6] [7] [8].

The cochlea itself is a very delicate organ and is to some extent isolated from the rest of the body through the blood-labyrinth barrier which, in a similar way to the blood-brain barrier, protects the cochlea from an influx of anything (be that hormones, free radicals, or any other toxin which may circulate in the blood stream) which could adversely affect its function [9]. This is necessary so that the cochlea stays in a state of homeostasis: it's function is dependent on a delicate balance in

the composition of the fluids which fill its interior [10][11]. Although this keeps a healthy cochlea functioning, it also makes the treatment of those that are damaged very difficult: if only those substances which the cochlea requires for healthy function can cross the blood-labyrinth barrier, systemic delivery of a drug via the bloodstream is very ineffective [12]. Not only does the drug have to be designed in order to cross the barrier, it has to be applied in sufficiently high doses such that the concentration once it reaches the cochlea is high enough to have any effect. In the case of steroid treatments, very common in inner ear therapies, this also leads to some quite serious side effects such as hyperglycemia, osteoporosis and even adrenal suppression [13]. Hence most delivery methods focus on local delivery, either by diffusion across a membrane known as the round window at the entrance to the cochlea, or by direct injection through it.

Diffusion across the round window occurs after application of a drug to the middle ear. The middle ear is the region of the ear which lies between the ear drum and the cochlea, and is normally filled with air, maintained at atmospheric pressure through the eustachian tube, which connects the middle ear to the throat. This tube's purpose is to regulate pressure and to remove mucus from the middle ear, necessary to avoid infection. Consequently, drug application to the middle ear suffers from the fact that the solution containing the drug is removed very quickly and swallowed by the patient [14][15]. Methods of delivery this way have fixed the patient's head in position for around 30 minutes, preventing the drug-filled solution from pouring through the tubes and allowing it to diffuse across the round window. Even with these measures, the concentration of the drug in the cochlear fluids is still relatively small, with concentrations at the first turn of the cochlea as low as 2.5% of that administered to the middle ear [16]. Not only is this percentage very low, but large gradients exist along the length of the cochlea [17]. For example, after an application of a suspension of the corticosteroid dexamethasone to the middle ear cavity, the concentration of the drug near the apex of the cochlea (the low frequency region) is 500 times smaller than at around halfway along it [18]. Hence apical and therefore low frequency damage is unlikely to be affected by such treatment.

Intracochlear injection involves the delivery of the drug directly into the cochlear fluids [4]. This method has the benefit of targeted delivery to the cochlea only, and hence the actual dosage delivered is well known compared to the round window diffusion technique, the results of which are known to vary widely between patients [19]. There are however a number of difficulties with this procedure. Firstly, the precision with which the procedure must be done make it very difficult. In order to reach the round window, a surgeon must first pass along the ear canal, through

the ear drum, across the air filled space of the middle ear, and into the small round window. Secondly, the volume of fluid which can be injected into the cochlea is very small, else the increase in pressure can lead to the destruction of the entire cochlear function [4]. Thirdly, the needle which delivers the injection passes through the membrane and causes a small rupture. This rupture must be perfectly sealed on removal of the needle to prevent fluid leakage and although gels and biocompatible tissue glues have proved to seal this hole well, they impact the mechanical properties of the membrane itself, which can lead to further problems [16] [20] .

The methods described here merely approach the issue of delivering drugs inside the cochlea: already a very complex task. However there is another problem: the distribution of drugs throughout the cochlea itself. Although the cochlea is completely fluid-filled, current therapies must rely on local, passive diffusion for drug transport throughout its entire length. Because of its dependence upon concentration gradients, this diffusion is very fast over small length scales. However once diffusion has begun, the concentration gradient reduces and the process slows [21]. To reach the apical region of the cochlea therefore requires very long timescales, turning the the problem into one of dosage and bio-availability. Under passive diffusion, the drug will redistribute evenly throughout the entire channel and the actual dosage at any one location will be much reduced. The reduction in availability of the drug is further compounded by processes such as absorption via the body and binding of the drug to proteins in the fluid itself [22]. Not only this, but a drug may only remain active for a certain lifetime, after which it becomes less effective. To overcome this issue, there are methods of delivery which delay the release of an active drug through the use of a so-called "carrier" (such as biodegradable micro-spheres and gels which can be loaded with a drug [18]), which can be triggered to release the drug in a variety of ways. Examples include utilising natural concentration gradients, using a chemical trigger such as the surrounding pH level or even through a variation in temperature [16]. These not only increase the active lifetime of the drug, but mean that the carrier can diffuse further towards the apex before releasing its payload, and potentially affect hair cells. However, the problem of re-absorption by the body still remains.

There is an emerging technology which looks to be very promising and manages to overcome almost all of these issues. The process works by the temporary implantation of precision micromechanical pump, which, over some time period, delivers the drug to the cochlea by a constant push-pull process. It overcomes volume conservation issues of normal injection techniques by ensuring that the total volume in the cochlea remains constant and also manages to mix the drug throughout the

entire cochlea, removing the need for passive diffusion as the main means of transport. The pump is implanted into a patient, and can be used over long timescales to deliver its payload. However, its biggest downfall is that it requires very invasive surgery: carrying its own, separate set of risks [13] [19]. It is therefore clear that a non-invasive, predictable method of delivering these drugs to a specific location in the cochlea is needed.

To summarise: research has shown that there are a number of ways that a drug can be delivered into the fluid-filled cochlea. These results, coupled with the pharmaceutical research being undertaken, provide a way in which to treat hearing damage and loss. However, these methods still rely on passive diffusion once the drug has been delivered or require invasive surgery to implement. This work will instead try to quantify and harness the natural fluid dynamics of the inner ear as a result of optimised sound stimulation to target locations along the cochlea and therefore increase dosage of therapies at a particular location.

Chapter 2

Introduction

2.1 The Anatomy and Physiology of the Ear

The anatomy of the ear consists of three main parts: the outer, middle and inner ear. Fig. 2.1 is an illustration showing the details of the anatomy of the human hearing organs.

2.1.1 The Outer Ear

The outer ear consists of the auricle (the visible part of the ear) and the ear canal. The auricle has its particular shape in order to funnel sound pressure waves in the air into the ear canal and onto the tympanic membrane. The tympanic membrane therefore oscillates at the same frequency as the waves in the air.

2.1.2 The Middle Ear

The tympanic membrane signifies the beginning of the middle ear. The membrane is forced to oscillate with the frequency of the incident sound, which in turn drives the oscillation of a series of three bones known as the ossicles: the maleus, incus and stapes (see Fig. 2.1 and Fig. 2.2). The purpose of these bones is to match the impedance between the air filled outer ear and the fluid filled inner ear (also known as the cochlea). When sound waves travel between media, there is usually a very large attenuation of energy due to the transition from a compressible medium (air) to a barely compressible fluid (the liquid contained within the cochlea). Without the intermediate stage of the middle ear, the vibration of the ear drum alone would have to drive vibrations in the fluid filled cochlea. If this were the case, the

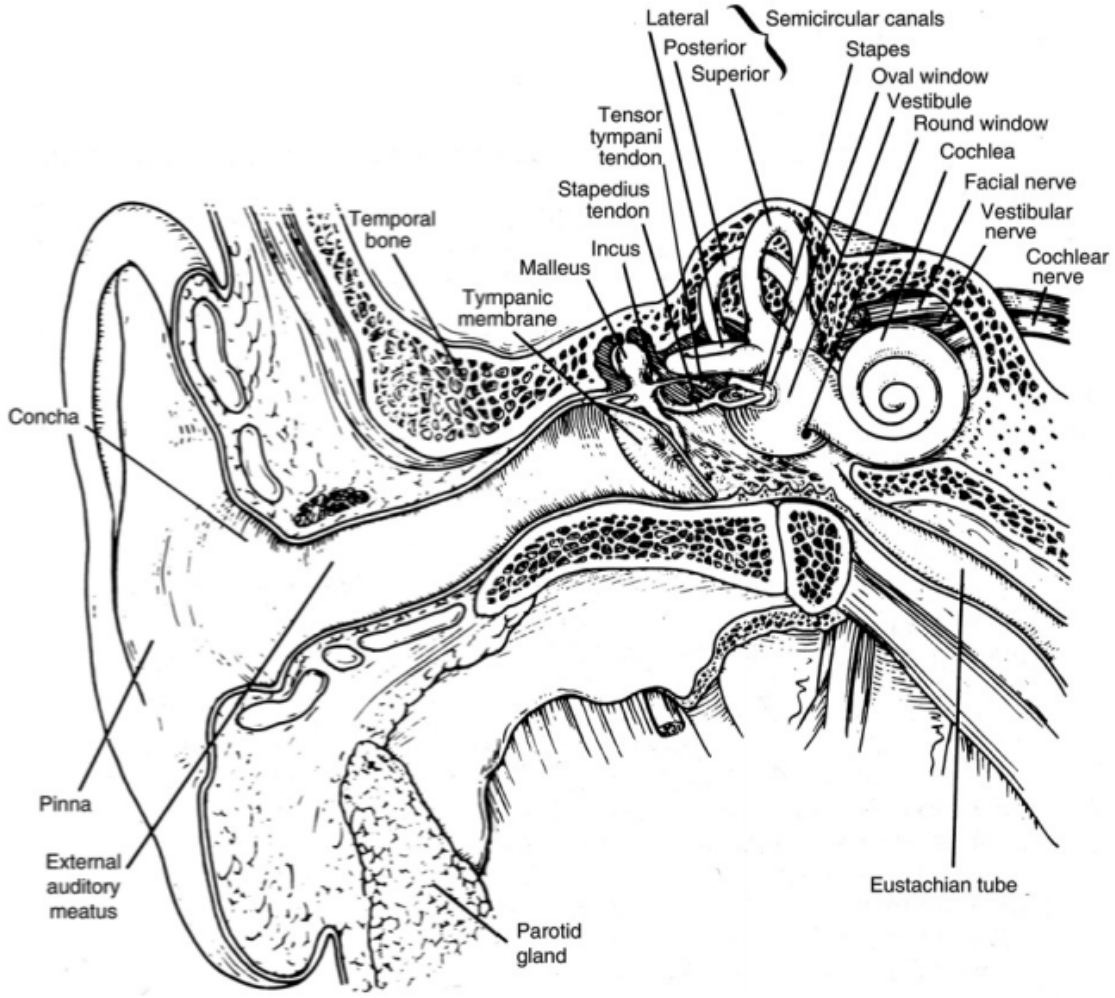

Figure 2.1: Illustration of the anatomy of the human ear detailing the outer, middle and inner ear. Taken from "An Introduction to the Physiology of Hearing" [3].

transmission of sound energy could be as small as 0.1% [3]. The ossicles therefore facilitate the transfer of force from the relatively large tympanic membrane onto a much smaller membrane known as the oval window, and the decrease in area results in an increased pressure at the oval window and hence a large enough energy transfer to drive the fluid motion inside the cochlea. This is possible through the geometry and lengths of the bones. Combined, they act as a compound lever, generating the increase in force necessary to drive the oscillation of the oval window.

2.1.3 The Inner Ear

We now reach the inner ear (or cochlea): the most complex part of the hearing apparatus. The purpose of this stage of hearing is to convert the mechanical signal

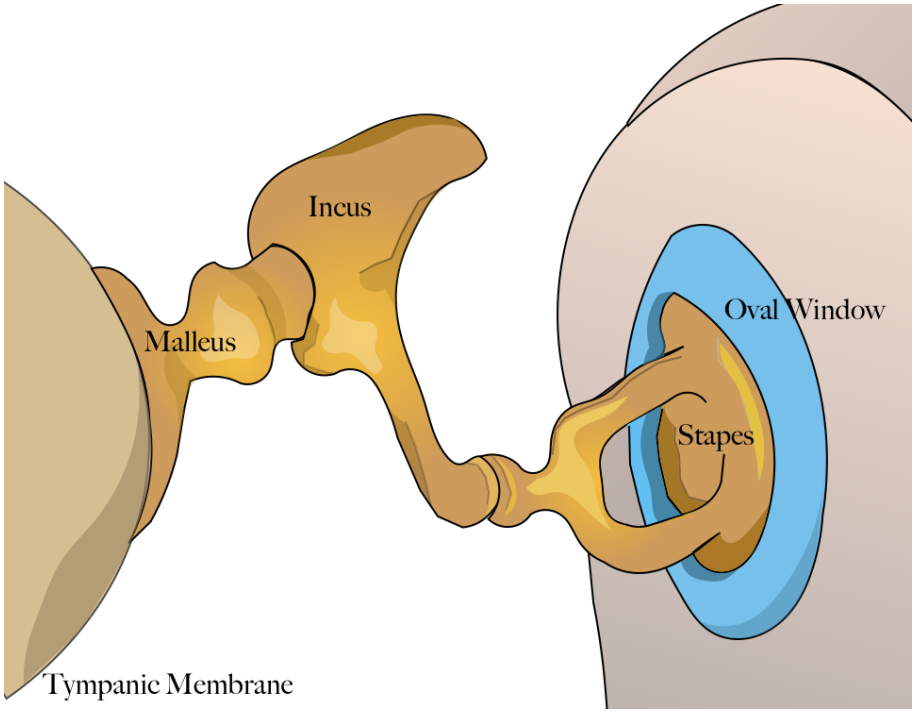

Figure 2.2: The tympanic membrane oscillates at the same frequency as the sound wave which is incident upon it. This in turn sets into motion the ossicles: three small bones whose purpose is to more efficiently transmit the oscillations from the air to the fluid in the cochlea. The ossicles connect the relatively large tympanic membrane to the much smaller oval window. The pressure exerted on the oval window and therefore onto the fluid within the cochlea is increased from that at the tympanic membrane. This impedance matching device means that the attenuation of the signal is drastically reduced relative to an air-liquid transmission.

received at the oval window into an electrical signal which can then be transmitted to the brain. The cochlea contains three coiled channels, separated by membranes, which form a spiral shaped structure (Figs. 2.3, 2.4).

The channels (scala vestibuli, scala media and scala tympani) are encased within the bony otic capsule. All three channels are completely fluid-filled. The scala vestibuli and tympani are connected at the apex of the channels by the helicotrema, allowing the exchange of fluid between the two. The scala media is isolated however, due to the composition of the fluid contained within: although the other channels are filled with a liquid which has a similar ionic composition to the extracellular matrix (perilymph), the scala media's fluid has a high concentration of potassium ions, K^+. This so-called endolymph has a potential of 80 mV: the endocochlear potential [23]. The channels are separated by two highly specialised membranes: Reissner's Membrane (separates scala vestibuli from media) and Basilar Membrane (separates scala media from tympanic). These two membranes as well as the scala media are grouped into what is known as the cochlear partition. Figure

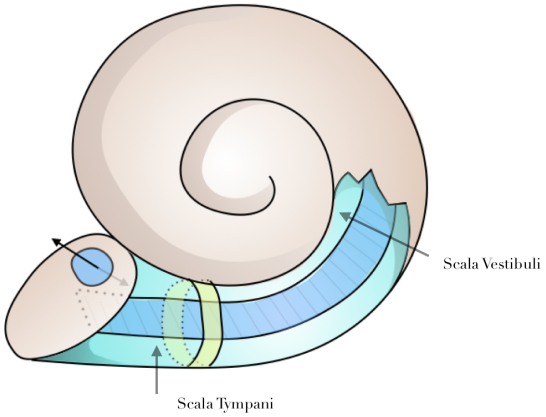

Figure 2.3: The spiralled cochlea, with a cut away section revealing the cochlear partition which coils throughout the cochlea. The arrows indicate the motion of the oval window (which is connected via the ossicles to the ear drum) which drives the fluid motion and consequently the travelling waves along the basilar membrane.

2.3 demonstrates this, showing the cochlea, with a section of the otic capsule cut away, revealing this cochlear partition, bounded from above by Reissner's membrane and from below by the basilar membrane with the scala media in between. Figure 2.4 shows these details further, and corresponds to a viewpoint which looks through the yellow section highlighted in Fig. 2.3. If we were to unroll the cochlea into a straight, tapered channel as in Fig. 2.5a, we would see that the BM is trapezium shaped (Fig. 2.5b). It is comprised of many fibres, which run perpendicular to its length, are attached at the cochlea walls and which have more mass and become more elastic the further along the cochlea we travel.

The structure of this membrane means that it has a spatially varying impedance, and it is for this reason that the cochlea is able to spatially resolve frequencies. The result of a sound wave of a particular frequency causing the fluid in the cochlea to move via motion of the oval window is a pressure difference between the top and bottom channels. The pressure difference causes motion of the BM in the vertical direction and elicits a travelling wave along the BM surface. Because of the physical structure of the membrane, with the mass increasing with distance from the base and the stiffness vice-versa, there is a spatial position at which the travelling wave abruptly decays. So, for a specific frequency, a resonance will occur at a certain location, causing the specialised cells at that location to send a signal to the brain. Because different cells are triggered at different frequencies, the brain can differentiate between signals of different frequency.

It is upon the Basilar membrane that the Organ of Corti is located. This organ is responsible for transducing the membrane motion into electrical signals through the triggering of action potentials in auditory-nerve fibers that are attached to hair

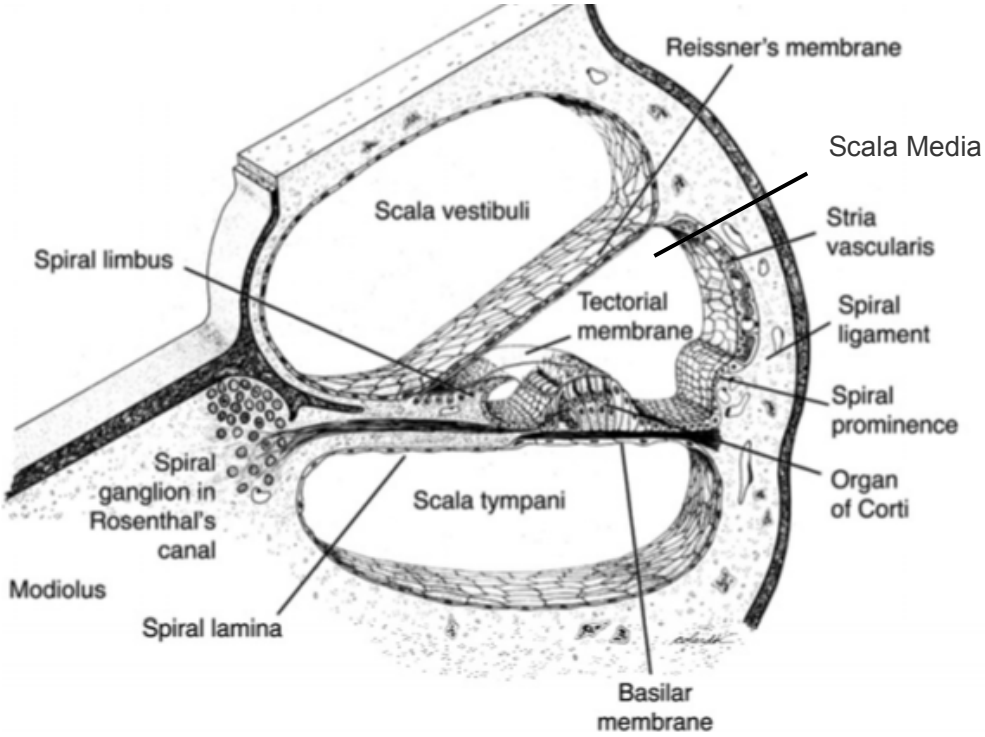

Figure 2.4: Cross section of the cochlea, corresponding to a viewpoint through the yellow highlighted section in Fig. 2.3 showing the basilar membrane and the various channels which run along the spiral. Taken from "An Introduction to the Physiology of Hearing" [3].

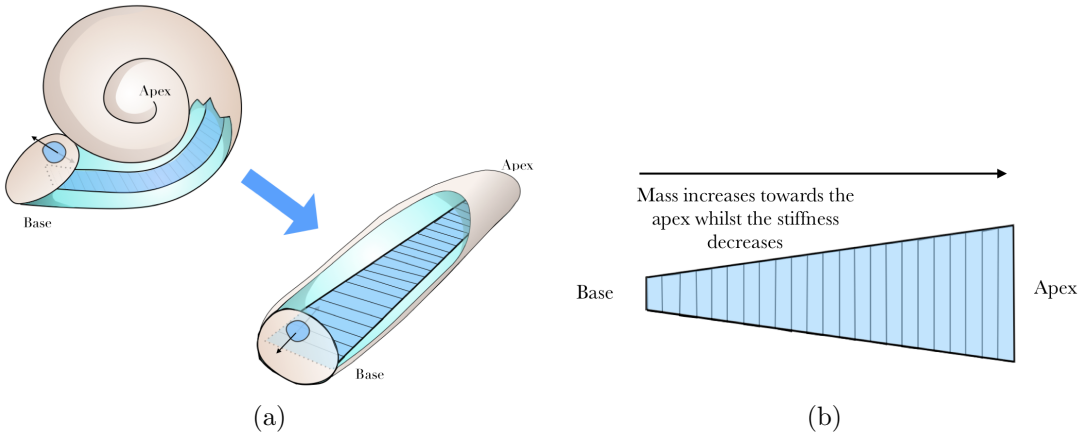

Figure 2.5: By unrolling the cochlea so that the channel is straight as depicted in (a), we find that the geometry of the basilar membrane which runs along the entire cochlear spiral, is trapezoidal:(b). It is composed of many radial components which are weakly coupled in the longitudinal direction (along the cochlea). At the entrance of the cochlea the components are stiffer and have smaller mass, whereas towards the apex of the channel they become more compliant with a greater mass.

cells. The vertical displacement triggers the transmission of electrical signals to the auditory fiber and thus the brain, by opening ion gates in the hair cells which lie upon

the membrane surface. Each hair cell consists of a central cell body with a set of stereocilia positioned at it's head (Fig. 2.6). These stereocilia are joined by filaments called tip links (Fig. 2.7) which, when the BM is deflected and the stereocilia bent, pull open ion channel gates and allow the flow of positive potassium ions into the hair cells.

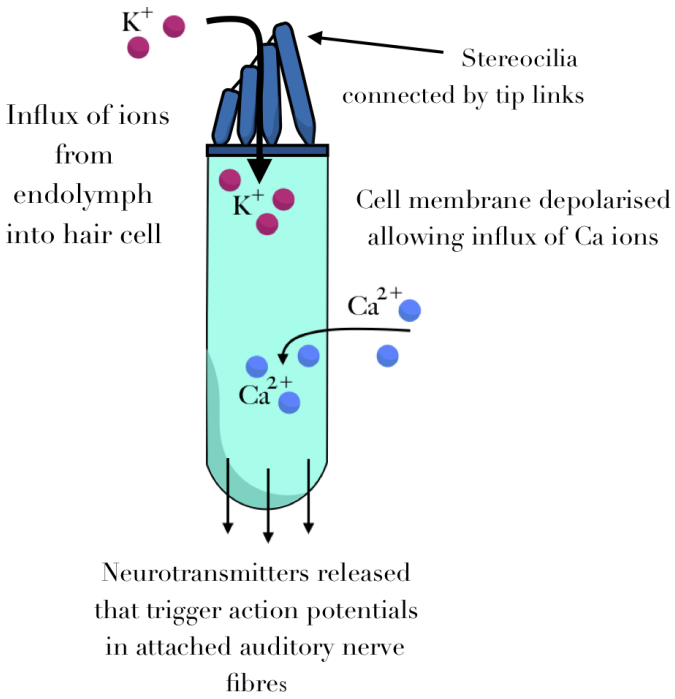

Figure 2.6: The hair cells which form part of the Organ of Corti on the BM are highly specialised. They allow an influx of Potassium ions from the endolymph into the hair cell through the gated channels of the stereocilia which open on deflection of the BM. Once the K^+ ions have flowed into the cell, its membrane becomes depolarized, and Calcium ions can also enter. The purpose of this ion flux is to trigger electrical signals which are sent to the auditory nerve and then the brain.

2.2 The Active Process

Measurements of the Basilar membrane response in a living (active) cochlea differ greatly from those of a dead (passive) one. In an active cochlea, the peak displacement of the BM is much larger than in the passive case. Not only is there an amplification of the BM displacement, but there is also a persistence in its oscillation in the fluid that cannot be explained by a model in which the membrane is driven by the mechanics of the middle ear alone. Experimental work by Gold on this matter [24][25] found that the quality (or Q) factor being measured for the oscillating system

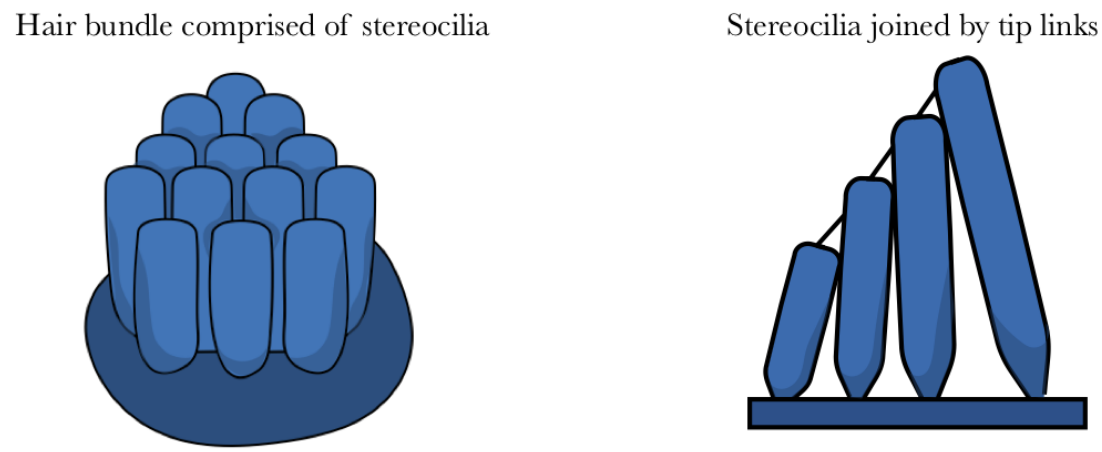

Figure 2.7: Stereocilia are grouped together into hair bundles, organised such that the stereocilia line up in height order creating a wedge profile (left diagram). Individual stereocilia are linked together via tip links (right diagram) whose role is to open the ion gates after deflection of the BM.

was impossibly high if it were true that the BM was driven only by the pressure difference between the channels. Consequently he hypothesised that there must be some other process which acts to amplify the displacement and prolong the oscillation.

The non-linear behaviour of the membrane displacement is the mechanism which allows the cochlea to resolve sounds of different orders of magnitude. Early experimental work [26] revealed that the membrane elicits a non-linear response to an increase in both sound pressure level (SPL) and frequency. The BM displacement away from the resonant position follows a linear behaviour, becoming sublinear as the peak is approached [27]. Quieter sounds have an amplification of up to 100 times those of louder ones.

Although these behaviours were known for a long time, it is only recently that a hypothesis for its origins has been put forward. It is now generally agreed upon that specialised hair cells upon the BM are responsible for the membrane amplification, through a process named "active feedback" [28][29][30][31]. The hair cells which lie along the BM are responsible for the mechanotransduction of signals from the membrane to the nerve fibres. When the hair cells are displaced by the BM, they exert a force back onto the membrane and cause an amplitude amplification. This amplification also aids the cochlea in hearing and processing low SPL inputs. Without the amplification it is impossible to explain how the ear succeeds in picking up such low energy signals. The active process is a feed back loop and is highly non-linear in nature. It is also the cause of otoacoustic emissions, sounds which are produced internally within the inner ear itself, rather than as a result of eternal

sound stimuli. The active process amplifies the BM wave and allows it to have enough energy to overcome the effects of viscous damping of the fluid, which lead to an increased wave amplitude. Although the mathematical model which we will describe in Chapter 3 does not include the details of this non-linear behaviour, we are able to incorporate the compressive non-linearity through empirically fixing the damping of the wave for different SPLs.

To summarise: the outer ear's role is to focus sound waves onto the ear drum; the middle ear's role is to transfer the energy received at the ear drum to the fluid in the cochlea through the impedance matching offered by the ossicles; the inner ear's role is to convert the mechanical waves into electrical signals for the brain to interpret as sound at a particular frequency. The displacement of the BM wave is different in an active vs passive cochlea due to the presence of the active process.

2.3 Steady Streaming

Steady streaming is the net motion of particles in a fluid in a fluctuating flow whose time average is zero. A simple example of this is in the case of a surface wave where the velocity field displays circular motion but with an amplitude that decays exponentially away from the surface. The time average of the motion of this fluid is zero, yet individual particle paths map out a translating circle: a spiral trajectory. There are a few factors which contribute to this effect, but the underlying principle is that energy is transferred to the fluid and results in a velocity field, which we will call the "steady streaming field" which is superposed onto the Euler velocity field of the fluid system. In general, the effect arises either due to a non-conservative body force in the fluid, through the momentum transfer from Reynolds stresses or from the boundary layer [32]. As will be discussed in further detail in the following chapter, it turns out that the nature of the fluid motion in the cochlea means that all three effects are present. Streaming in the cochlea has been a topic of interest for many years: Lighthill studied steady streaming of the cochlea theoretically and in particular found that a combination of effects cause the steady streaming: Stokes drift in the bulk flow and boundary layer, and momentum transfer due to Reynolds tangential and normal stresses [33]. Edom and Obrist built upon this work and found additional streaming effects which result from slight membrane motion along the channel as well as perpendicular to it. [34]. The work of Steele in 1968 focused on the effects of the streaming within the perilymph-filled space between the two main channels [35]. Whereas research has been conducted into the process of steady

streaming in the cochlea, the focus has been towards the physiological implications of such an effect or the determination of its magnitude and importance for the overall dynamics of the cochlea [36]. In this work we are instead interested in the question: are we able to use the steady streaming flow in the cochlea to efficiently transport an injected drug to a specific location along the basilar membrane?

To discuss the simplest steady streaming, we must use two interpretations of the velocity field in the fluid, depending on the reference frame used: Euler (fixed reference frame) or Lagrangian (reference frame which moves with the fluid parcel). Of course in a linear system, the time average of these two velocities are equal. However, as will be seen in the full treatment of steady streaming in the cochlea in § 3, when higher order terms are taken into account, this difference is non-zero and proportional to the square of the velocity amplitude.

In the work which follows, we investigate whether or not the steady streaming in the cochlea occurs fast enough and over sufficient length scales such that when presented with a sound, the underlying steady streaming field can be used as a transport mechanism. The fact that the streaming is proportional to the square of the velocity amplitude (where in the case of the cochlea this refers to the membrane's vertical velocity) implies that the effect is greater near the position of resonance for a particular frequency. It is therefore hypothesised that by changing the frequency of the stimulation via frequency sweeps for example, the location of the resonance and hence maximum steady streaming could be changed also. By optimising the sound stimulus it could be possible to harness this effect and transport an injected drug through the cochlea to a specific location: something which is currently impossible to achieve with any significant dosage.

Chapter 3

The Mathematical Formulation: Cochlear Mechanics and Steady Streaming

3.1 Basilar Membrane Waves

3.1.1 Cochlear Fluid Mechanics

We begin by reducing the geometrical complexity of the system significantly in two ways. Firstly, by unrolling the cochlea [37]. The validity of this simplification can be argued for two reasons. The first is that in the high frequency region (the region of focus of this work) the curvature of the cochlear channel is much larger than the local wavelength of waves elicited upon the BM, and so we can locally assume the channel to be straight. The second is that the energy transferred to the fluid because of the curvature is small for most of the channel, becoming significant only near the apex [38][39]. In this work we focus on high frequency stimulation, which occurs at the base of the cochlea, because it is not only better understood, but physically lies in the region of interest in terms of drug delivery along the cochlea [40][41]. Secondly, by treating it as two channels instead of three: effectively treating the scala media and scala vestibuli as one compartment [42] [43]. The justification for this simplification is that Reissner's membrane which separates the scala media and scala vestibuli, is much thinner than the BM and hence has a much smaller impedance [26][44]. Figure 3.1 shows the geometry and associated variables of the problem.

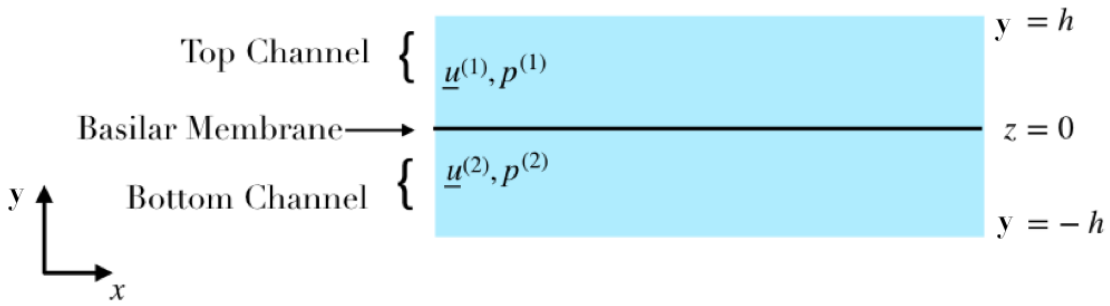

Figure 3.1: The geometry of the problem: the top (1) and bottom (2) channels of the cochlea are separated by the Basilar membrane. Velocity and pressure fields are defined in both channels.

Beginning with the full Navier Stokes equations:

$$\rho \frac{D\underline{u}}{Dt} = -\nabla p + \rho F + \mu \nabla^2 \underline{u} \tag{3.1}$$

where $\underline{u} = (u, v, w)$ is the velocity field vector and $\frac{D\underline{u}}{Dt} = \frac{\partial \underline{u}}{\partial t} + \underline{u}\nabla . \underline{u}$ is the material derivative, we make the following assumptions:

- no external body forces act upon the fluid
- the fluid is inviscid
- the amplitude of the BM waves, is small. [44] This long wavelength approximation means that $\frac{a}{\lambda} \ll 1$. Using this fact, the advective, non-linear term $(\mathcal{O}(\frac{a^2\omega^2}{\lambda}))$ is much smaller than the unsteady term $(\mathcal{O}(a\omega^2))$ and can be neglected.

These assumptions leave us with the reduced Navier Stokes equations:

$$\rho \frac{\partial \underline{u}}{\partial t} = -\nabla p. \tag{3.2}$$

Next we consider the continuity equation:

$$\frac{D\rho}{Dt} = \rho \nabla \cdot \underline{u} \tag{3.3}$$

Only very small displacements are present in the cochlea ($< \mathcal{O}(10^{-6})m$). Consequently, we employ a Taylor expansion of the fluid density around a mean displacement, x_0:

$$\rho = \rho(x_0, t) + (x - x_0)\frac{\partial}{\partial x}\rho(x_0, t) + \frac{(x - x_0)^2}{6}\frac{\partial^2}{\partial x^2}\rho(x_0, t) + ... \tag{3.4}$$

and take ρ to be equal to the leading term, $\rho_0 = \rho(x_0, t)$. Thus we remove the x dependence of the density, but its time dependency remains. Now Eq. 3.3 becomes

$$\frac{\partial \rho_0}{\partial t} = -\rho_0 \nabla \cdot \underline{u}. \tag{3.5}$$

Notice the spatial derivatives of ρ have now vanished after invoking Eq. 3.4.

Time dependent density is equivalently described in the context of a pressure change, and the two vary according to the fluid's compressibility, κ as follows:

$$\frac{\partial \rho_0}{\partial t} = \rho_0 \kappa \frac{\partial p}{\partial t} \tag{3.6}$$

combining Eq. 3.5 and Eq. 3.6

$$-\nabla \cdot \underline{u} = \kappa \frac{\partial p}{\partial t} \tag{3.7}$$

and by combining the divergence of Eq. 3.2:

$$\rho_0 \frac{\partial}{\partial t} \nabla \cdot \underline{u} = -\nabla^2 p \tag{3.8}$$

with Eq. 3.7, we find the wave equation for the pressure in the fluid:

$$\frac{\partial^2 p}{\partial t^2} = -\frac{1}{\rho_0 \kappa} \nabla^2 p \tag{3.9}$$

which defines the wave speed, c for a sound wave travelling through the fluid:

$$c = \frac{1}{\sqrt{\rho_0 \kappa}}. \tag{3.10}$$

The longitudinal pressure wave which travels through the fluid is not important for the fluid dynamics. It has a wavelength of the order of a metre, significantly larger than the size of the cochlea, even in large mammals.

At this point, we can introduce the time dependency to the $\underline{u}^{(1,2)}$ and $p^{(1,2)}$ fields. We begin by assuming a pure-tone, with frequency ω, such that

$$p^{(1,2)} = \tilde{p}(x)^{(1,2)} e^{-i\omega t} + c.c \tag{3.11}$$

$$\underline{u}^{(1,2)} = \underline{\tilde{u}}(x)^{(1,2)} e^{-i\omega t} + c.c \tag{3.12}$$

where c.c indicates the complex conjugate. We now consider the boundary condi-

tions. Firstly, apply the no slip condition at the top and bottom walls:

$$\underline{u}^{(1,2)}\big|_{(y=h,-h)} = 0 \tag{3.13}$$

and at the BM:

$$\underline{u}^{(1,2)}\big|_{(y=0)} = V \tag{3.14}$$

where V is the vertical velocity of the basilar membrane, defined through the impedance, Z, as:

$$V = \frac{1}{Z}\left(\tilde{p}^{(2)} - \tilde{p}^{(1)}\right) \tag{3.15}$$

and all walls are treated as rigid boundaries such that:

$$\left.\frac{\partial p}{\partial y}^{(1,2)}\right|_{(y=h,-h)} = 0. \tag{3.16}$$

Starting now again with Eq. 3.7 we set the y-dependent velocity to 0 and use the common simplification of making the system 2D [45] [46], with the x direction along the channel and the y direction across the channel height. Taking a volume integral (where volume here refers to volume per unit span) described in Fig. 3.2 over both sides:

$$-\int_V \nabla\cdot\,\underline{u}dV = \kappa\int_V \frac{\partial p}{\partial t}dV \tag{3.17}$$

and using Gauss's theorem:

$$\int_V \nabla\cdot\,\underline{u}dV = \oint_S \underline{u}.\underline{\hat{n}}dS \tag{3.18}$$

we rewrite Eq. 3.17 as

$$-\oint_S \underline{u}\cdot\,\underline{\hat{n}}dS = \kappa\int_V \frac{\partial p}{\partial t}dV \tag{3.19}$$

Integrating over a fluid control volume in the top channel , leads to 1 dimensional expression for the velocity $\underline{u} = (u, v)$ and the pressures:

$$-h\,u|_{(x)} + v|_{(y=h)}\,x - h\,u|_{(x+dx)} - v|_{(y=0)}\,dx = \kappa h\frac{\partial p}{\partial t}dx \tag{3.20}$$

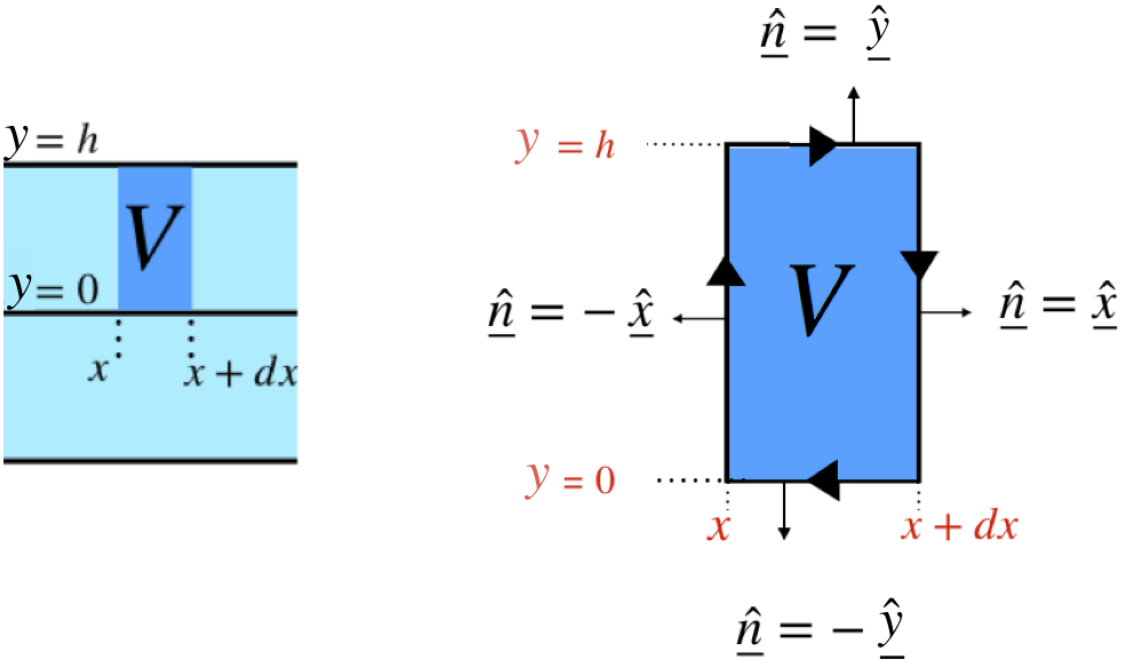

Figure 3.2: The left hand diagram shows the control volume, V, over which we integrate. Due to Gauss's theorem, we can calculate this as a surface integral with normal vectors and the direction of integration defined in the right hand diagram.

the second term, $v(h)x = 0$ by definition (no flow through solid boundaries). Grouping the terms multiplying h and dividing through by dx:

$$h\frac{\left(u|_{(x)} - u|_{(x+dx)}\right)}{dx} - v|_{(y=0)} = \kappa h\frac{\partial p}{\partial t} \tag{3.21}$$

and after using the definition of the derivative:

$$h\frac{\partial u}{\partial x} = v|_{(y=0)} + \kappa h\frac{\partial p}{\partial t}. \tag{3.22}$$

The vertical component of the fluid velocity at the membrane, $v(x, y = 0)$, is equal to the membrane's vertical velocity, V. Now we can implement Eq. 3.11, Eq. 3.12 and Eq. 3.15 in each of the channels which gives

$$h\frac{d\tilde{u}^{(1)}}{dx} = \frac{1}{Z}\left(\tilde{p}^{(2)} - \tilde{p}^{(1)}\right) - i\omega\kappa h\tilde{p}^{(1)} \tag{3.23}$$

The two terms here show the two ways in which the longitudinal velocity can be altered: a membrane motion (induced by a pressure difference across it) or a compression of the fluid.

By taking the x differential of the x-component of Eq. 3.2, we can eliminate

the velocity from Eq. 3.23 to form an equation in terms of the pressure for the top and bottom channel respectively:

$$\frac{d^2\tilde{p}^{(1)}}{dx^2} = -\frac{i\omega\rho_0}{hZ}\left(\tilde{p}^{(2)} - \tilde{p}^{(1)}\right) - \omega^2\rho_0\kappa\tilde{p}^{(1)} \tag{3.24}$$

$$\frac{d^2\tilde{p}^{(2)}}{dx^2} = \frac{i\omega\rho_0}{hZ}\left(\tilde{p}^{(2)} - \tilde{p}^{(1)}\right) - \omega^2\rho_0\kappa\tilde{p}^{(2)}. \tag{3.25}$$

Combining these expressions and defining the pressure difference: $\tilde{P} = \tilde{p}^{(2)} - \tilde{p}^{(1)}$ and neglecting compressive effects due to the large wavelength of compression waves leads to the one dimensional wave equation for the pressure difference across the BM:

$$\frac{d^2\tilde{P}}{dx^2} = \frac{2i\omega\rho_0}{Zh}\tilde{P} \tag{3.26}$$

This wave equation gives the local wave speed as

$$c(x) = \sqrt{\frac{i\omega Zh}{2\rho_0}} \tag{3.27}$$

which leads to the wave number (through $c = \omega/k$):

$$k(x) = \sqrt{\frac{2\omega\rho_0}{iZh}} \tag{3.28}$$

The nature of the wave number is important. It is dependent on the impedance, which is itself a result of the balance between the mass and stiffness properties of the membrane.

So far there has been no mention of the mathematical nature of the impedance. In reality, the BM is not a continuous membrane at all, but rather a series of radially connected elastic beams, which are coupled together by the fluid, rather than each other. This means that each beam has its own resonant frequency dependent upon its mass, m and stiffness, K. We now implement this spatial dependence, using the following expression for the impedance [37],[40],[43]:

$$Z = \frac{1}{A}\left(\frac{-iK}{\omega}\left(1 - \frac{\omega^2}{\omega_0^2} + \frac{i\xi\omega}{K}\right)\right) \tag{3.29}$$

where the resonant frequency, ω_0 is

$$\omega_0^2 = \frac{K(x)}{m(x)}. \tag{3.30}$$

and ξ is a damping factor, necessary to ensure that the resonance peak behaves in a physical manner. ξ therefore represents the viscous damping of the BM by the fluid.

3.1.2 The WKB Approximation

The WKB approximation is a method used to solve spatial and temporal differential equations where the coefficient has a spatial dependence. Usually the WKB approximation is used in the case of a "short wavelength" assumption: seemingly opposite to the model requiring the long wave assumption we have presented here. However, it has been argued that the short assumption is still valid in this case, as the wavelength is only long in comparison to the small amplitudes of the BM motion. In fact we compare the wavelength scale to the lengthscales over which the impedance of the membrane changes [47]. In this way the wavelength is "short". This assumption is borne from the observations that waves travel only in one direction along the membrane [26][43]. In order for no travelling wave reflections to occur at any point along the membrane, the structure of the membrane must change slowly and smoothly [42][47][48].

We are now at the stage where we can begin the process of finding the surface deflection which we shall need to pursue the next stages of the work. The purpose of using this method, is that it will enable us to greatly simplify the computational costs of simulation the membrane motion in the cochlea. This is due to the fact that the results of the WKB method incorporate the mechanical properties of the membrane and allow us to use the deflection to drive the flow, rather than applying a pressure field to the fluid and implementing a fluid structure interaction to deflect the membrane as a result. This is discussed in further detail in the following chapter. Once we take Z to be $Z(x)$, Eq. 3.26 becomes a differential equation with a spatially varying coefficient, and so we can use the WKB approximation to solve it. We begin by introducing the ansatz

$$\tilde{P} = \hat{P}(x)e^{-i\int_0^x k(x')dx'} \tag{3.31}$$

into the wave equation:

$$\hat{P}'' - 2ik(x)\hat{P}' - ik(x)'\hat{P} - k(x)^2\hat{P} = \frac{2i\omega\rho_0}{Z(x)h}\hat{P} \tag{3.32}$$

To find the leading order behaviour of this equation, we use the fact that the wave number, $k(x)$ is much larger than the relative change in pressure amplitude, $\frac{\partial\hat{P}}{\partial x}/\hat{P}$. Doing so gives the dispersion relation:

$$k(x) = \sqrt{\frac{2\omega\rho_0}{iZ(x)h}} \tag{3.33}$$

and taking the next order gives an ordinary differential equation for $\hat{P}$:

$$\frac{\hat{P}'}{\hat{P}} = -\frac{k'}{k} \tag{3.34}$$

the solution of which is

$$\ln(\hat{P}) = \ln(k^{-1}) \tag{3.35}$$

leading to

$$\hat{P} = \frac{1}{\sqrt{k}}. \tag{3.36}$$

and thus

$$\tilde{P} = \frac{1}{\sqrt{k(x)}}e^{-i\int_0^x k(x')dx'} \tag{3.37}$$

Finally, using Eq. 3.15 and Eq. 3.33, we arrive at an expression for the vertical velocity of the BM as a function of the impedance:

$$\tilde{V}(x) = \left(\frac{-h}{2i\omega\rho_0 Z(x)^3}\right)^{1/4} \mathrm{e}^{-i\int_0^x \sqrt{\frac{2\omega\rho_0}{ihZ(x')}}\mathrm{dx}'} \tag{3.38}$$

and we define the velocity amplitude, $\hat{V}$ as

$$\hat{V} = \left(\frac{-h}{2i\omega\rho_0 Z(x)^3}\right)^{1/4} \tag{3.39}$$

Finally, the full expression including time dependence for the BM velocity is:

$$V(x,t) = \tilde{V}(x)e^{i\omega t}. \tag{3.40}$$

To elucidate the behaviour of the BM, we consider the nature of $\hat{V}(x)$. The integral term in the exponential depends on the impedance, $Z(x)$. Before the wave reaches the resonant location, the impedance has a large, real part, and the exponent is imaginary, resulting in a propagating wave. Once the resonant location is reached however, the impedance becomes imaginary and the exponent real. This is an evanescent wave, which promptly decays, allowing the cochlea to achieve spatial frequency resolution.

3.1.3 Matching the Theory to the Experimental Data

Now that the function governing the mechanics of the membrane has been derived, the parameters will be fixed in order to use Eq. 3.40 to generate realistic BM deflections in the computational model. Experimental data for the mass and stiffness of the BM in gerbils is used, from the work of Emadi et al [1]. Henceforth, all parameters will be fixed using rodent data and so the work effectively calculates the steady streaming fields for much smaller mammals than humans. Although the geometry is much smaller and the frequency range different to humans, the model can be easily adapted for a human cochlea on addition of the equivalent experimental data to that which follows.

x Position (mm)	Mass (ng)	Stiffness (Nm^{-1})
0	32	1
7	65	0.03

Table 3.1: Experimental data taken from the work of Emadi et al [1]

Using the convention that their spatial variation is approximately exponential [42][47]:

$$m = m_0 e^{x/l_m} \qquad K = K_0 e^{-x/l_K}. \tag{3.41}$$

combined with the data in table 3.1 gives the empirically determined decay length-scales as $l_m = 115$ nm and $l_K = 501$ nm respectively. Higher frequencies should resonate closer to the entrance of the cochlea and lower frequencies resonate at the base of the cochlea. Figure 3.3 verifies that these functions behave in this way.

The amplitude of the BM wave envelopes scale with increasing SPL. The next value we determine is the scale factor between SPLs, the normalisation pressure. The normalisation pressure, p_N for each curve is the root mean square pressure in

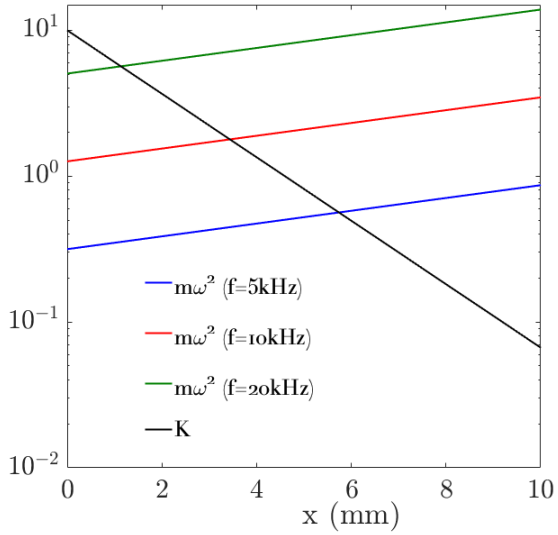

Figure 3.3: Resonance curves for 80 dB SPL stimulation across a range of frequencies. The intersection of the mass and stiffness curves indicate the location of the resonant location for different frequencies. Higher frequencies resonate closer to the base of the cochlea.

air for a specific SPL, determined through the conversion:

$$\text{dB SPL} = 20\log\left(\frac{p_N}{p_{ref}}\right) \tag{3.42}$$

where $p_{ref} = 2 \times 10^{-5}$ Pa is a reference pressure: the threshold for human hearing. These values will scale the entire envelope to simulate increasing energy of the stimuli sound. However, the scaling is not the same across the entire envelope. This leads us to the final parameter to fix: the damping factor, ξ. This affects the shape of the envelope itself, by altering the shape around the peak, and can be fixed such that some of the non-linear behaviours can be captured. Specifically, we want to try, as far as possible, to recreate the compressive non-linearity around the resonance peak. Figure 3.4 shows the experimental results of Cooper and Rhodes [2], who measured the sensitivity (the displacement normalised by p_N) at different frequencies, but always at the same location in the cochlea: in this case at the position of the 17 kHz resonance for a chinchilla.

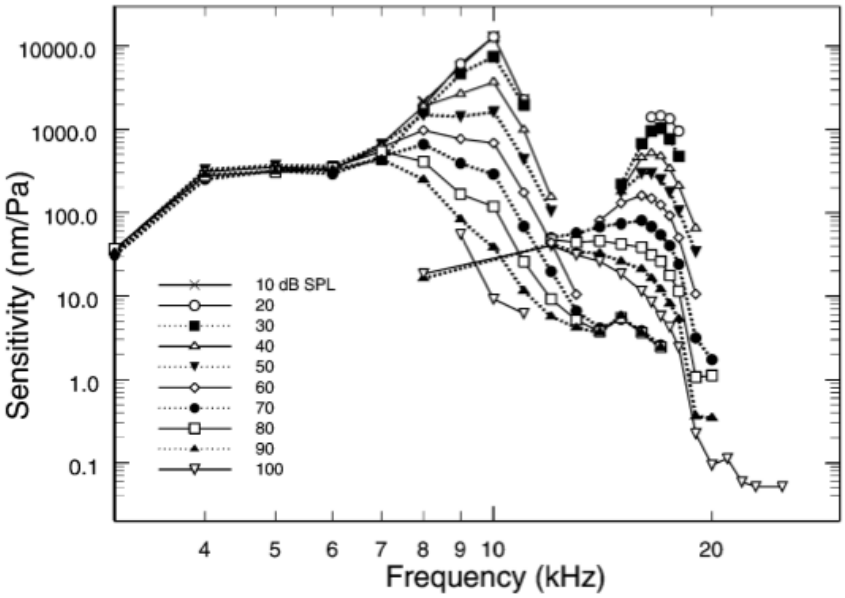

Figure 3.4: Experimental data taken from the original work of Cooper and Rhodes [2]. The higher frequency curves are of interest for us. We chose the 60, 80 and 100 dB SPL curves respectively. The data was found from measurements made at the 17 kHz resonance location in a chinchilla cochlea.

In order to fix ξ, the value was varied until the the wave amplitude at a fixed x-location (the longitudinal coordinate of the 17 kHz resonance) as well as the relative amplitude between SPLs at that location was matched to the experimental data. We are able to capture some of the non linear behaviours without actually having a nonlinear wave input; the ratio between the envelopes far from the peak is ≈ 10 but at the peak location, it is ≈ 3. However, the damping factor can only do so much in capturing the shape of the envelope of the waves. Indeed, our wave envelopes are indeed more sharp than is observed physiologically, and this can be seen in Fig. 3.5 when compared with the shape of the curves in Fig. 3.4. This is because we are limited by the use of a linear theory in a non-linear system. We therefore decided to make a trade off, prioritising the amplitude of the wave envelope over the ideal shape. The reason for this was that the steady streaming is proportional the square of the velocity envelope (see Section 2.2) which is determined by the amplitude of the function. Because the aim of this work is to determine whether or not streaming can effectively transport drugs, the magnitude of the streaming is more important than the width of the region of influence of the BM wave. Thus, in the work which follows, the reader should keep in mind that the steady streaming fields will be more spread than they appear here. Figure 3.5 shows the displacement envelope of the waves as well as the sensitivity curves after fixing all of the parameters, collated in Table 3.2 below.

SPL (dB)	Normalisation Pressure, p_N (Pa)	Damping Factor ξ (Nsm^{-1})
60	0.02	10×10^{-8}
80	0.2	5×10^{-7}
100	2	2×10^{-6}

Table 3.2: Parameters for the BM wave model, fixed using data acquired from the work of Cooper and Rhodes [2]

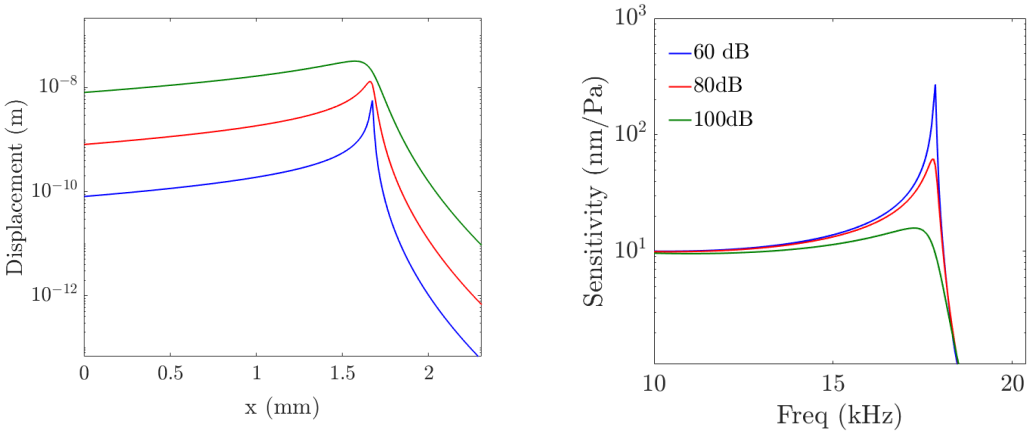

Figure 3.5: Curves for the membrane displacement at 17 kHz with increasing SPL. By fitting the damping factors to fit the experimental data, the compressive non-linearity around the resonance can be captured approximately: note the ≈10 fold increase in amplitude far from the resonance compared to ≈3 fold increase between the maxima.

3.2 Steady Streaming

The derivation for the steady streaming in the cochlea is completed in full by Lighthill, and we merely summarise the contributions to steady streaming that he presents (the Stokes drift, and Reynolds stresses)[33] as well as a more recent contribution from work completed by Edom and Obrist [34]. In the sections which follow, several assumptions about the nature of the fluid solutions in the channels have been made, specifically about the behaviour of the wave number, k. Following Lighthill [33], if k varies smoothly as a function of x only:

- at a specific location along the BM, the wave number takes on a constant, local value and is described by the dispersion relationship value at that location
- the local waveform is assumed to be that of a wave with a constant value of the local wave number everywhere.
- the amplitude variation along the membrane is due to the transfer of energy at the group velocity speed.

- any error associated with these assumptions is $\mathcal{O}(\frac{dk}{dx}\frac{1}{k^2})^2$.

Lighthill used these rules in order to derive his solutions for the fluid fields in the cochlea, which have been shown by comparisons by Steele [43] to be valid to as high an accuracy as the WKB method. Thus we implement his method in our work to the same end. For what follows, we approximate k as locally constant.

3.2.1 Stokes Drift

The first contribution we explore is the Stokes drift, u_S, a second order effect resulting from the difference between the time averaged Euler and Lagrangian velocities:

$$u_S = u_L - u_E. \tag{3.43}$$

The mean Euler velocity is calculated as the time average of instantaneous velocities at a fixed points in the field. The Lagrangian mean velocity however is the time average of a particle along some trajectory. So a particle moves through the Eulerian field on its Lagrangian path. The time average at a specific fixed coordinate in an oscillating field is zero, whereas this is not necessarily true along a particle's trajectory for the same time average. We calculate these differences in the bulk flow and the boundary layer flow.

Bulk Flow

We take the Euler mean velocity to be zero, and so are only interested in u_L for now. The velocity field in the x and y directions in the bulk flow take on the well known values of:

$$\tilde{u} = i\tilde{V}e^{-kz} \tag{3.44}$$

$$\tilde{v} = \tilde{V}e^{-kz} \tag{3.45}$$

such that the transverse (y-component) and longitudinal (x-component) fields are out of phase by $\pi/2$. Note that these variables are the Fourier coefficients of the velocity fields. Using the fact that [33]

$$u_L = \left\langle \frac{\partial \tilde{u}}{\partial x}\frac{\tilde{u}}{i\omega} + \frac{\partial \tilde{u}}{\partial y}\frac{\tilde{v}}{i\omega} \right\rangle \tag{3.46}$$

(angular brackets indicate an average over time) and substituting in the relevant

fields leads to

$$u_L^{(B)} = \frac{k}{\omega}\tilde{V}^2 e^{-2ky} \tag{3.47}$$

which is the same as the well known result for deep water waves. This deep water result is valid within the apparently shallow cochlea because the depth of penetration of the energy associated with the BM wave is of the order of k^{-1}. For a BM wave with $\lambda \approx 10^{-3}$m, this corresponds to a penetration depth of $\approx 1.5 \times 10^{-4}$m at the peak of the BM wave, which is around 1/3 of the entire depth of the channel (5×10^{-4}m) Completing an analogous process with w_L results in $w_L = 0$.

Boundary Layer

Now we can repeat this process for the flow in the boundary layer along the Basilar membrane. The velocity fields here are

$$\tilde{u} = i\tilde{V}(1 - e^{-y(\frac{i\omega}{\nu})^{-1/2}}) \tag{3.48}$$

$$\tilde{v} = i\tilde{V}(1 + (1 - e^{-y(\frac{i\omega}{\nu})^{-1/2}})) \tag{3.49}$$

using the same definition of u_L gives

$$u_L^{(b.l)} = \sqrt{\frac{i\omega}{\nu}}\frac{\tilde{V}^2}{2\omega}\mathrm{e}^{-y\sqrt{\frac{i\omega}{\nu}}} \tag{3.50}$$

If we integrate $u_L^{(B)}$ and $u_L^{(b.l)}$ to get the total mass flow, we find that they in fact have the same magnitude ($\frac{\tilde{V}^2}{2\omega}$) but in different directions. Hence the net mass flow as a result of the Stokes drift is zero: mass transport in the bulk of the flow is balanced out by an equal and opposite mass transport in the boundary layer.

3.2.2 Reynolds Stresses

The next contribution to steady streaming is through the Reynolds stresses: the mean value of the momentum flux. Whereas Stokes drift is present even in deep free surface water waves, these stresses originate in the boundary layer due to the BM and result in the application of a resultant force upon a fluid volume, causing non-zero mean motion to occur.

The Reynolds stresses are commonly seen in the theory of turbulence, where they appear in the Navier Stokes equations as a result of decomposing the velocity

fields into a mean and fluctuating component. For a fluctuating velocity component, u_i' in the x_i direction ($i = 1, 2, 3$), the Reynolds stress tensor is defined as:

$$\tau_{ij}^R = \left\langle \rho u_i' u_j' \right\rangle \tag{3.51}$$

Which can be understood as the flux of the j^{th} component of the mean momentum per unit volume, $\rho u_j'$, in the x_i direction [49].

For our purposes, we are interested only in the transfer of x momentum in the y direction (the tangential (shear) stress):

$$R_T = -\rho \frac{\partial}{\partial y} \langle u' v' \rangle \tag{3.52}$$

as well as the transfer of x momentum along the x direction (the normal stress):

$$R_N = -\rho \frac{\partial}{\partial x} \langle u'^2 \rangle \tag{3.53}$$

The result of spatial changes in the stress is the generation of a thin vortex sheet, which leads to a non-zero value of u_E. u_E then sharply decreases from its value at the BM, causing a large momentum gradient. Considering these momentum balances leads to the determination of the value of u_E and because forcing of fluid elements in the bulk flow will come from the value of u_E at the edge of the boundary layer, we calculate its value at that point. This is known as the slip velocity, and comes from these shear and normal stress contributions as well as an extra contribution to the shear stress due to the spatial dependence of the BM wave amplitude ([33] Eq. 91). Taking these things into consideration results in the steady streaming velocity:

$$u_{ss} = \frac{k\tilde{V}^2}{4\omega} - \frac{3}{4}\frac{\tilde{V}}{\omega}\frac{\mathrm{d}\tilde{V}}{\mathrm{dx}} \tag{3.54}$$

To derive this expression, Lighthill realised that the Stokes drift is cancelled out in the flow in some fashion. To ensure this was the case, he made an assumption that the Euler velocity at the position $y = 0$,(the surface of the Basilar Membrane) was

$$u_E|_{y=0} = \frac{\tilde{V}^2}{\sqrt{8\nu\omega}} \tag{3.55}$$

The work of Edom and Obrist however leads to a more intuitive boundary condition through their new contribution to the streaming velocity.

3.2.3 Edom and Obrist's New Term

The new term introduced by Edom and Obrist [34] is a result of the motion of the BM itself: that the elastic restoring forces of the membrane result in a force on the fluid in the direction of the travelling wave. The contribution to the streaming velocity from this effect is:

$$u_{BM} = \frac{\tilde{V}^2}{\sqrt{8\nu\omega}} \tag{3.56}$$

This velocity is equal and opposite to the value of the Stokes drift. It was hypothesised that this contribution to the flow is what cancels the Stokes drift, not a contrived boundary condition as mentioned above. If instead a more natural boundary condition is implemented at the boundary:

$$u|_{y=0} = 0 \tag{3.57}$$

it yields an altered Reynolds stress contribution to the streaming velocity and a different expression than that derived by Lighthill:

$$u_{ss}^{E} = \frac{-\tilde{V}^2}{\sqrt{8\nu\omega}} + \frac{\tilde{V}^2 k}{4\omega} - \frac{3\tilde{V}}{4\omega}\frac{d\tilde{V}}{dx} \tag{3.58}$$

For the work which follows, we take only Lighthill's solution, u_{SS} (Eq. 3.54) in any mention of the theoretical streaming value. This is because our BM deflection model uses a 1D stiffness in the model, as opposed to the 2D stiffness used by Edom and Obrist to derive u_{BM}.
In summary:

- Steady streaming has a contribution from the Stokes drift: the difference between the mean Euler and Lagrangian flows. However, the streaming in the boundary layer is equal and opposite to the streaming in the bulk flow, hence the Stokes drift has no contribution to overall mass transport.

- The streaming is therefore primarily driven by the transfer of momentum due to Reynolds stresses present in the boundary layer. These stresses result in generation of a vortex sheet and consequently a forcing from the boundary layer on the bulk flow. The maximum streaming velocity occurs at the boundary layer edge.

- For a membrane with 2 dimensional motion, there is a further contribution to the streaming. Our model however does not include this 2D BM motion.

3.3 Dimensionless Parameters

Dimensionless parameters are important in fluid dynamics because they give an idea of the regime that the flow is in. This informs us of whether or not the assumptions we made in order to derive the equations which govern the flow are correct. There are two dimensionless parameters which are of interest here. The first is the Reynolds number, the ratio between inertial and viscous effects:

$$R_e = \frac{U_{max} L}{\nu} \tag{3.59}$$

where L is a typical length-scale, taken to be the height of the channel: 0.5 mm. For a pure-tone stimulation of 20 kHz at 80 dB SPL, the value of U_{max} is 2×10^{-4} ms^{-1} and the kinematic viscosity is assumed to be the same as water. As expected for an incompressible viscous, laminar flow the Reynolds number for the cochlea is small and here its value is 0.125, agreeing with previous calculations, which have placed the value between 0.06 and 1 [50][51][46]. The Reynolds number is interpreted as a measure of the flows resistance to viscosity and low value is expected as it implies that the effects of viscous damping in the fluid are important. The second parameter of interest for oscillatory flows is the Strouhal number, defined as:

$$S = \frac{fL}{\tilde{U}} \tag{3.60}$$

and is the ratio of the oscillation and mean speeds, $\tilde{U}$, with f being the oscillation frequency and L the characteristic length, as above. A high value of S is expected in this case, as we have a high frequency system with a relatively slow flow. Indeed, for the same system as above, we find that $S \approx 10^5$, again agreeing with previous investigations [50].

Chapter 4

Computational Fluid Dynamics

4.1 Setting up the Problem

Many factors must be considered when undertaking the creation of a new CFD simulation. In this chapter, the process of creating, testing and using the CFD simulation is described.

The simulations were used for all results and hypothesis testing once the realistic wave forms had been generated. All simulations were done in OpenFOAM, an open source software run from the Linux terminal and written in C++. The software is powerful due to the fact that every piece of the code is fully user manipulable meaning that the user has full control over the entire computational process, from the equations of motion and turbulence models to implementation of geometries and boundary conditions.

It is compatible with the paraView software for visualising the flow, and all figures involving direct simulation output were generated using this software.

All simulations were run on a discrete mesh, and finite difference schemes used for the spatial and temporal derivatives. There are several factors which determined the size and scale of the spatial and temporal discretisation.

4.1.1 Mesh Size and Timestep Considerations

The initial mesh was tested for convergence using increasing spatial resolution. The aim of these initial tests was to confirm that the velocity and pressure fields in the domain were independent of the mesh used. This gives a "lower limit" on the mesh resolution: a coarser mesh will not give valid results. Once this limit is determined, there are three factors which influence the choice of mesh resolution:

- The amplitude of the travelling waves along the basilar membrane surface. There must be enough mesh points along the BM surface in order to accurately capture the shape of the wave. For this consideration, the more points defining the membrane, the better the wave resolution.

- The stability of the mesh due to the dynamic mesh changes. The motion of points on the membrane drive the motion of all local points through the implementation of a dynamic mesh. Large deflections using a coarse mesh will lead to deformation of cells which causes poor derivative calculations. The mesh must have the correct refinement near the surface as a result of this constraint

- The stability of the mesh due to the speeds present in the system, parameterised by the Courant-Friedrichs-Lewy number, C_o. This is the ratio of the maximum speed present in the domain and the speed of propagation across a cell. This determines the stability of the simulation and is very important in this case where we need to track particles over very small displacements.

The first two points were found to be resolved fairly naturally as a result of the final, stronger restriction. The Courant-Friedrichs-Lewy, or CFL constant, was described by the authors in their work on the discretisation of partial differential equations (PDEs) [52]. It describes the necessary condition for the PDEs to converge, namely that the time taken for a wave to propagate across a cell must be larger than the timestep. Hence the timestep and grid size choices are not independent of one another. The condition for convergence is that

$$C_o = \frac{u_{max}\Delta t}{\Delta x} \leq 1 \tag{4.1}$$

The cell velocity, $u_{cell} = \frac{\Delta x}{\Delta t}$ is therefore fixed by the maximum magnitude of the fluid velocity, u_{max}. This gives a first estimate of the way in which we need to set the spatial and temporal timesteps. The next step is to ensure that the timestep can capture the frequency we want to stimulate. A range of frequencies were required and initially, 5 kHz to 20 kHz were chosen. In order to capture very highly resolved particle paths, a sample rate of 10 steps per cycle was selected. This set the timestep at values between a maximum of 2×10^{-5} s for 5 kHz to a min value of 0.5×10^{-5} s for 20 kHz stimulation.

4.1.2 Dynamic Boundary Implementation

Often, cochlear CFD models use a fluid structure interaction to simulate the flow [53] [54] [55] [56]. The structural properties of the BM would be encoded and then an oscillating pressure field caused by an oscillating wall in the basal side of the channel would cause the pressure difference between the top and bottom channels, resulting in a travelling wave across the membrane. In order to simulate this entire process, a fluid structure interaction (FSI) is required, something which is computationally difficult and expensive. Instead, the method elucidated here removes the need for an FSI. By using MATLAB to numerically solve Eq. 3.38, the solution is found at every timestep and a matrix generated with each row corresponding to the full set of coordinates for the BM deflection at time timestep. This information is then used as an input to the CFD simulation[1]. Therefore there is an accurate BM wave shape which propagates with the temporal resolution required by our simulation and without the need for the FSI we can drive the flow in the two channels.

4.2 Evolution of the CFD Simulation

The simulation has undergone drastic changes over its lifetime, primarily due to changes in the mesh geometry and generation, and changes in the fluid dynamic solver.

4.2.1 Evolution of the Mesh

Initial work tried to simplify the problem of a double-channelled flow with fluid exchange as a closed half channel flow, the idea being that simulating only half the flow would halve the computational time. It also meant that there was no need to simulate an immersed, dynamic boundary which seemed more challenging at the time. These runs used a rectilinear grid generated by OpenFOAM's built-in mesh generator tool, blockMesh. The edge and bottom walls were static and the top wall (corresponding to the basilar membrane) dynamic: its motion defined by the numerical solution of 3.38, calculated using MATLAB.

Initial successful test cases were run where the left and right hand walls had pe-

[1]This capability was made possible in the early stages of the project by code supplied by Nikola Ciganovic.

riodic boundary conditions applied and the top, dynamic surface supported a simple sine wave. The model was then ran as a closed system, with no slip boundary conditions applied at every wall and the WKB wave along the BM. These half channel closed models resulted in an anomaly in the fluid and pressure fields, attributed to a break down in volume conservation which can be seen clearly in Fig. 4.1.

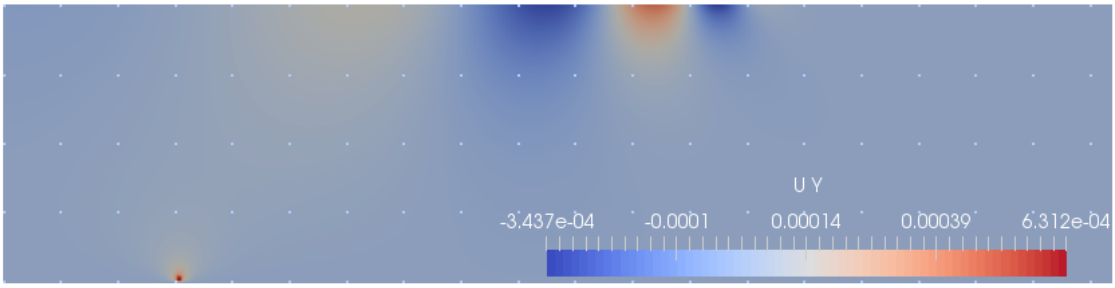

Figure 4.1: Simulation output of the y-component of the velocity field for an 8kHz BM wave, used here to illustrate the volume conservation problems of the half channel geometry. A "singularity" can be seen in the bottom left corner and originates from the fact that the top surface being redefined in a closed incompressible system induces small but important errors in the mass conservation. The field from the surface interacts with this feature at higher frequencies and cannot be ignored.

The top surface deflection is not symmetric and so the integral of the area in the positive and negative parts of the displacement are not equal. Although the deflection of the surface is very small and the mismatch between the integrals also very small, this effect was enough to allow error propagation in the flow and affect the final field. The location of the "singularity" was not dependent upon the frequency the BM was stimulated at. For low frequencies therefore the affect on the flow was negligible, but for high frequencies these flows would interact and affect the result.

To resolve issues of volume conservation and in fact make a more robust, meaningful simulations, the computational cost worries of doubling the domain were set aside, and the entire domain, detailed in Fig. 4.2, simulated. In this way the BM becomes a fully immersed, solid, deformable boundary, implemented numerically by the definition of a "master" and "slave" walls (the top and bottom surfaces of the BM respectively) to which boundary conditions can be applied. The stimulation is in 2D but there is still an extrusion of the 2D geometry, leading to a top and bottom surface of the BM. In this case, the top surface is the master wall and the bottom the slave. The front and back walls of the simulation are "empty" leading to the 2D solution in the end. The two coupled walls are merely the top and bottom face of the basilar membrane. The helicotrema is modelled as an "blank" wall with no solid structure, and so allows for fluid exchange between the top and bottom channel.

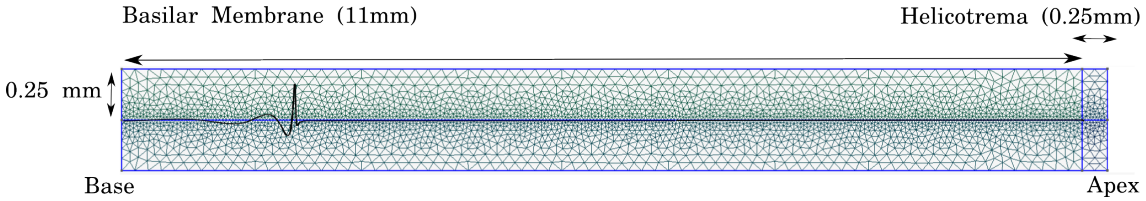

Figure 4.2: Triangular Delaunay mesh created using the Gmsh meshing software. A greatly exaggerated BM surface deflection has been included for illustration. All walls are rigid, and the helicotrema portion of the membrane is open, allowing exchange of fluid between the channels. All boundary walls are static with non-slip conditions applied.

Aside from this issue which related to the fundamental flow fields being unreasonable, there were further issues regarding the particle tracking. Once particles were added into the simulations, these meshes led to very unstable and strange trajectories. It was unclear why this should happen. It was hypothesised that the particle moving across a cell boundary could be redefined as being in another location. However this issue was difficult to understand because the nature of the odd behaviour was quite varied. Sometimes the particle would simply move from one timestep to the next to another location in the domain and carry on with the same trajectory from there. Other times the amplitude of the oscillation would vary suddenly, as if the velocity had discretely jumped. In all cases it was thought that the motion across a boundary must have resulted in a change of velocity due to the discrete nature of the fields, but this was never confirmed. Because the flow has underlying rotation due to the creation of the vortices, it was determined that an unstructured triangular mesh may be better suited to this model, thereby ensuring that on average more cell edges were orthogonal to the flow direction[2] [57]. The mesh was generated using the external software, Gmsh. OpenFOAM has built in capabilities for interpreting the mesh files outputted by Gmsh. Indeed, the results of the simulations after implementing this were much improved, but still required a very small CFL number in order to output stable particle trajectories. Figs. 4.3 and 4.4 show the kind of strange results that would be seen after post processing of the data when the CFL number was below 1, but larger than around 10^{-5}. For clarity a result with only one rogue particle is shown, but for all simulations with a CFL number which was much higher than this value these results were much more common, especially near the BM where there were large velocity gradients.

Updated mesh tests were completed on the new mesh and although coarser meshes were stable and converged, a finer mesh (resulting in a compromise in computational time) was required in order to capture the particle behaviours nicely.

[2]Issues with particle tracking were also related to the solver, which will be addressed in the following section.

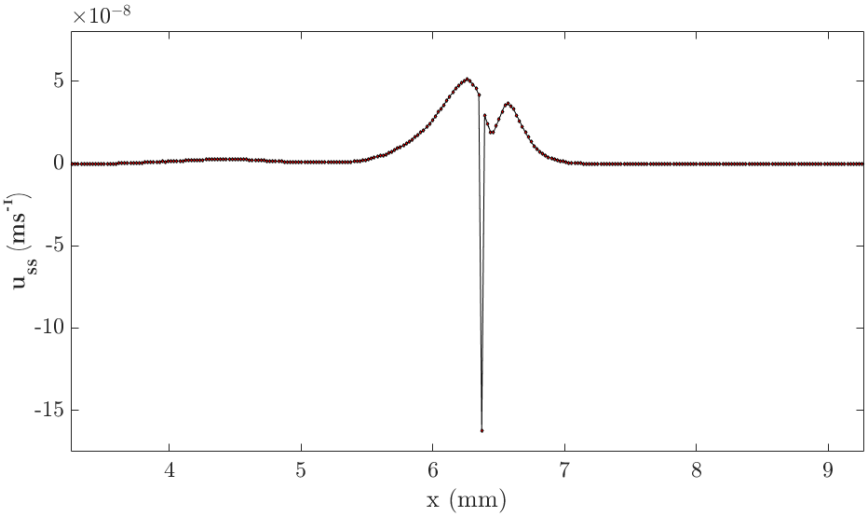

Figure 4.3: u_{ss} for a row of particles injected along the cochlea from the base to the apex. The stimulation frequency was 5kHz. Each velocity value comes from the analysis of the trajectory of an individual particle placed at that location. Particle displacements are very small, so for these timescales (in this example, 12.5ms) we can assume the steady streaming field value to be the value of the particle. Anomalous results such as the one clearly seen here were difficult to handle. The underlying problematic trajectories were not always so distinctive from the normal ones.

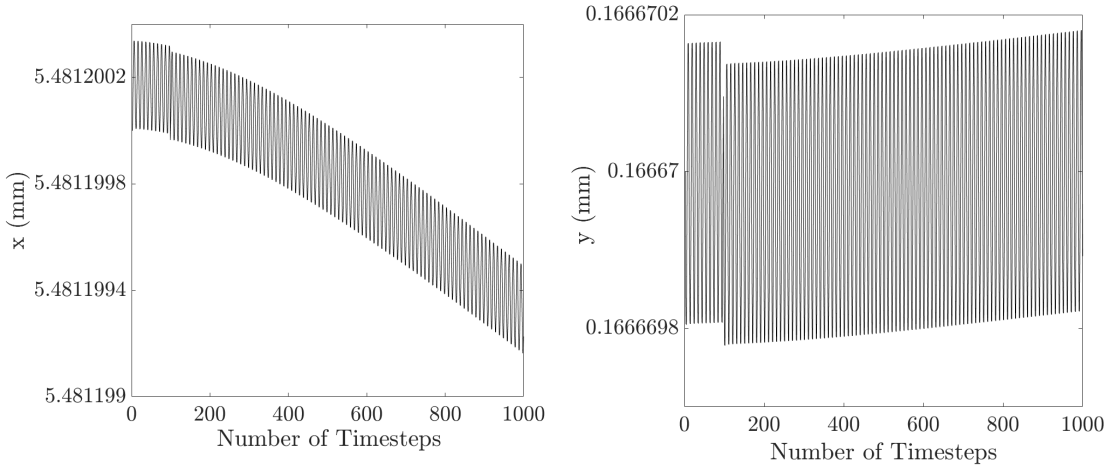

(a) (b)

Figure 4.4: Typical example of problematic particle trajectories. (a) x-trajectory showing the oscillatory behaviour and the translation in the negative x-direction. (b) Problematic particle y-trajectory showing the subtle jump at around 100 timesteps. This discontinuity caused errors in the determination of the steady streaming velocity fields.

After all of these considerations, a mesh with 975 points along the BM (corresponding to a Δx of 1.12×10^{-5} m) was chosen, which satisfied all of the points discussed here. These simulations turned out to be incredibly stable and yielded very smooth results for the particle trajectories: the main goal.

4.2.2 Evolution of the Solver

The cases were run using the homemade solver, BMicoFoam which was originally formed from the creation of a merged pimpleFoam solver and solidParticle tracking algorithms. The problems encountered throughout the CFD were mainly in the particle tracking. Initially pimpleFoam was used to simulate the flow because of its more complete treatment of fluid systems (it has capabilities for both laminar and turbulent flow and so was thought to cater for the fast flow at the membrane surface and the transition to the almost static flow regime far from the surface). Ultimately it was too unstable in this particular context due to its formulation being inherently set up for large timesteps (pimpleFoam is used in larger-scale turbulent flows where the averaged behaviour is more important than that of the small spatial and temporal scales). The problem with this was a CFL number which was too high to capture the particle paths, which would be erratic and disjointed. To overcome these issues, the much simpler icoFoam solver was implemented.

4.3 The BMicoFoam Algorthim

The icoFoam formulation is a transient, incompressible laminar solver, which is required in this case because of our high frequency flow: the timestep should be small enough to fully capture the oscillation of the wave and therefore the trajectory of the particles. It also keeps the full Navier Stokes equations without such simplifications as neglecting non-linear terms. The steady streaming phenomenon is a consequence of these non-linear terms so they must remain. Its core solver is built around the PISO (Pressure Implicit with Splitting of Operators) algorithm and an overview of its function follows here.

4.3.1 The PISO Algorithm

In all of the simulations that follow throughout this work the fundamental fluid solver was not changed. Instead only boundary conditions (i.e the BM deflection for different frequencies and sound pressure levels) or parameters relating to the particles moving within the fluid (their initial coordinates or injection speed for example) were altered.

Fig. 4.5 shows a general overview of the processes followed by the PISO algorithm in order to calculate the pressure and velocity fields. The algorithm begins by

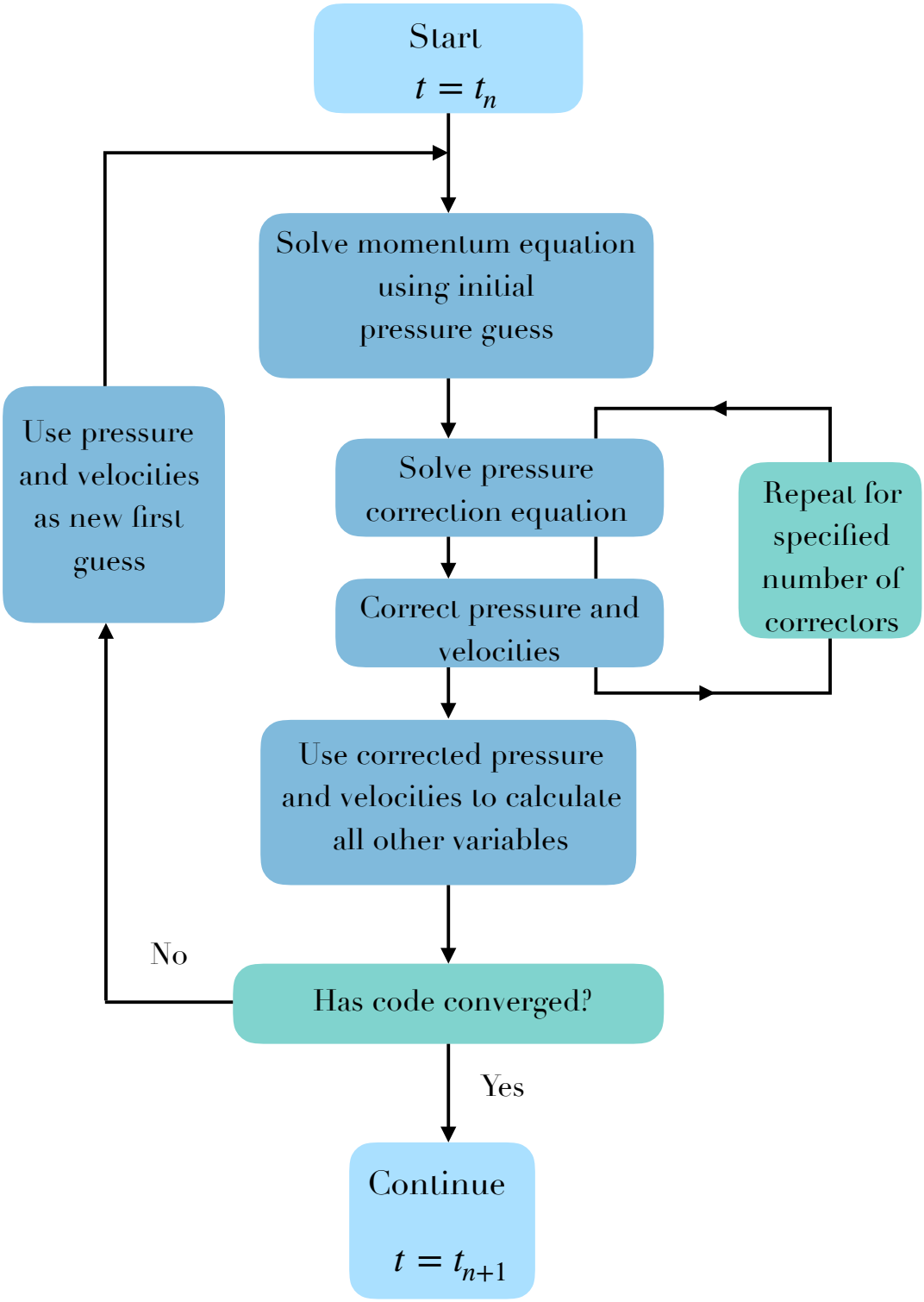

Figure 4.5: The PISO algorithm simply explained. The algorithm relies on a few "corrector" steps. Once an initial guess for the pressure field is made, the equations of motion are solved under that first restriction. They are then corrected and this process repeated for as many times as the user specifies, in our case only twice. Then the remaining fields are determined from these calculations of the pressure and velocity fields. A convergence test is done and if successful the next timestep is calculated. If the fields have not converged the process is repeated from the equation of motion this time, with the improved estimates now used as the first guess.

choosing a "guessed" pressure field and using it as an input to solve the discretised momentum equations. The backwards Euler (implicit) scheme is used for all time differentials. In simplified terms, if we have a differential equation for a velocity, u:

$$\frac{du}{dt} = f(t, u) \tag{4.2}$$

the backwards Euler scheme determines the value of u at a certain timestep, i for a timestep of size Δt through

$$u_{i+1} = u_i + hf(t_{i+1}, u_{i+1}) \tag{4.3}$$

The method is implicit because it relies on information from the next time step in order to calculate the information for the time step that precedes it. Spatial derivatives are found using the Gauss linear scheme, a finite volume method. In this scheme, the field values for a cell are evaluated using the cell centre as the node, illustrated in Fig. 4.6.

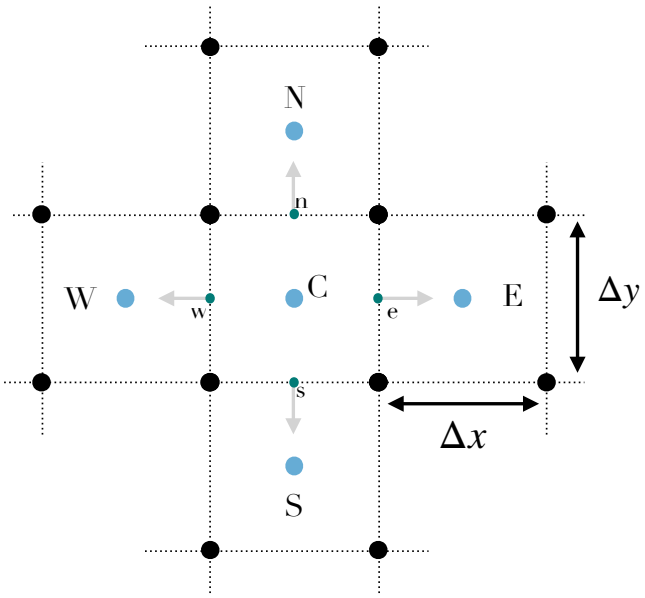

Figure 4.6: The values for the variables are calculated by taking the nodes to be at the centre of the cells, denoted by the capital lettered labels (blue points). The dotted lines show the grid points of a Cartesian grid and so black dots correspond to the cell corners. The face centres are indicated by lower case labels and the arrows show the direction of the outward facing normal, necessary when using the divergence theorem to form the surface integrals.

The Gauss linear scheme refers to the method of volume integration (Gaussian), the method of discretisation of the domain (central differencing defines values at the cell centres, as opposed to face centres) and the fact that linear interpolation is used

for calculation of diffusion coefficients, in this case, merely the viscosity, ν.

The pressure is then recalculated using a pressure corrector equation, after which the disparity between the velocity and pressure fields is determined, and used to re-correct the fields. The PISO algorithm allows the user to repeat this stage up to 4 times: this work found 2 to be sufficient. Once the velocity and pressure fields have been found, any remaining fields (such as temperature) are calculated from their corresponding equations, using the pressure and velocity fields as input. A convergence test is then completed, according to a user defined input for the tolerance of the residual. The residual of the particular solution is just the difference between two iterations of the solution, and if this value falls below the specified tolerance the system is said to have converged and the simulation moves on to the next time step, and so on until all timesteps have been calculated. The tolerances used in this work are 10^{-6}Pa for the pressure fields and 10^{-5}ms^{-1} for the velocity fields.

4.4 Particle Tracking

OpenFOAM has a somewhat built in capability for particle tracking. Initially this analysis was attempted using the post-processing tools supplied with paraView to insert tracer particles into the pre-calculated flow. This was prohibitively slow however and not very elegant to implement. Instead, the particle tracking was written into the solver so that the coordinates would be calculated at every timestep during the simulation run. In order to achieve this, the work of Aurélia Vallier from the Chalmers Institute of Technology was followed [58], and updated to account for significant software update since its time of writing. The particle tracking works by defining the injection coordinate and speed of particles in the domain, as well as their size and density, and then the forces acting upon each particle as a result of the pressure field in the flow are applied to each particle resulting in particle displacement at each timestep. In all simulations, a set of 5000 particles spaced evenly on a grid covering the entire bottom channel (Fig. 4.7), were injected at the first timestep and their trajectories calculated throughout the run. In this way then, only the initial coordinate of the particle needed to be supplied through the use of the particleProperties dictionary.

Further to the properties already mentioned, there are also two more dimensionless parameters which need to be defined: the restitution ratio and friction coefficient. The restitution ratio is a parameter which controls the way in which the

Figure 4.7: An example of the paraView output, here showing the x-component of the fluid velocity field at an instant in time. The particles are injected in rows which fill the bottom half of the channel.

particles interact with each other/boundaries in the simulation. In the implementation used here, the simplest coupling between particles was used. The argument for this decision comes from exploration for the velocity fields due to the membrane. It became clear that the flow is so small that the flow is laminar and we can safely say for small sound pressure levels that no mixing occurs and so particles are very unlikely to collide. For those that do, the effects are so small that it was not considered worthwhile to implement a more complicated particle coupling. The restitution ratio, e is defined as:

$$e = \sqrt{\frac{KE_{before}}{KE_{after}}} \tag{4.4}$$

where "before" and "after" are in reference to a collision between another particle or a solid boundary. The friction coefficient is added so that the particles can be seen as separate to the main fluid. A small value of 0.001 was used in this case so that the particles are separate to the fluid but do not interact strongly.

In summary: the simulation uses an unstructured, triangular mesh, whose cell size is a result of numerical stability and wave amplitude constraints. The timestep is determined by the frequency of the waves simulated. The numerical scheme uses an implicit Euler method of the time differentiation, and a discrete volume Gauss linear scheme for the spatial differentials. All walls are impermeable, the bounding walls are also static. The BM is modelled as an immersed dynamic boundary, whose motion is a result of a redefinition of its coordinates at each timestep. These coordinates are supplied externally through a set of matrices generated by numerical solution of the wave equation detailed in the preceding chapter. Finally, particles with a simple coupling and with an almost elastic collision model are injected at zero velocity into the domain according to a set of coordinates such that all of the domain volume is filled and the steady streaming velocity can be extracted from the coordinates of the particle trajectories. The table below summarises all parameters used in the CFD simulation. The fvSolutions and fvSchemes dictionaries which contain all of the information pertaining to the numerical solution implementation

in OpenFOAM are included in the appendix.

Parameter	Symbol	Numerical Input Value	SI Unit
Fluid Density	ρ	1000	kgm^{-3}
Fluid Kinematic Viscosity	ν	10^{-6}	m^2s^{-1}
Particle Diameter	dP	0.2	μm
Injected Particle Density	ρ_p	1000	kgm^{-3}
Coefficient of Restitution	e	0.95	n/a
Friction Coefficient	μ_P	0.001	n/a
Particle Injection Speed	UP	0	ms^{-1}

Table 4.1: Parameters used in the CFD simulation for the cochlear channel, including those of the fluid itself, and the injected particles.

Chapter 5

Results: Pure-Tone Stimulation

The following chapter presents a subset of results obtained from the OpenFOAM simulations. In total, 18 simulations were run, covering a range of frequencies (5, 8, 10, 15, 18, 20 kHz) at each SPL (60, 80 and 100 dB). In each simulation 5000 particles were injected throughout the bottom half of the domain, and their motion tracked throughout the simulation. Throughout the following, the steady streaming velocity is $\underline{u}_{ss}(x, y) = (u_{ss}(x, y), v_{ss}(x, y))$. Simulations were undertaken on a HP EliteDesk 800 desktop machine (8 core, 32GB RAM). Each simulation of 20000 timesteps took around 30 hours to complete.

5.1 Post Processing

The aim of the analysis of the data from the simulations is to find the steady streaming velocity of the particles injected into the field. OpenFOAM gives an output of the coordinates of each particle at every timestep of the simulation, and these coordinates were read into MATLAB. We know that due to steady streaming the particle trajectories map out spirals, which means the x and y-components of the motions will be oscillatory, with one full oscillation per BM wave cycle. By ensuring that the timestep was small enough (10 timesteps per cycle), we captured these oscillations very well. For a circular trajectory, these oscillations have their centres at the same x-coordinate. However a spiral trajectory translates in x and so mapping the x-coordinate of the centre of the spiral in time should give a line with some gradient. This gradient is the steady streaming velocity and will tend to some constant value as the steady state is reached. All simulations started from both zero particle injection speed as well as zero fluid speed, so some time was needed for the system to accelerate to the steady state. In order to find these gradients, we

implemented the MATLAB smoothing function on the coordinates. The function used a weighted linear least square regression model with a moving average span that was chosen to be 0.5, correspondong the half of the data points at each step of the smoothing algorithm. This means that the span is very wide, which was necessary in order to resolve both the very small changes in the gradients and in order to reduce edge effects. The model further used weighting to scale the value of outliers: reducing a data point's weight if it lay far from the mean. At 6 standard deviations, the data points had 0 weight. An example of the extraction of this information from the raw coordinates is illustrated in Fig. 5.1. It should be mentioned that this is a relatively steep slope, chosen here for illustration so that the spiral centre tracking is more evident.

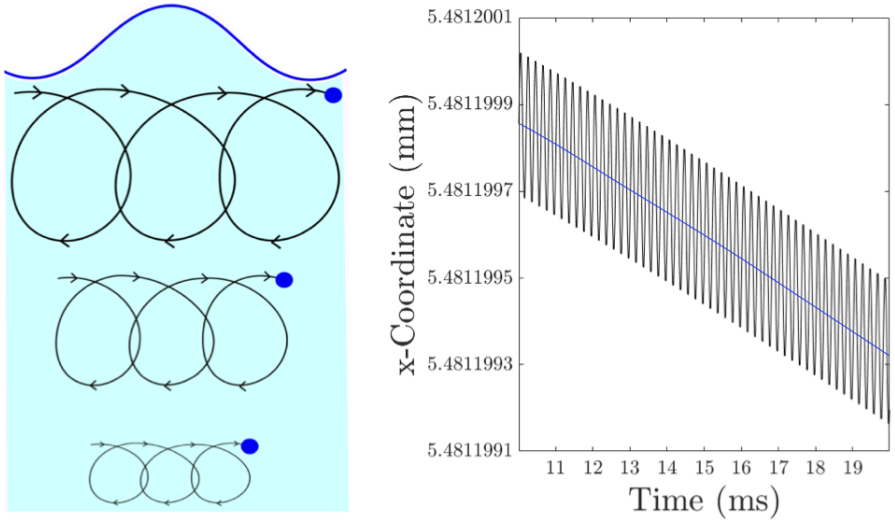

Figure 5.1: The spiral trajectories of the individual particle paths can be decomposed into sinusoidal oscillations in the x and y directions. The zero point of the oscillations are tracked using a smooth function: illustrated by the blue line.

From this example we can see that the gradient of the line mapping the centre of the spiral is very small. The fluid velocities away from the basilar membrane are small and mean that within a single cycle the particle's translation is very tiny. Significant particle translation is only possible over large timescales. For all the following results, the zero line tracking was completed using 20000 timesteps. This timescale was chosen because it was long enough to ensure the steady state was reached, and also supplied the smoothing function with enough information in order to calculate the gradients accurately. For every separate simulation, convergence tests were undertaken for this stage of the post processing to ensure that the streaming velocities had reached their steady state.

The convergence tests also served another purpose: to define an upper limit on the timescales used. As well as ensuring that enough information was available in order to capture behaviours, it was important that not too many timesteps were used. The reason for this comes from the way in which we present the data: as a steady streaming field. The particles were injected in a grid formation and their streaming velocity after 20000 timesteps were then used as the approximate value of the streaming field at their injection point. This is only an approximation because the particles do not remain in a singular point throughout the sound stimulus, but it was found that for small enough timescales and for a large enough number of particles, this approximation is valid. The more particles, the higher the resolution of the streaming field and so the better the approximation of a smooth field from the discrete values.

Finally this process was followed for both the x and y-components, and their respective steady streaming fields determined. With these velocity components, it was also possible to create a vector map of the steady streaming flow, using the symmetry of the system to present the top channel results as well. These plots reveal a pair of counter rotating vortices in the top and bottom channel.

To summarise:

- The particles were injected into the fluid domain according in the geometry of a grid, using 10 rows of 500 particles in the bottom channel. The simulations then run for 20000 timesteps.
- After the simulations had run, the coordinates of the particles at each timestep were read into MATLAB for analysis.
- This analysis began with the use of the smooth function, which effectively traced out the centre point of the oscillations of the x and y -coordinates respectively (see Fig. 5.1) for each particle in the domain.
- This so-called "centre line" has a gradient corresponding to the steady streaming velocity.
- We defined the steady streaming field by assigning the particle's streaming velocity to the location in the field at which is was injected, thereby creating a velocity map of the entire domain. Using the symmetry of the system to also display the top channel streaming fields and vector maps.

In the sections which follow, the velocity component maps and vector plots for 10 kHz and 20 kHz frequency stimulations are presented at each SPL.

5.2 Results: 60 dB SPL

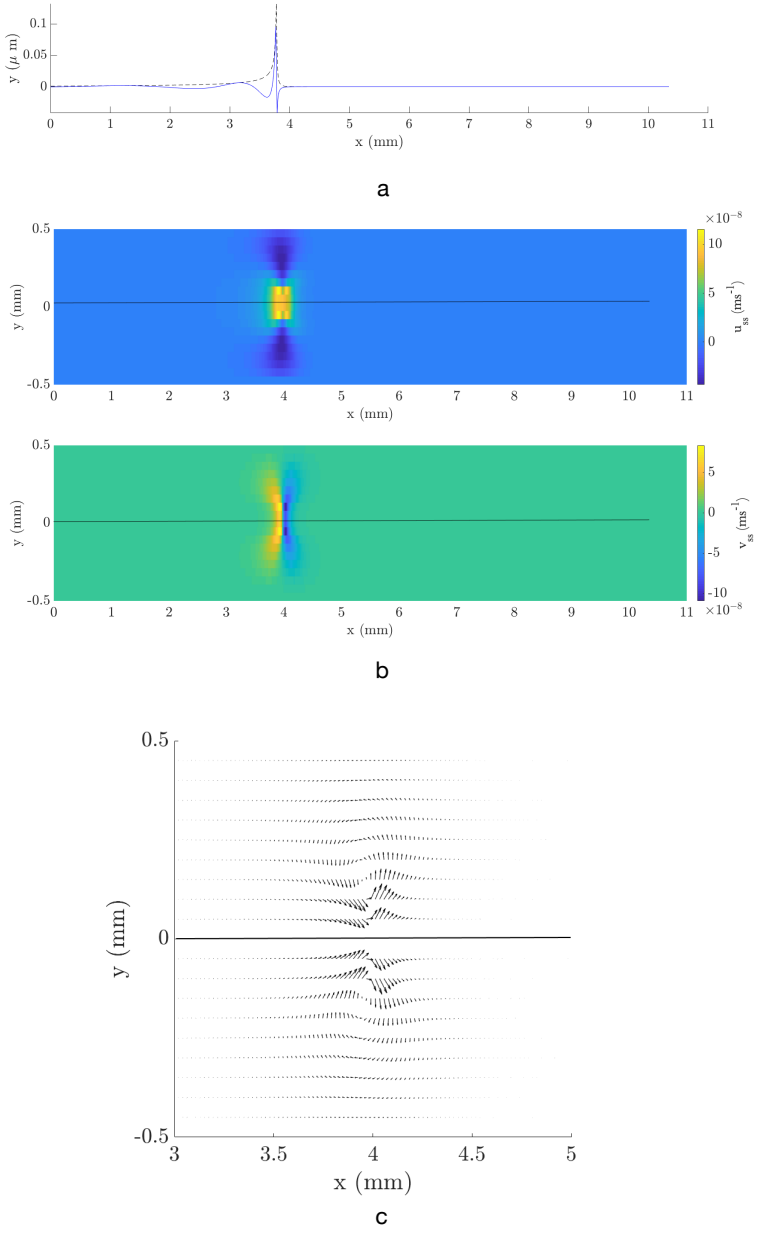

Figure 5.2: a) Travelling wave shape and envelope at 60dB SPL with a 10kHz pure tone stimulation. b)Resulting u_{ss} and v_{ss} fields after 20000 timesteps. The black line at $y = 0$ indicates the location of the basilar membrane. Note that the region closest to the membrane is an interpolation of the streaming fields, due to problems with particle tracking inside the boundary layer. c) Vector field around the characteristic place, showing that there is a recirculation zone which particles move within.

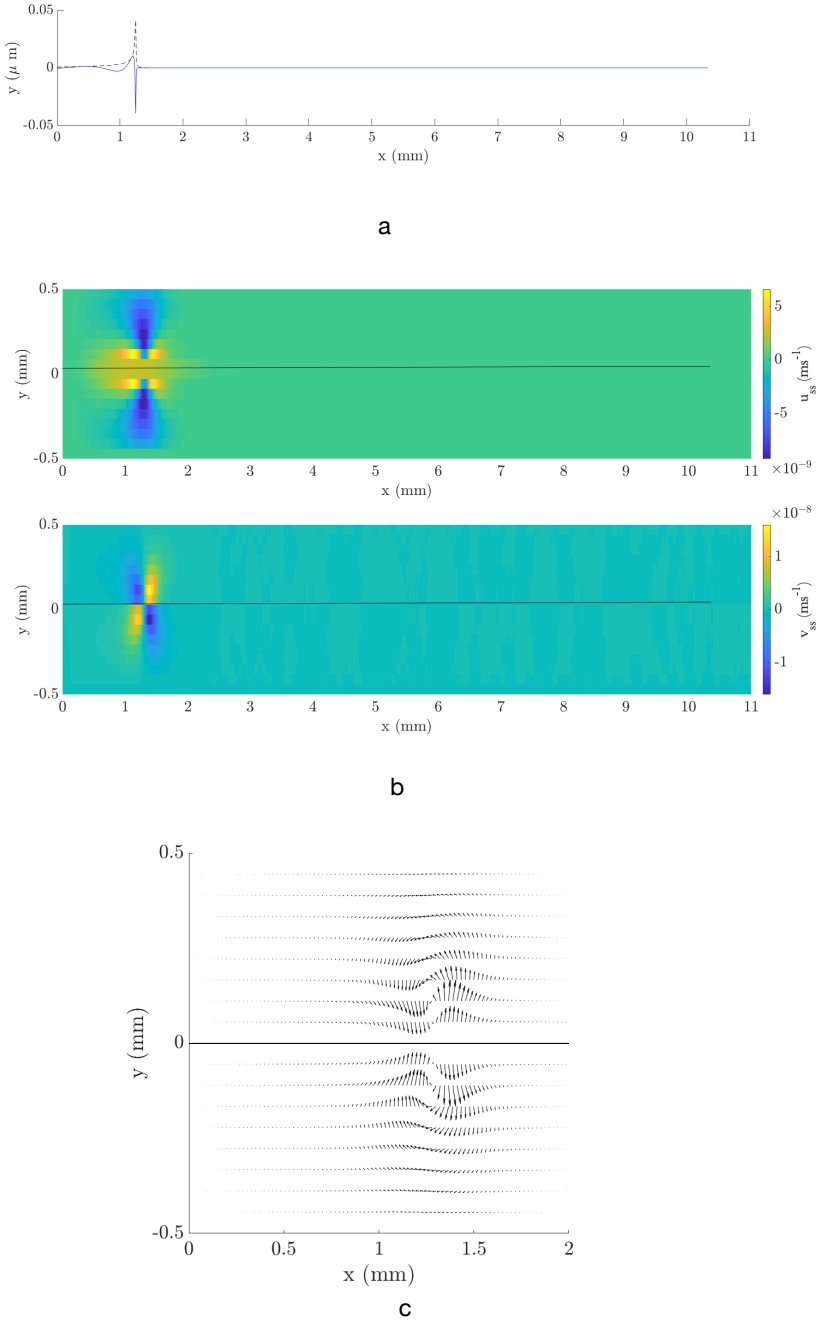

Figure 5.3: Same as previous figure, except at 20kHz stimulation.

5.3 Results: 80 dB SPL

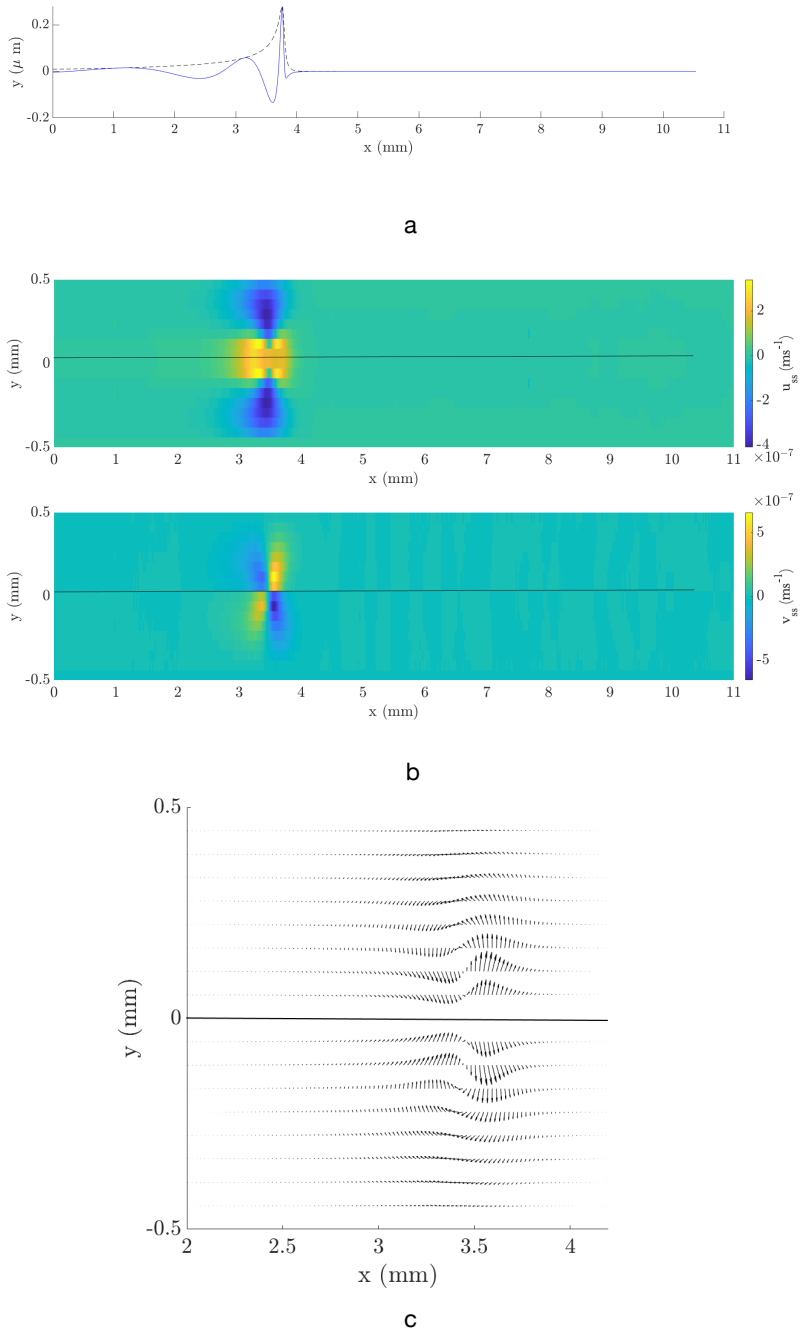

Figure 5.4: Same as Fig. 5.2 at 80dB SPL.

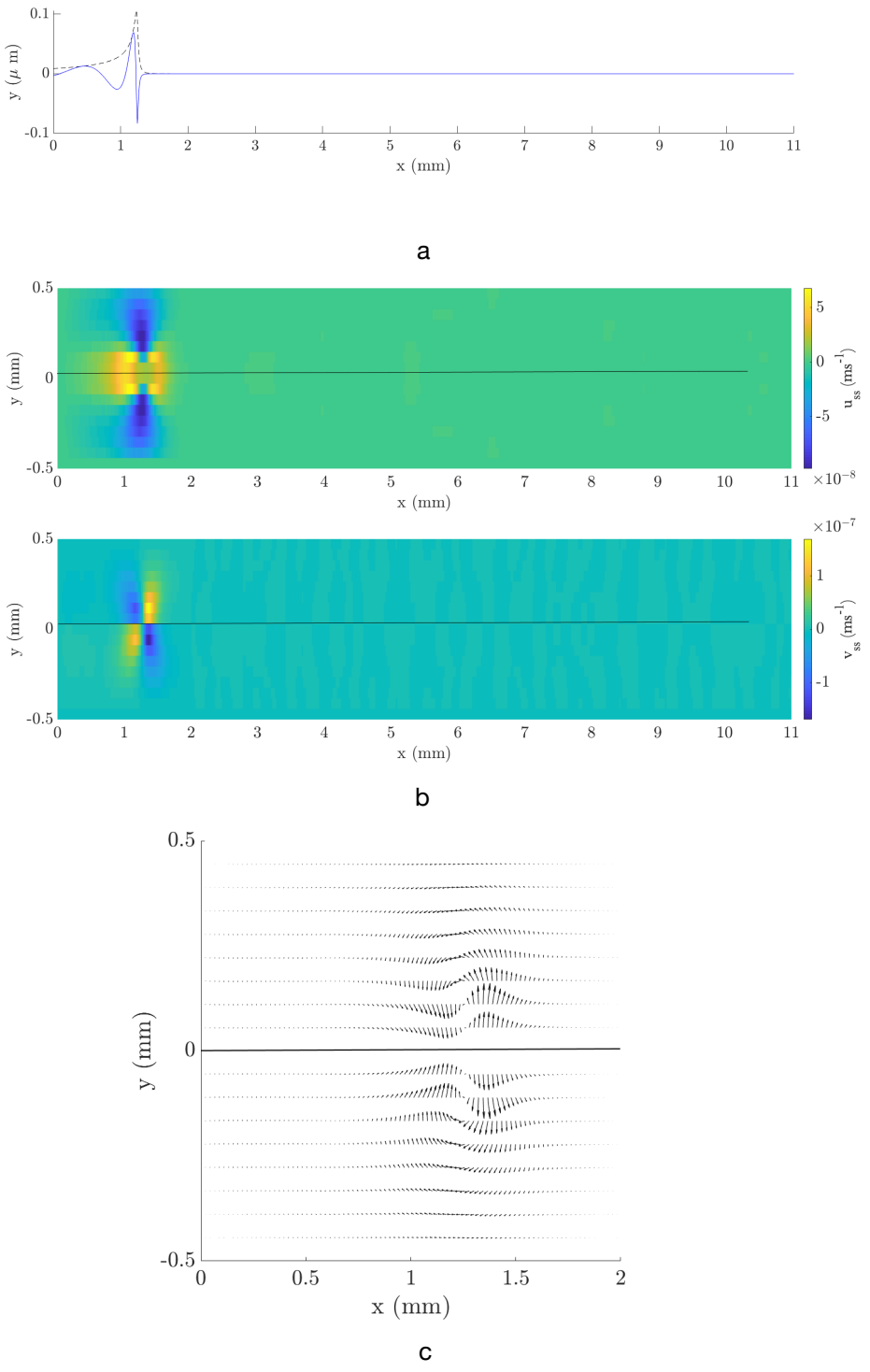

Figure 5.5: Same as Fig. 5.3 at 80dB SPL.

5.4 Results: 100 dB SPL

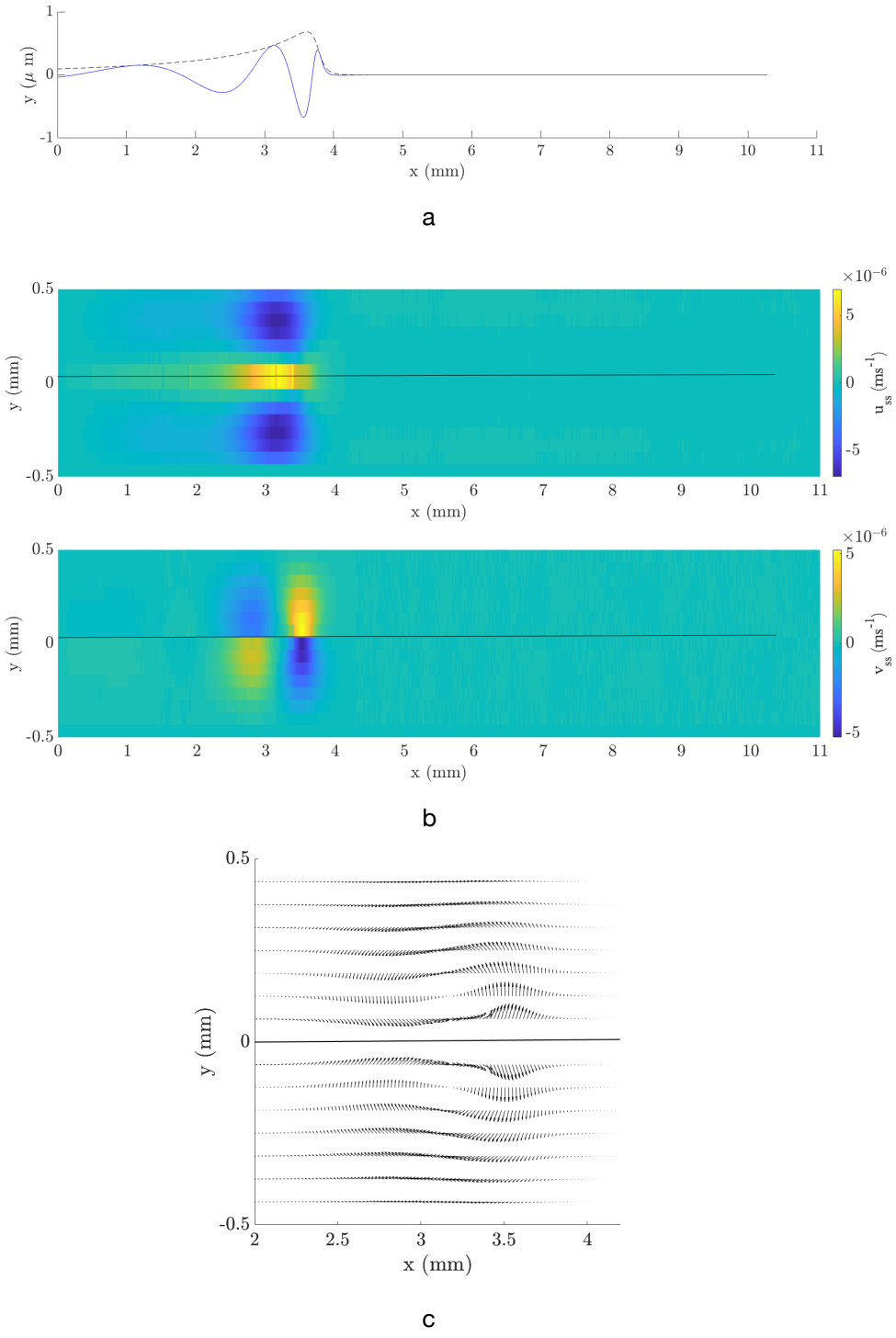

Figure 5.6: Same as Fig. 5.2: stimulation of 20kHz at 100dB SPL.

.

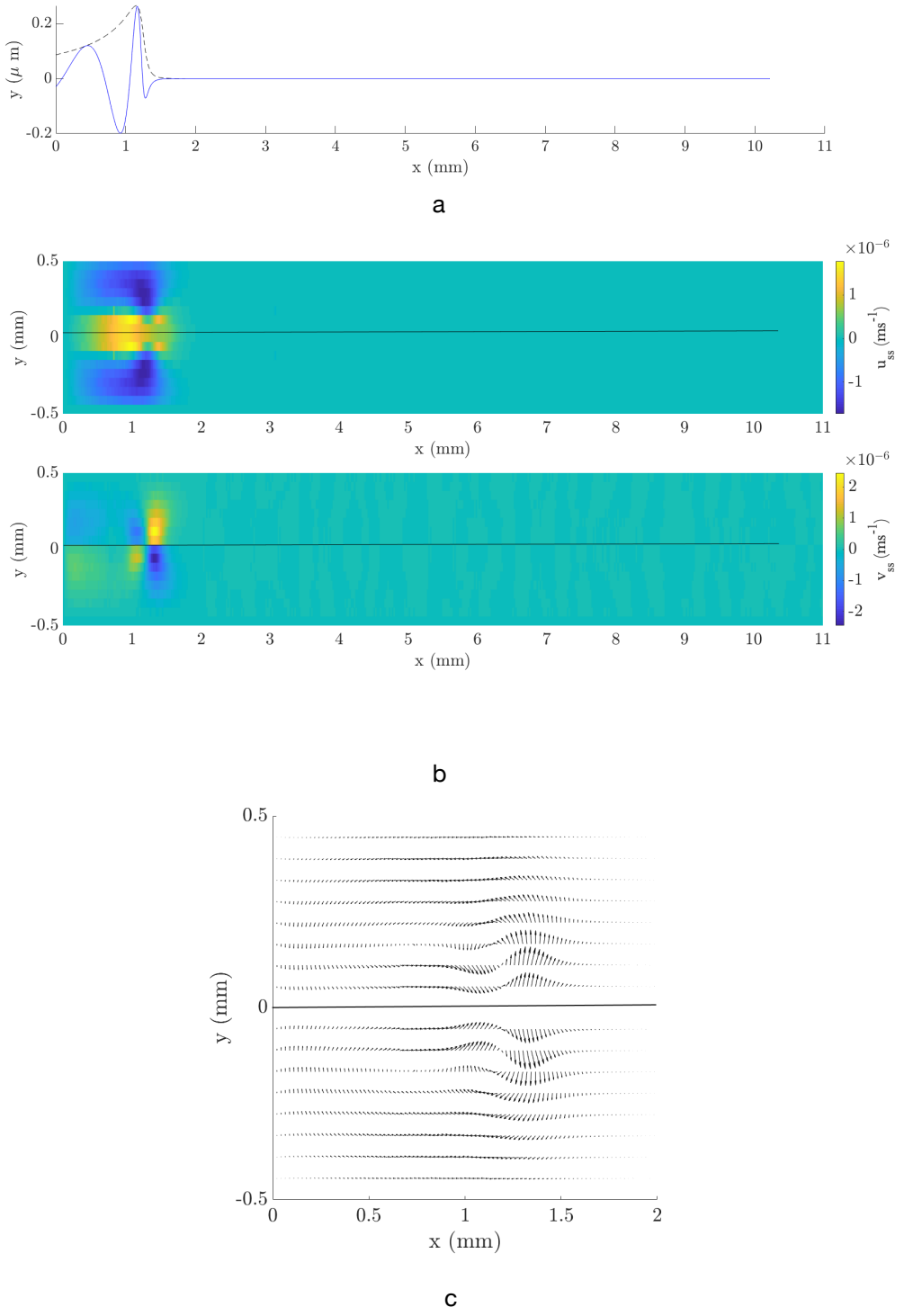

Figure 5.7: Same as Fig. 5.3: stimulation of 20kHz at 100dB SPL.

The separate vertical and horizontal velocity profiles for both the x and y-

components at the resonant location are detailed in the following pages. Following this, Fig. 5.14 then collects all of this information into a comparison to the theoretical prediction.

We also begin to see the boundaries affecting the flow. At 100 dB the amplitude of the waves is large enough such that, at high frequencies, the fluid interacting with the wall changes the underlying streaming field. These effects were not included by Lighthill in his theoretical treatment of cochlear steady streaming, hence we expect some discrepancy between the values found here and those predicted by his work.

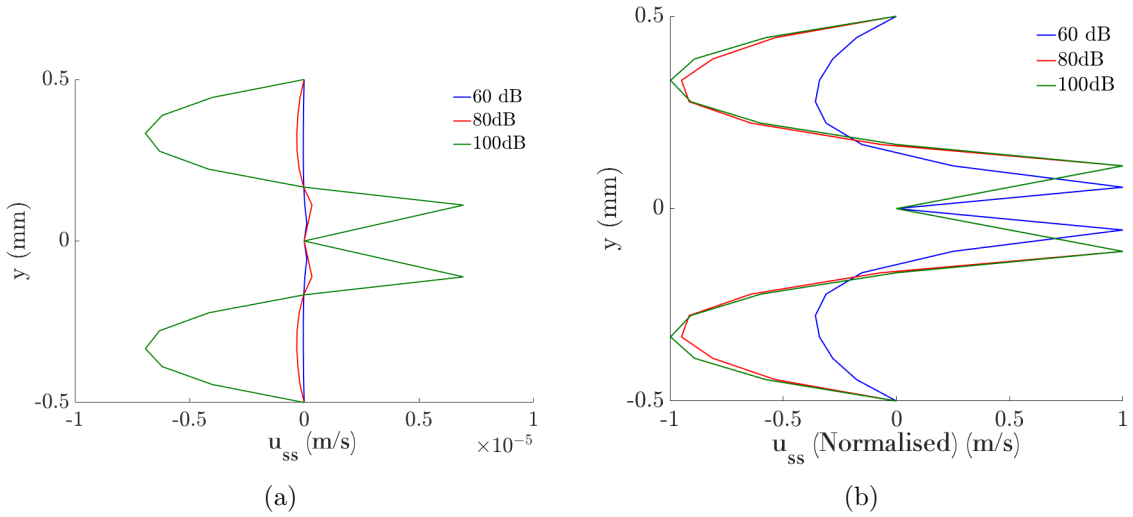

Figure 5.8: (a) Comparison of u_{SS} at fixed x location (the 10 kHz resonance location) for different SPL, showing the increase in streaming velocity from 0 at the BM to a maximum at the edge of the boundary layer and the subsequent decrease back to 0 to satisfy no-slip at the top and bottom walls. (b) Curves are normalised by the maximum streaming velocity at each SPL for comparison. We can see that the larger SPL have a larger depth over which they influence the flow, indicated by the depth at which the inflection point of the curve occurs.

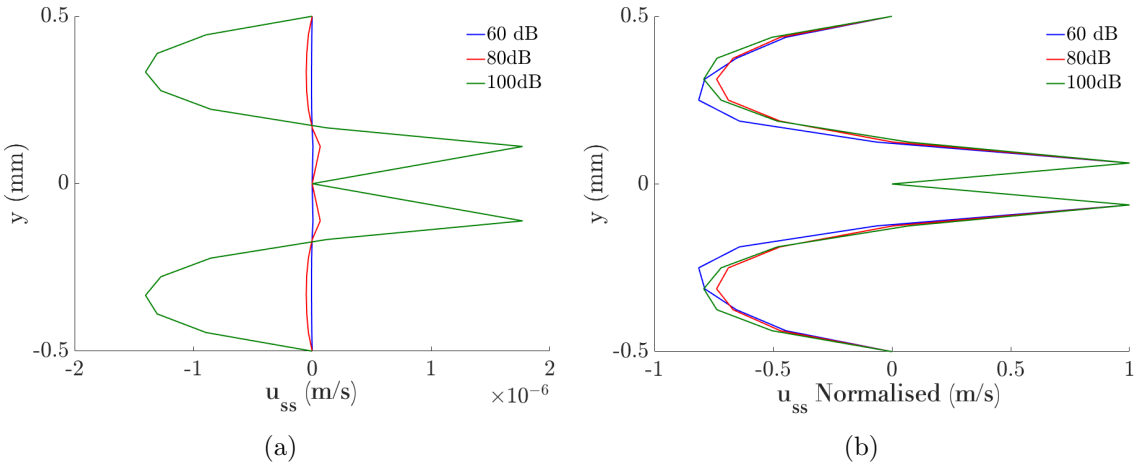

Figure 5.9: (a) Same as Fig. 5.8a but taken at the 20 kHz resonance location (b) Curves are normalised by the maximum streaming velocity at each SPL for comparison.

.

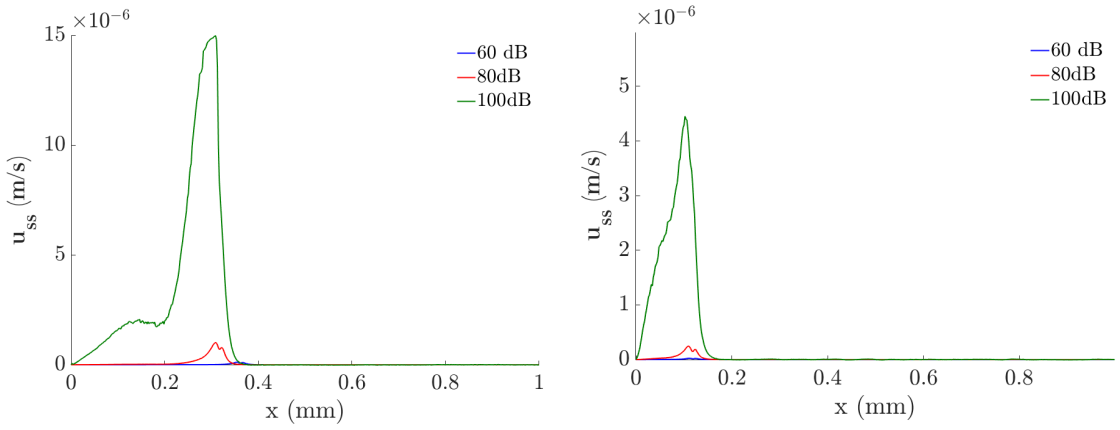

(a) (b)

Figure 5.10: (a) Comparison of u_{SS} at fixed y (edge of the boundary layer) for different SPL. (a) 10 kHz stimulus and (b) 20 kHz stimulus. The influence of the walls on the 100 dB waves can be seen by the spread of the curves.

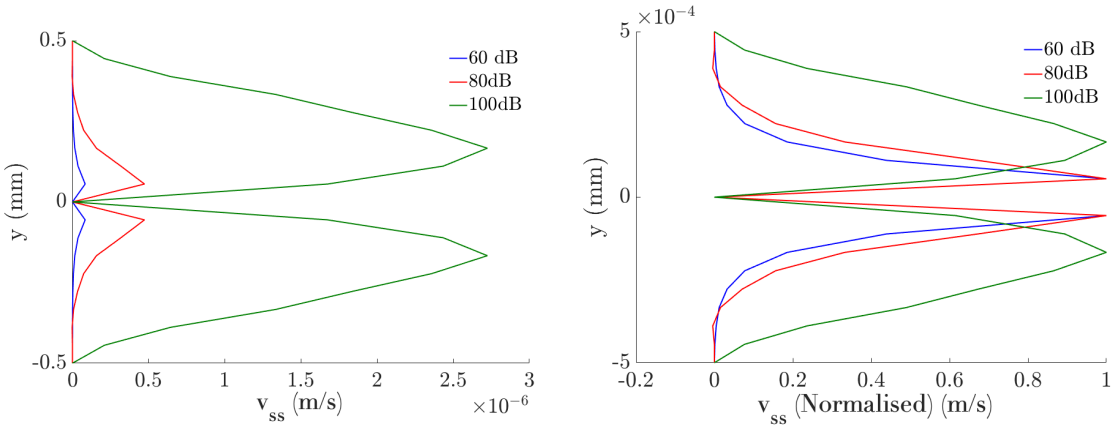

(a) (b)

Figure 5.11: (a) Comparison of v_{SS} at fixed x location (the 10 kHz resonance location) for different SPL, showing the increase in streaming velocity from 0 at the BM to its maximum value at the edge of the boundary layer and the subsequent decrease back to 0 to satisfy no-slip at the top and bottom walls. (b) Normalised curves to better show the detail near the BM across SPL. The SPL increase changes the magnitude of the steady streaming.

.

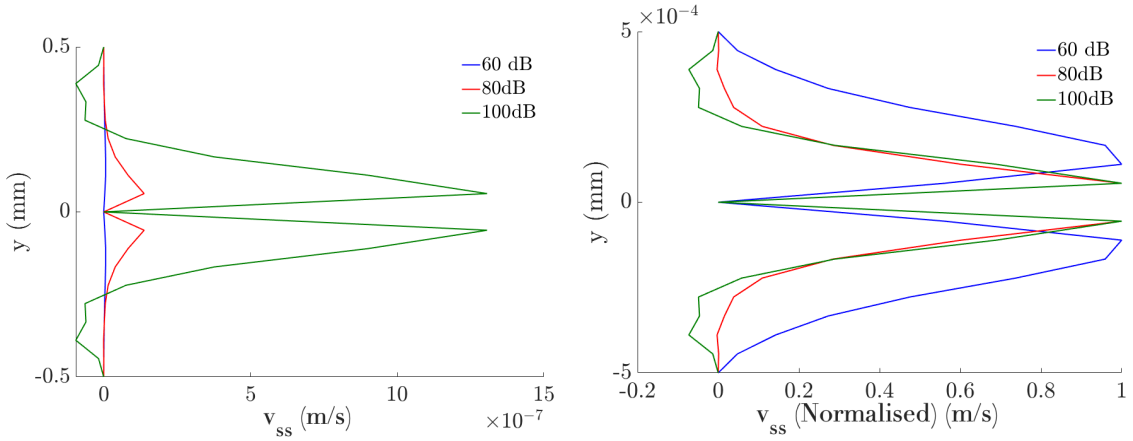

Figure 5.12: (a) Same as Fig. 5.11 but now at 20 kHz (b) Curves normalised by the maximum v_{SS} at each SPL

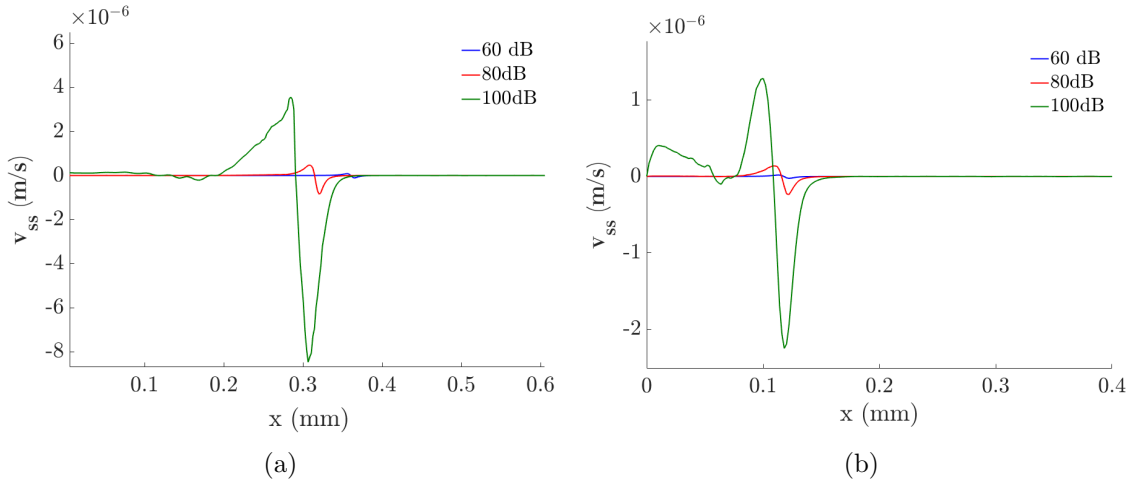

Figure 5.13: Comparison of v_{SS} at fixed y (edge of the boundary layer) for different SPL. (a) 10 kHz stimulus and (b) 20 kHz stimulus. The influence of the walls on the 100 dB waves can be seen by the spread of the curves.

5.5 Discussion of Results

The results are qualitatively sensible, we see an increasing steady streaming velocity near the resonance location, as well as an increase with SPL. Figs. 5.8 and 5.12 shows the vertical velocity profiles for the x-component of the streaming at the characteristic place for the 10 kHz wave. The scale of the streaming increases with SPL as expected, and we can see that the width of the circulation region generated by the pure-tone also increases significantly with an increased SPL, whereas the depth of the eddies remains constant. Fig. 5.13 shows the velocity profile along the boundary layer, close to the BM, and we see the character of the waves is preserved

in the flow: lower SPL have a narrower peak and higher SPL more spread, which explains why the vortices at higher SPL are wider.

The hypothesis of the work was that we could use a changing frequency stimulus in order to drag fluid through the cochlea and target damaged hair cells at a particular site. In order to do this, we need to ensure that the rate at which we change the frequency is optimised such that it matches the streaming rate of the particles. If it is changed too quickly, particles will be "left behind" but if it is moved too slowly the process becomes very inefficient and could be comparable to passive diffusion alone. We use the results from all pure-tone simulations to compare the maximum steady streaming velocity to the predictions of the theoretical model. Fig. 5.14 (a) details the raw simulation output compared to the theory, whereas (b) has employed a shift in order to better match the theory and numerics.

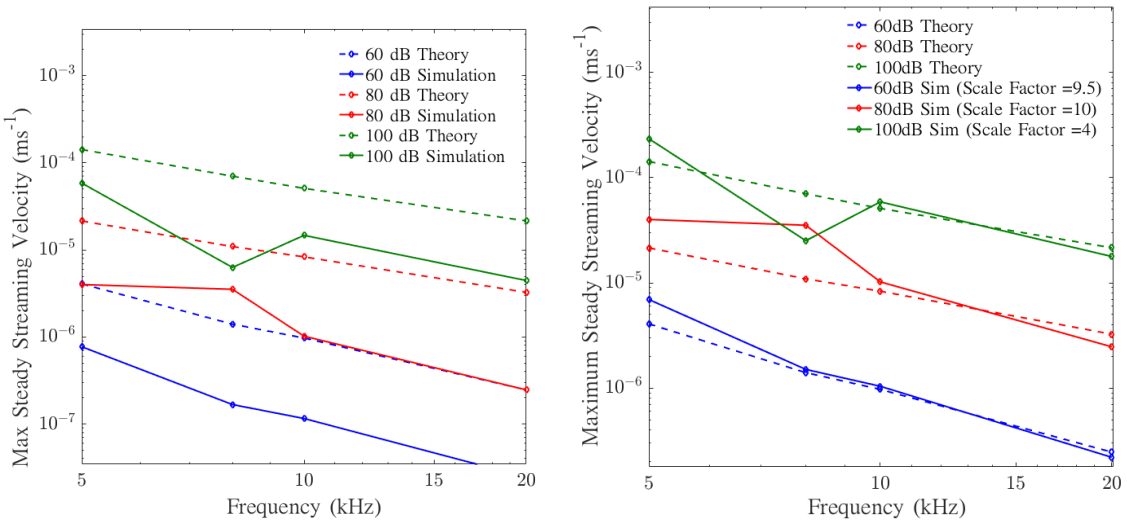

(a) (b)

Figure 5.14: (a) Comparisons between u_{ss} from Lighthill's theory (Eq. 3.54) and these simulations showing a discrepancy in the functional behaviour of the numerics at lower frequencies as well as an offset in the actual values of the solutions. (b) Scaled numerical results compared with the theory, showing that with the use of a scale factor the functional behaviour of the streaming can be reproduced from the simulations.

Here we see that our simulation doesn't follow the correct functional behaviour for frequencies below 10 kHz. Because the entrance to the cochlea is where we are most interested in (for now) and the WKB and steady streaming models are anyway only valid for high frequencies, we decide to only focus on the region down to 10 kHz stimulation. Figure 5.14 shows that for frequencies over 10 kHz, the numerical model and theoretical model agree up to a scale factor. By scaling the numerical results we can find the relation

$$U_{theory} = CU_{num}$$

where C is the scale factor to be determined empirically and U_{theory} and U_{num} are the maximum streaming velocities from the theory and numerical simulation respectively. We can now use the theoretical model to find the sweep rate required to move to a certain location in the cochlea, and the scale factor to convert that into the required sweep rate in the numerical model to get the equivalent motion.

5.6 Frequency Sweep Formulation

5.6.1 Calculating the Sweep Rate

Now that we have the scale factors for each SPL, they can be used to determine the way in which we must alter the frequency in order to move the particles through the cochlea. We can use the analytical expressions (which are now scaled accordingly) to see how much time is required to move from one position in the cochlea to another, if the particles act in the ideal way and move along the cochlea with the resonance peak of the membrane. The ultimate goal is to find the rate at which to change the frequency of the stimulus waves. In order to determine this, the max steady streaming velocity at every input frequency was determined numerically from Eq. 3.58, and through this, the position of the resonance as a function of frequency, ω was found. Fig. 5.15 shows these results, for a frequency range down to 10 kHz and for a SPL of 80 dB. We focus on 80 dB now because it is a reasonable SPL for a patient to listen to for an extended time (100 dB could be too much over longer time spans) but more powerful than the 60 dB which has much slower steady streaming velocities.

Now, using these values, we can determine the time it would take to move a particle from one location to another: necessary if we are to calculate the frequency sweep function, $\omega(t)$. In our discrete setup, we must approximate the velocity between successive frequency resonance locations by taking the average. Then by dividing this average velocity between the spatial distance moved we can estimate the time taken between the two locations. Fig. 5.16 illustrates this point.

Using the variables from Fig. 5.16, where we now generalise using the index i, if the average of the velocities at x_i and x_{i+1} is simply:

$$\bar{v}_i = \frac{v_i + v_{i+1}}{2} \tag{5.1}$$

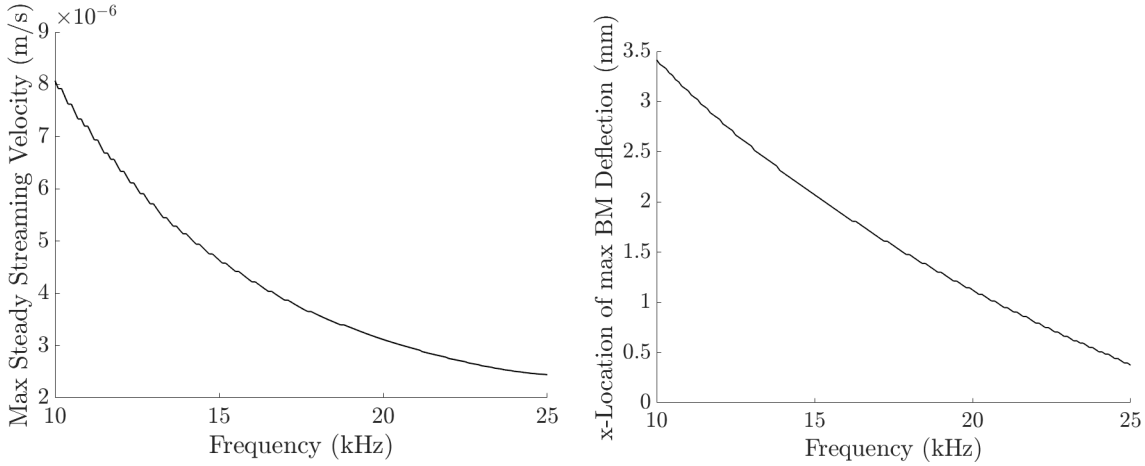

(a) (b)

Figure 5.15: (a) The maximum value of u_{ss} for an 80 dB SPL wave, extracted from numerically solving Eq. 3.58 for many frequencies. (b) The corresponding x-coordinate of the maximum value of u_{ss}.

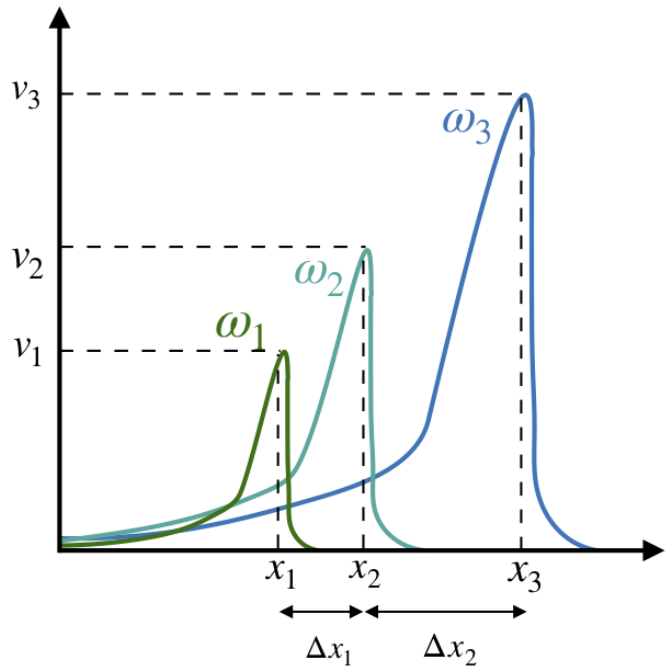

Figure 5.16: An illustration of the variables outlined in the description of the sweep rate calculation. The wave envelopes for different pure-tone frequency stimuli, ω_i have their resonance location at different locations along the cochlea, x_i, with corresponding steady streaming velocities at that location, v_i.

then the time taken to move through the distance

$$\Delta x_i = x_{i+1} - x_i \tag{5.2}$$

is

$$t_i = \frac{\Delta x_i}{\bar{v}_i} \tag{5.3}$$

and the total time, T to move though N steps in frequency is:

$$\sum_{i=1}^{N} t_i = T \tag{5.4}$$

Using this method, the time for the particle to move from the entrance of the cochlea to the 10 kHz position were determined.

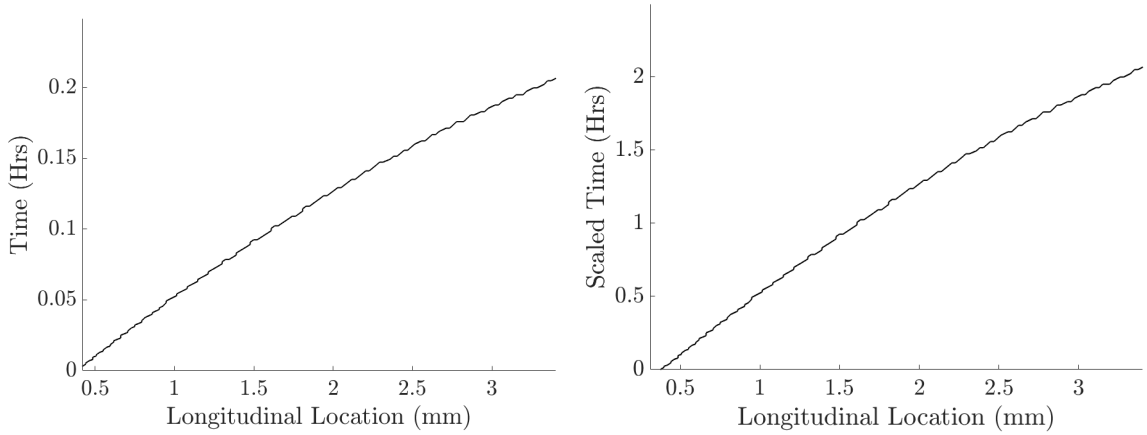

(a) (b)

Figure 5.17: (a) The cumulative time required to move a particle from the entrance of the cochlea to a location along is length. Only frequencies down to 10 kHz have been considered due to the discrepancy between the theoretical and numerical model below that point. This puts the estimate of the time required to move an injected particle from the entrance of the cochlea to approximated 1/4 along its length as 12 minutes. (b) The cumulative time time now scaled by 10 times as given by our numerical results. Only frequencies down to 10 kHz have been considered due to the discrepancy between the theoretical and numerical model below that point. This puts the estimate of the time required to move an injected particle from the entrance of the cochlea to approximated 1/4 along its length as 2 hours.

For a particle to move around 1/4 of the way along the cochlea at 80 dB would take 2 hours. In terms of a therapy this is quite promising, as it is not a prohibitively long time to be sat listening to the stimulus. Of course this timescale increases if we need to reach frequencies much lower than 10 kHz, but an order of magnitude time estimate from simply extrapolating Fig. 5.17b still would leave us with a feasible time-frame: after all a patient could even be under general anaesthetic during the process. The more pressing problem with this timescale is the computational time. From these results, we see that in order to move a particle near the membrane

along with the flow, it is necessary to change the frequency incredibly slowly: a change of 10 kHz across 2 hours corresponds to a change of approximately 1.4 Hz every second. The simulations undertaken thus far have run for 100 cycles of each frequency, ranging from 0.005 seconds of real time (for 20 kHz) to 0.02 seconds (for 5 kHz). The computational time of these runs is significantly larger, with the smallest timescale simulations taking approximately twelve hours to compute. So to even simulate a change of 1 Hz would take a very long time. As well as this, a change of 1 Hz corresponds to a minute change in spatial position: the meshes being used will not be able to capture it. The next logical step would therefore be to reduce the mesh size to a scale which enables the behaviour to be resolved, which in turn means a reduced timestep in order to keep the simulation stable. It was therefore decided that simulating the sweep at these amplitudes would be prohibitively slow, as we would require a nanometre resolution in the mesh in order to sweep slowly enough to affect the particles.

5.6.2 Scaling Solution to the Problem

The steady streaming velocity is related to the square of the membrane amplitude, so increasing the wave amplitude means we increase the lengthscales over which particles travel in a certain time. The problem with increasing the SPL and forming realistic waves for simulations is that the method must be suitable for therapeutic purposes: the method is useless if it works only for SPL which themselves cause hearing damage after sustained delivery. To overcome the problem of computational time, we have scaled the wave forms for an 80 dB stimulation (a reasonable SPL for a patient to listen to for a sustained amount of time) by 300 times, corresponding to a 129.5 dB SPL in loudness. By keeping the shape of the envelope of the wave the same as 80 dB, we can find the streaming velocities and scale them back down (time scales at 129.5 dB SPL are therefore 90000 times faster than at 80 dB with the same physical behaviour). In this case, because the amplitude of the waves (and therefore the speed) was much increased, the mesh resolution also changed to keep the simulation stable. Specifically it was reduced by a factor of three, such that $\Delta x = 3.36 \times 10^{-5} m$). Figs. 5.18a- 5.19b show the much higher speeds and therefore smaller timescales now required for the same displacement of the injected particles. The analyses undertaken for pure-tone stimuli at the beginning of this chapter were repeated to find the scaling for the 129.5 dB SPL waves. This scaling was found to be 15.

This now means that a sweep of 10 kHz takes place at a rate of 5 kHz per second.

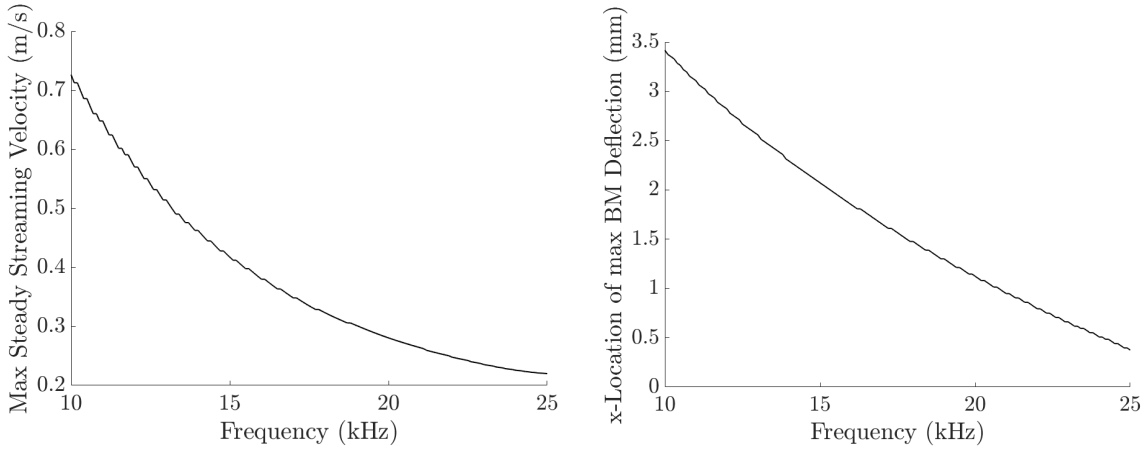

(a) (b)

Figure 5.18: (a) The maximum value of the u_{ss} for an 129.5 dB SPL wave, extracted from numerically solving Eq. 3.58 for many frequencies. (b) The corresponding x-coordinate of the maximum value of u_{ss}.

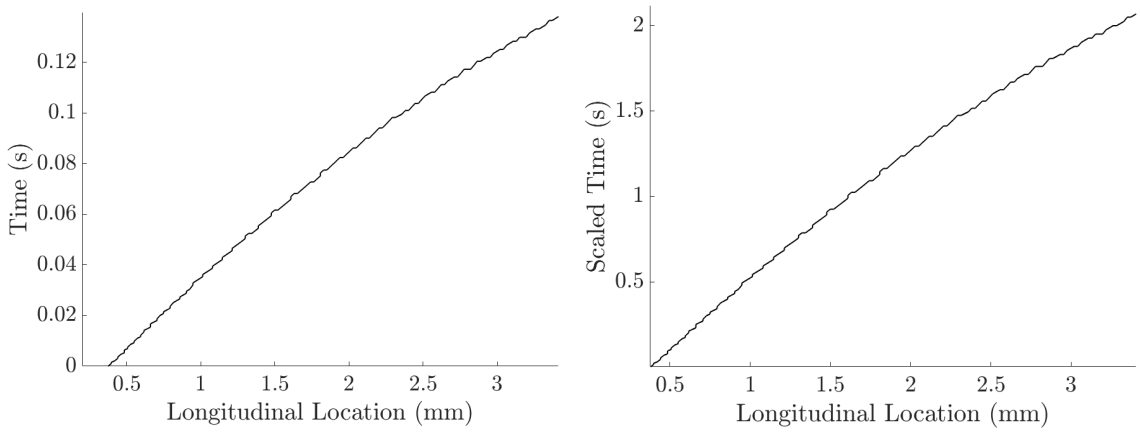

(a) (b)

Figure 5.19: Same as Fig. 5.17 but now scaled as described. (a) Now a particle takes only takes 0.12 seconds to move 1/4 of the length of the cochlea. (b) The cumulative time time now scaled by 15 times as given by our numerical results. A particle now takes 12 seconds to move 1/4 of the length of the unrolled cochlea.

These scales are much more manageable now, as even a small timescale will still translate particles over a significant distance which the mesh can easily resolve. In order to simulate the changing frequency input, the frequency sweeps were generated by approximating the change in max streaming velocity as locally linear for a small frequency change (Fig. 5.19a) then a simple linear function spanning two frequencies in some number of timesteps was generated. In the same way as for the pure-tone stimuli, the wave forms at each timestep were generated and fed into the OpenFOAM simulation.

The details which follow show the process of optimising the frequency input, and were done mostly qualitatively from viewing the outputs after each simulations. In these cases no further processing was completed because the downfalls of each method and the way to improve them became immediately clear from the first simulation outputs. The particles were indeed moved along via the frequency sweep, but due to the region of circulation set up by the BM motion, they would enter the back-flow and be moved back towards their initial injection points. It was also obvious that a simple sweep alone would not be very efficient. Many particles were "left behind" by the translating wave, and those who had been translated initially were either lost to the backwards part of the streaming circulation (Fig. 5.20) or simply stagnated in the region downstream from the resonance peak location. The next trials therefore tried a pulsing sweep (Fig. 5.21). The idea was to repeatedly sweep the particles (much like sweeping leaves) to pull those particles which may have been left behind into the main circulation region as the waveform translated along the BM. However the problems of back flow and stagnation still remained.

The next sweeping trial then aimed to "capture" the particles in the circulation region by adding a second, simultaneous sweeping wave beginning from a lower frequency along the BM which would act to trap the particles and aid in their motion. The frequencies were chosen such that the difference in frequency was constant during the sweep. This causes a widening of the distance between resonance peaks as they move from the base to the apex of the cochlea. This did not have the effect desired, but it became immediately clear that the combination of the eddies induced by the membrane motion could lead to much more efficient transport.

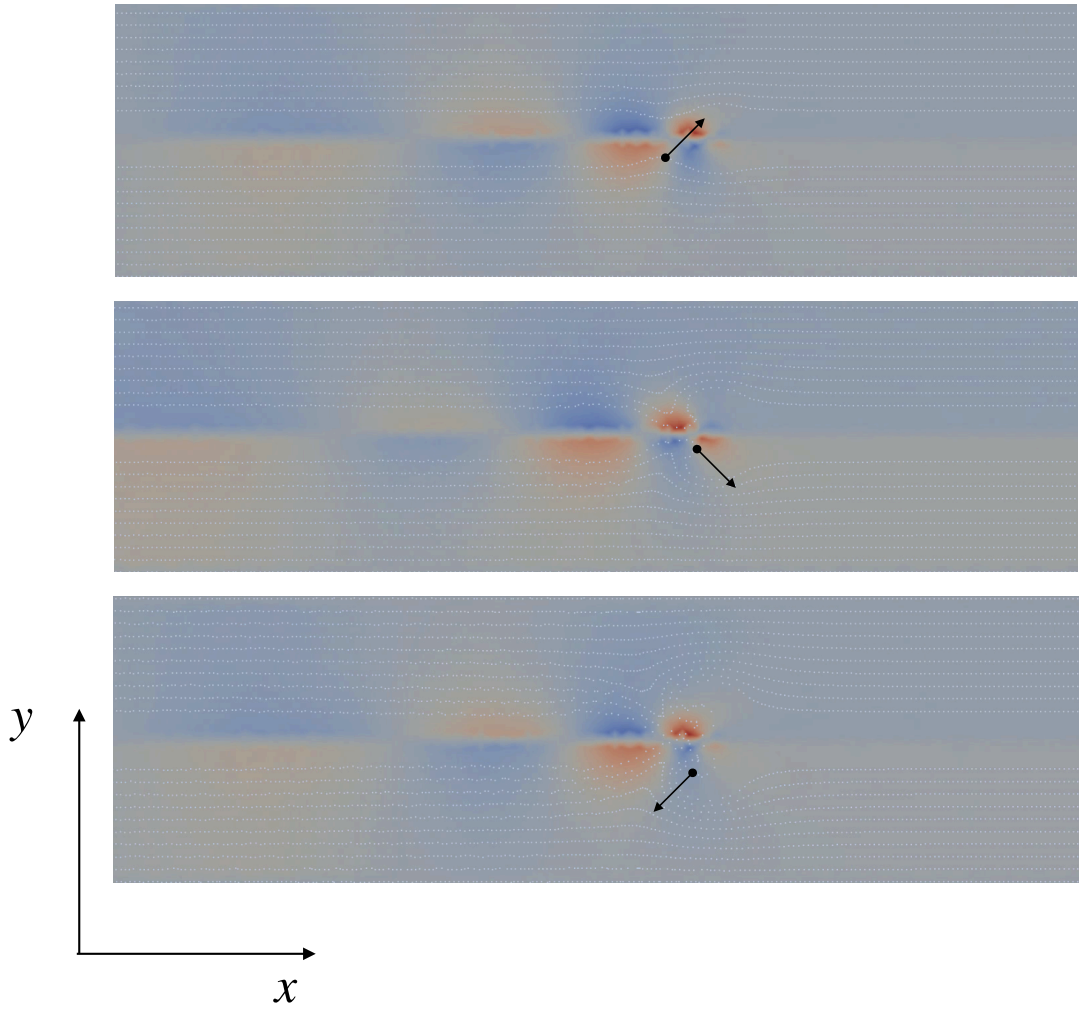

Figure 5.20: OpenFOAM output, included here as an illustration of the behaviour of the injected particles when a linear frequency sweep over a small frequency range (12-10 kHz) was implemented. The colour mapping represents the x-component of the fluid field velocity and the red and blue colouring indicates positive and negative field values respectively. The fluid field becomes static after the resonance location. The white points are individual particles which are traced through the flow and the images are snapshots from the start middle and end of the simulation (after 1.2 ms 3.5 ms and 5.9 ms respectively). Particles begin to move in the opposite direction at the edge of the sweep, and the amount of particles even affected by the sweep is quite small. Many particles lying further from the membrane are barely affected by the sound stimulus at all.

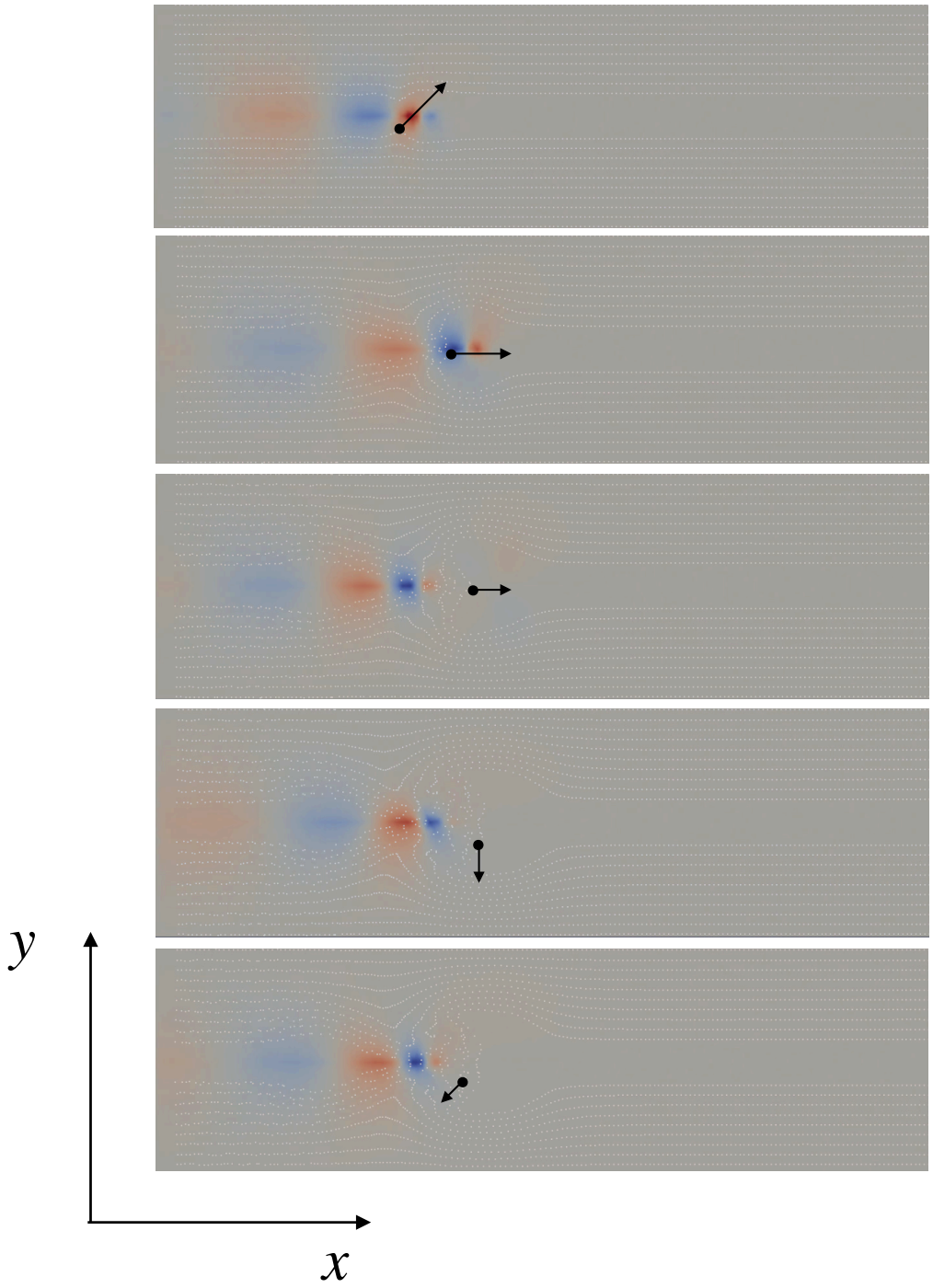

Figure 5.21: OpenFOAM output, included here as an illustration of the behaviour of the injected particles when a linear frequency sweep over a small frequency range (20-18 kHz) was repeated three times. The colour mapping represents the y-component of the fluid field velocity where the red and blue indicate positive and negative field values respectively. The fluid field becomes static after the resonance location. The white points are individual particles which are traced through the flow and the images are snapshots from throughout the simulation (at 1 ms, 9.1 ms, 18 ms and 23 ms respectively). In the third snapshot, the wave begins again to sweep from its initial frequency. This is repeated and it is clear that this is more efficient than the simple sweep in Fig. 5.20.

Instead of focusing on the sweeping, more tones were added to see if this could increase the transport efficiency. Fig. 5.22 shows the result of 6 (at this stage quite arbitrarily chosen) frequencies played at the same time, showing how much the particles are displaced from their initial to final positions. This stimuli is very effective at transporting the particles, setting up a streaming channel along which particles are accelerated due to the addition of the local eddies into a larger global circulation region, preventing back flow from individual eddies and stretching further along the channel. Importantly for both the pure-tone and the tone complex simulations, particles which lie far from the membrane in the y-direction are pulled up and along the streaming channel, an important result when it could be very difficult to inject a drug into a specific region of the cochlea.

After this simulation, the focus was shifted to a new question: how can the sound stimulus be optimised for multiple frequencies such that the maximum horizontal speeds are reached in the streaming channel?

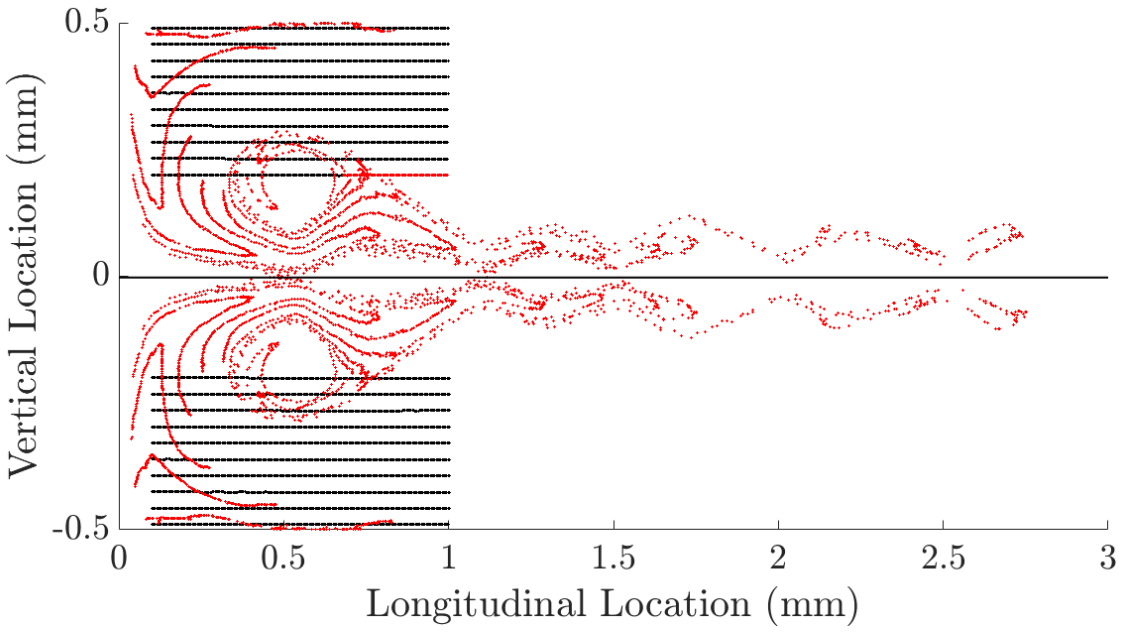

Figure 5.22: The initial (black) and final (red) coordinates for 5000 particles injected near the entrance of the cochlea as a result of 6 frequencies played simultaneously for 12.5 ms of real time. The bumpy shape of the path the particles travel is a consequence of the interaction of multiple vortices, which superpose to form into one global circulation region. Not only do the particles move a significant distance, with 3mm corresponding to more than 1/4 of the length of the cochlea, but the particles which lie far from the membrane are also pulled up and along the channel.

Chapter 6

Results: Multiple Frequency Stimulation

The results of the previous chapter show that steady streaming causes particles which lie further from the BM to be pulled into the region of higher streaming velocity nearer to the BM. This effect is very promising for therapeutic applications. As discussed in § 1, injection of a drug into the cochlea through the round window is already very difficult. If the method is capable of drawing an injected drug from the entire volume near the base of the cochlea, it removes the need to worry about where exactly the drug is being deposited on injection. If a drug is placed on the outside of the round window membrane and allowed to diffuse across it (a much safer and less invasive method) it is hard to control where it will be concentrated on the other side. Having a method of delivery where this does not matter is therefore very powerful.

6.1 Frequency Superposition

The linear superposition of multiple pure-tone frequency stimuli is effective because for each frequency, a local circulation region is generated. Once these circulation regions come into contact, they combine, creating a global circulation region. By choosing the frequencies carefully, it should be possible to optimise this effect and create a circulation region which extends from the highest frequency resonance location to the lowest. There are a number of factors which affect this choice. Firstly, the circulation regions should be close enough that they actually combine as explained in Fig. 6.1.

Secondly, although the maximum speeds are possible when the circulation re-

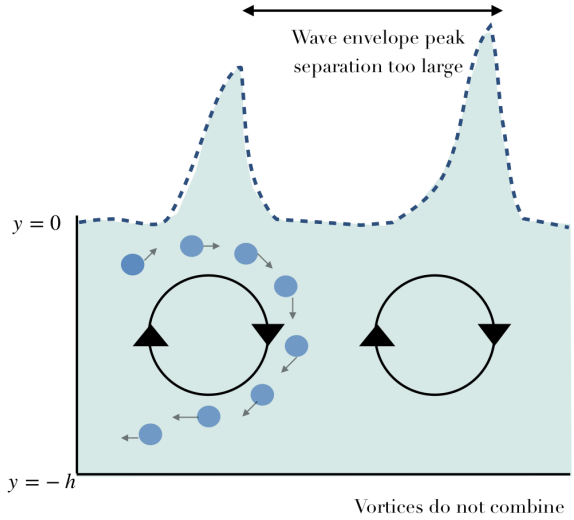

(a)

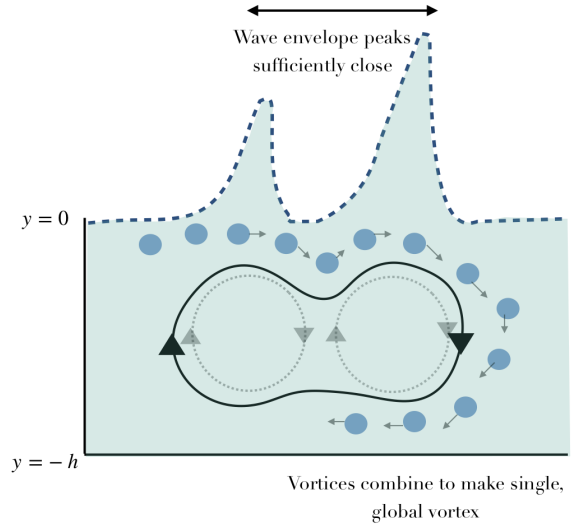

(b)

Figure 6.1: Considering only the bottom half of the channel, when two pure tones are linearly superposed, their combined wave envelope (exaggerated for illustration here by the dotted line) will have two peaks if the difference in frequency is large enough. If the difference is too small the peaks will overlap and the envelope will become smeared out. For wave envelopes where the peaks are too widely spaced as in (a), the individual circulation regions generated by each tone are spatially separated such that they do not combine. If however the frequencies are chosen such that the peaks are separated sufficiently close, as in (b), the individual circulation regions combine to form one global circulation region, which is much more efficient at transporting injected particles.

gion centres are closer together, they cannot be too close. Not only because of the fact that the peaks will no longer be resolved, but also because our simplified model uses the fixing of damping parameter, ξ in order to recreate the compressive non-linearity around the peak, meaning that a linear superposition of the waves is only

valid outside of this region. Therefore we can only linearly superpose waves as long as their non-linear regions do not overlap. This gives us a lower limit on how small the change in frequency between successive tones can be. Using experimental data from the chinchilla cochlea [59], a non-linear interaction region width of 100 μm was chosen as a lower limit on the peak-to-peak distance between wave envelopes.

At a constant SPL, the circulation region diameters are not a strong function of frequency in the range that we consider. The wave envelopes are more spread, and hence the circulation region diameters wider, for lower frequencies at the same SPL, but because we are only considering frequencies down to 10 kHz, the circulation region diameters can safely be assumed to be constant. So we look for a superposition of frequencies which lead to an equal spacing in the spatial domain. The spatial location of resonance along the BM scales linearly with the logarithm of the frequency such that choosing a constant difference in the spatial coordinates corresponds to a scaling in frequency of:

$$f_{j+1} = f_j e^{-R}. \tag{6.1}$$

Therefore when $j = 1$ we have the initial frequency (chosen to be 24 kHz in all results that follow) and all f_j scale from there onwards. R is what we will refer to as the ratio, and is defined as

$$R = m\delta \tag{6.2}$$

m being the constant of proportionality between $\ln(f)$ and x: equal to 301.5m^{-1}. The constant δ is the distance we desire between resonance peaks along the BM. From the 80dB simulation results, the longitudinal distance between circulation region centres was estimated as 1 mm, meaning an upper bound on the ratio value of 0.3. Hence a change in R is a scaling of the change in the distance between the circulation region centres. Fig. 6.2 shows the implementation of this method for different ratios of 10 frequencies and shows that indeed the peaks are equidistant. Already we find that a spatial separation of 1 mm is too large: the BM wave envelope extends across the entire cochlea, into the low frequency region which we do not account for in our model. This in turn gives another restriction on the choice of ratio, and leads to the maximum ratio considered as R=0.15. Fig. 6.3 shows the frequency functions used in the OpenFOAM simulations after invoking Eq. 6.1 with R=0.05, 0.1 and 0.15 respectively, with corresponding spatial separations of $\delta_{0.05} =$ 0.17 mm, $\delta_{0.1} = 0.33$ mm and $\delta_{0.15} = 0.5$ mm.

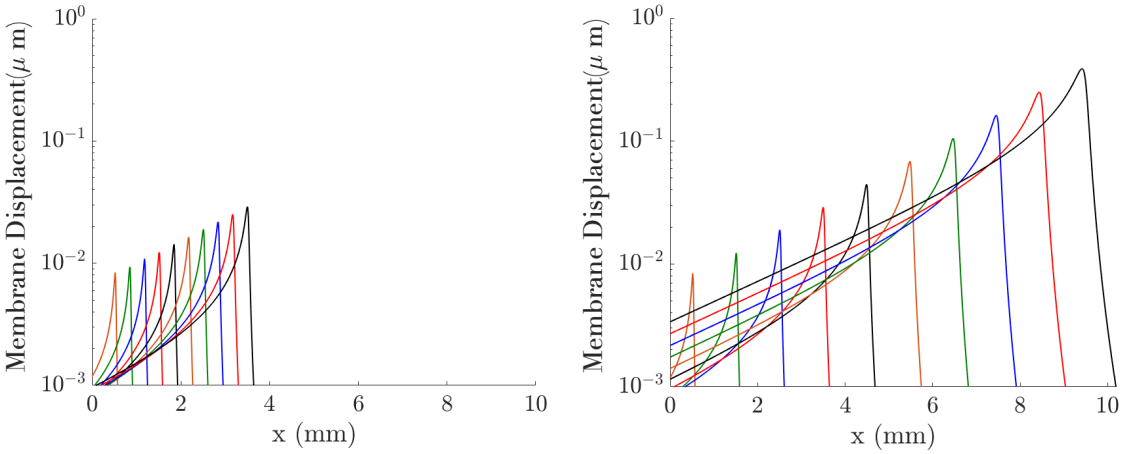

Figure 6.2: Plots showing the pure-tone stimuli wave envelopes for (a) R= 0.1 (with a corresponding peak to peak distance of 0.33 mm) and (b) R= 0.3 (with a corresponding peak to peak distance of 1 mm). Each envelope was calculated separately using the same parameters and only changing the frequency. The peaks are equidistant in space, and their total spatial extent increases as R is increased, as expected. These travelling waves were linearly superposed and used as input to the simulations as a multi-frequency BM deflection.

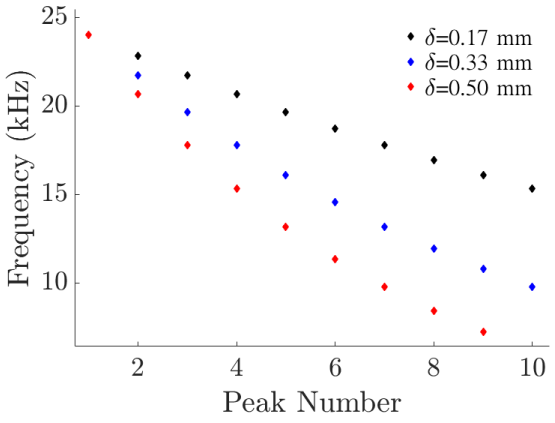

Figure 6.3: Frequency curves for the three values of R presented in this work. Each pure-tone is linearly superposed such that the envelope consists of ten equally-spaced peaks. The peak separation distances were: $\delta_{0.05}$ = 0.17 mm, $\delta_{0.1}$ = 0.33 mm and $\delta_{0.15}$ = 0.5 mm.

6.2 Post Processing

The metric against which we measure the efficacy of the transport is the velocity of particles the streaming channel when the steady state has been reached. In order to determine these velocities, the domain was decomposed into a grid, and the average velocity of particles in each cell of the grid calculated. Fig. 6.4 illustrates

such a grid on one half of the domain and defines the lengths of the cell edges Δx and Δy.

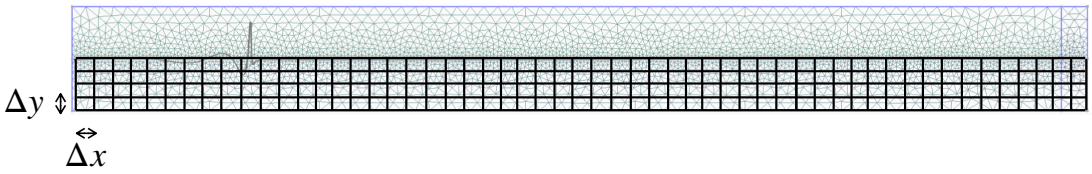

Figure 6.4: Example of a coarse grid taken over the lower half of the domain in order to define cells within which the statistics for the average velocity of particles can be determined. Δx and Δy are the lengths of the cell edges.

In order to find the time averaged velocity of particles in each cell of the domain, $\underline{\bar{u}}$ where the overbar indicates time averaging, the following method was undertaken:

- At a certain timestep, t_i, find the particles contained in each cell by sorting all of the particles in the domain into the corresponding cells in the grid which contain their coordinates.

- For each cell, store the coordinates (x_i, y_i) of every contained particle at t_i and t_{i+1}.

- Calculate their instantaneous velocity between successive timesteps:

$$\underline{u}_i^A = (u^A, v^A) = \left(\frac{x_{i+1} - x_i}{\Delta t}, \frac{y_{i+1} - y_i}{\Delta t} \right)$$

  where Δt is the timestep of the simulation.

- Find $\underline{u}^A$ for every particle in the domain at $t = t_i$.

- Repeat for every timestep (for all i).

- Average these values over time to get $\underline{\bar{u}}$ in each cell of the domain.

In order to define the grid through which we decompose the domain, the maximum displacement between adjacent timesteps was found such that the cells of the grid would contain even the largest displacements between two timesteps. If particles translated more than a cell size between timesteps, the velocity statistics would be inaccurate.

6.3 Results

All simulations were run for 10000 timesteps and each took around 25 minutes to run.

6.3.1 129.5 dB SPL

The initial and final coordinates of the injected particles for a range of δ are shown in Figs. 6.5 to 6.7 and show how much more effective the smallest separation was at drug transport: almost all particles were dragged into and along the streaming channel. Not only does the vicinity of each recirculation region play a big role in this process, but for smaller separation values, the amplitude of the BM wave is higher and so therefore are the speeds. For δ= 0.5mm, we start to see why the larger spread is less efficient: whereas some particles were transported along the centre of the streaming channel and have almost no component of their velocity in the y-direction, some were in the region where their y-velocity component is non-zero, reducing the average horizontal velocity and hence the efficiency. This is more apparent in the time averaged velocity maps in 6.8 to Figs. 6.10. Reducing the separation to 0.17 mm caused particles to move so effectively that in the same time, they reached the edge of the global circulation region and began to move into the back flow. This was the smallest separation considered, because it approaches the lower limit of 100 μm imposed earlier in this chapter. In total 10 OpenFOAM simulations were run for values of δ between 0.17 mm and 0.5 mm and the maximum steady streaming velocities as a function of ratio were found and are presented in Fig. 6.11. For the displacements and average particle velocity maps, only the results for 0.17 mm, 0.33 mm and 0.5 mm are presented.

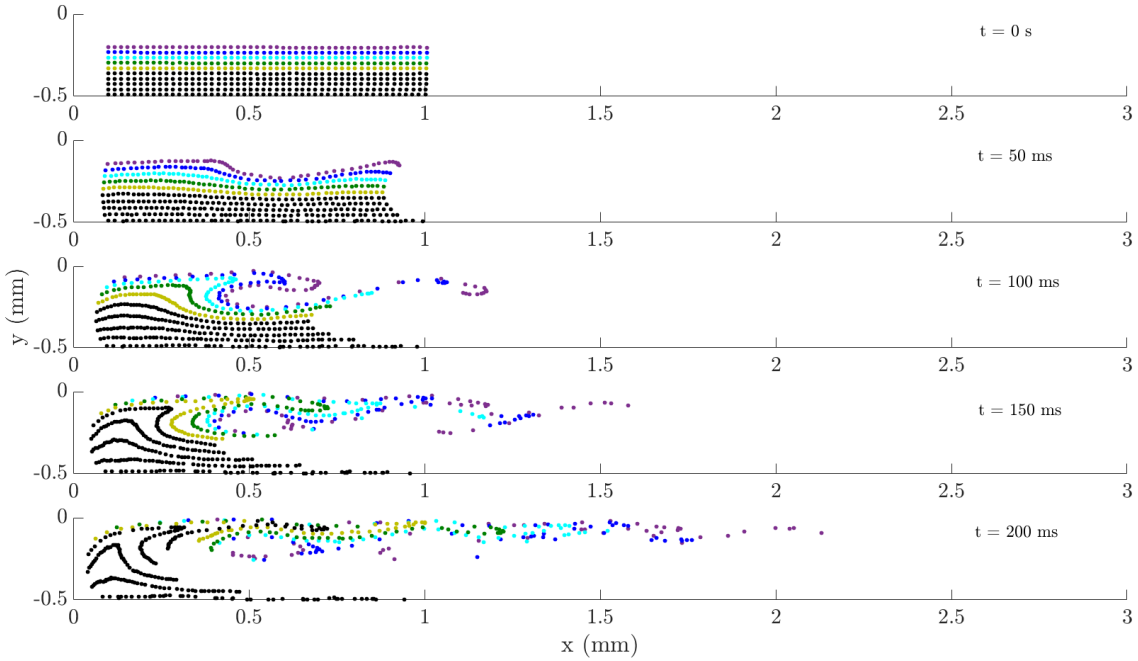

Figure 6.5: Displacement of particles injected into the fluid when a sound stimulus with $\delta = 0.5$ mm is applied. Each point represents a particle and the top five rows of particles have been colour coded in order to better track their displacement throughout the domain.

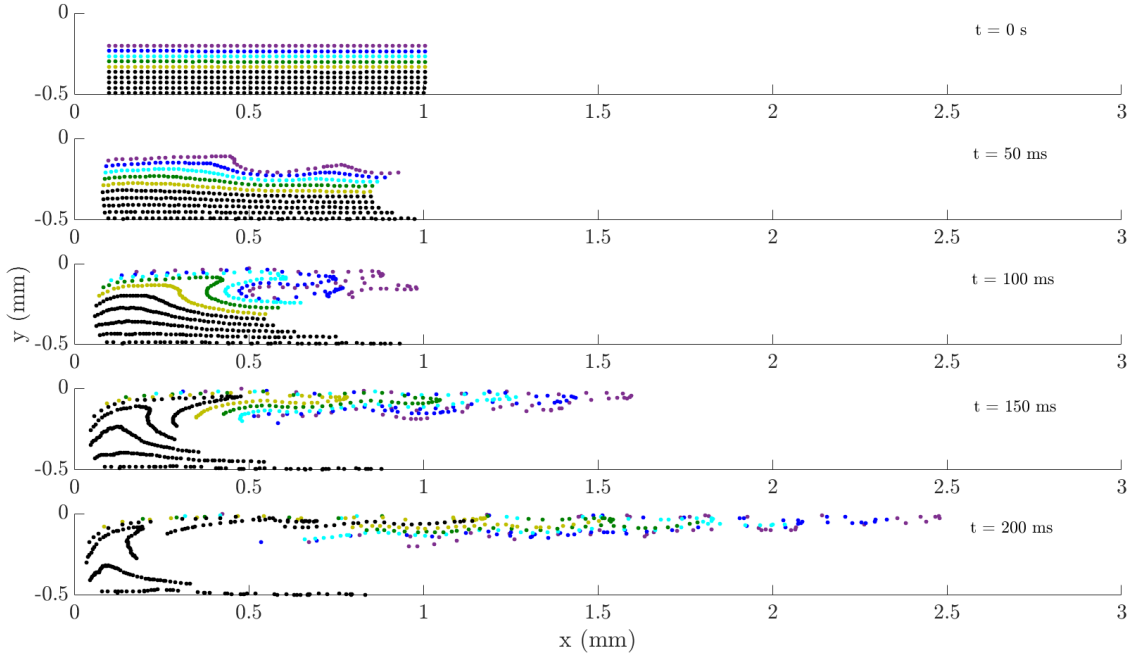

Figure 6.6: Same as Fig. 6.5 but with $\delta = 0.33$ mm

.

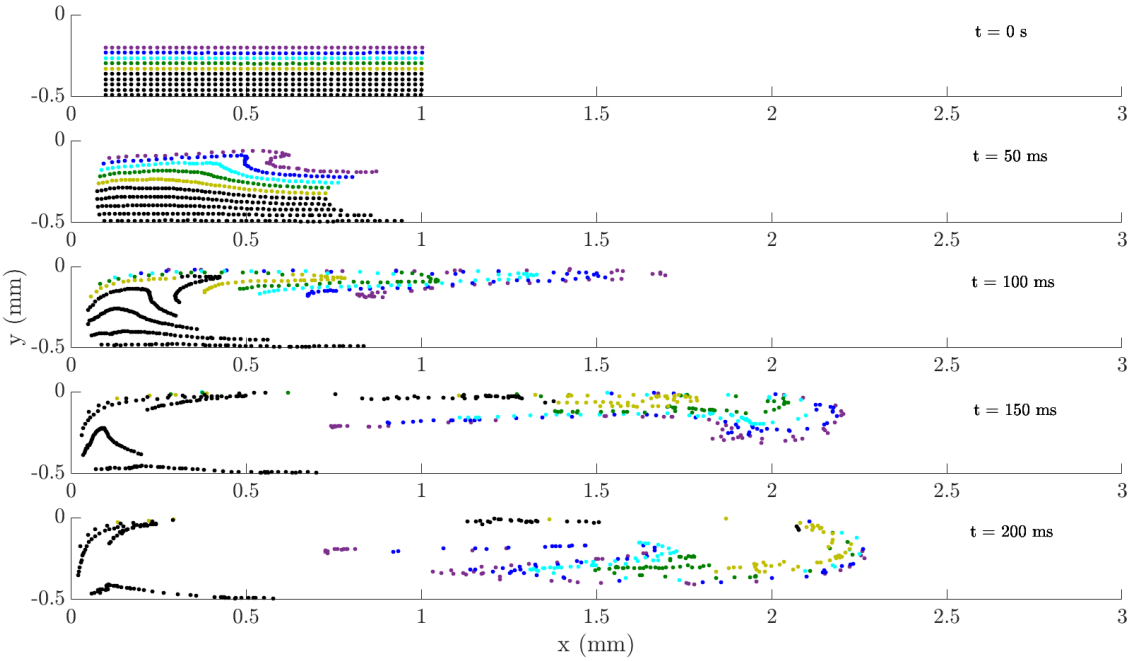

Figure 6.7: Same as Fig. 6.5 but with $\delta = 0.17$ mm. Here we see the particles have began to move back towards the base of the cochlea after entering the backflow. This effect would be diminished on addition of more tones to the stimuli in order to elongate the region of oscillation of the BM.

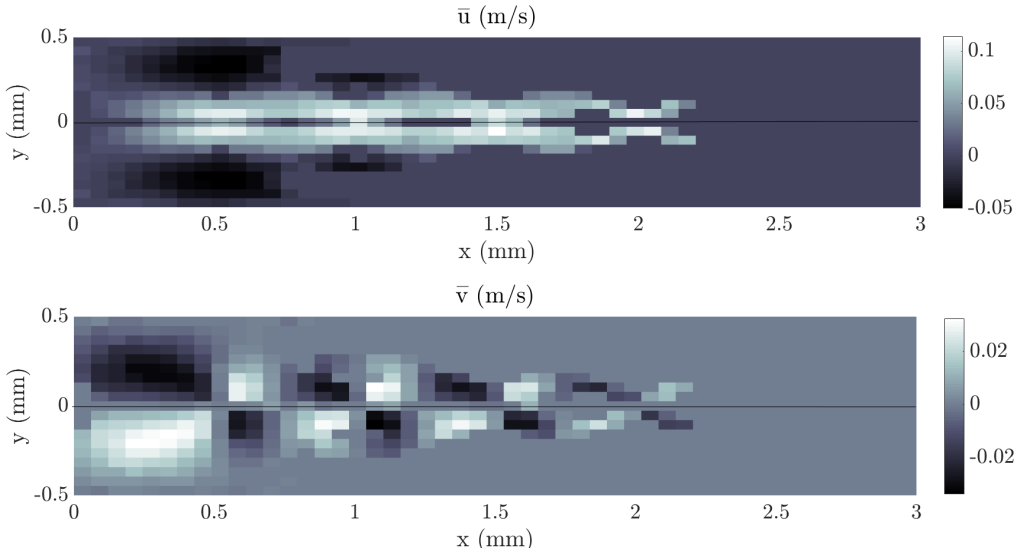

Figure 6.8: Average velocity maps for $\bar{u}$ (top panel) and $\bar{v}$ (bottom panel) when δ= 0.5 mm, averaged across 250 timesteps (1.25 ms) once the steady state was reached. The domain has been split into a 20x50 grid of cells according to the method outlined above. The upper panel shows the streaming channel whereas the lower panel reveals the circulation regions due to the non-zero y-component.

.

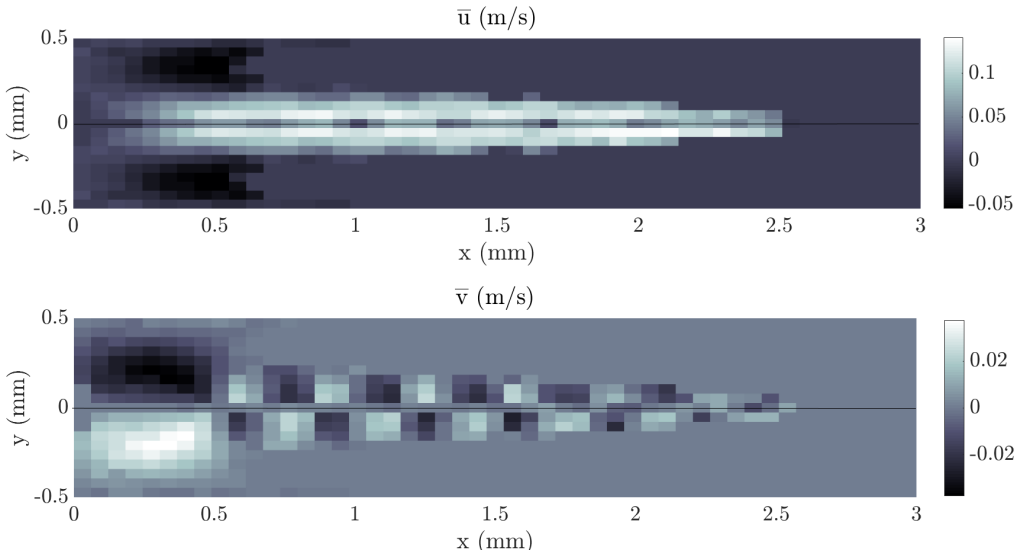

Figure 6.9: Same as previous figure except δ= 0.33 mm. The upper panel shows the streaming channel, which is narrower and hence more efficient than for R=0.15. The lower panel reveals the circulation regions due to the non-zero y-component which is weaker in this case than for δ= 0.5 mm.

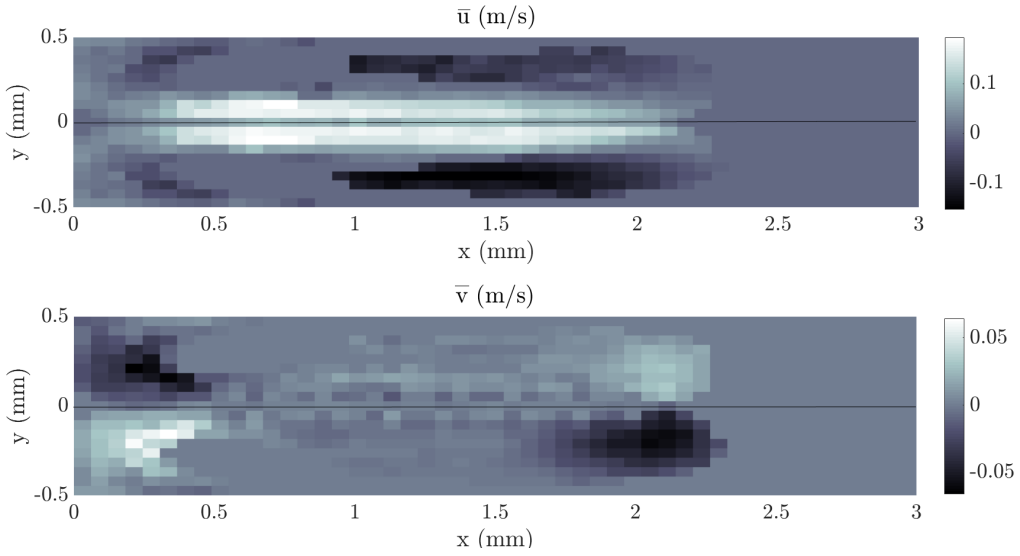

Figure 6.10: Same as previous figure except δ= 0.17 mm. Here the particles have travelled to the edge of the BM stimulation region and have began to move back towards the entrance of the cochlea. The x-velocity values are higher than for the previous ratios and the y-velocity along most of the channel is almost zero, meaning virtually all of the energy is given to motion in the x-direction, as desired.

.

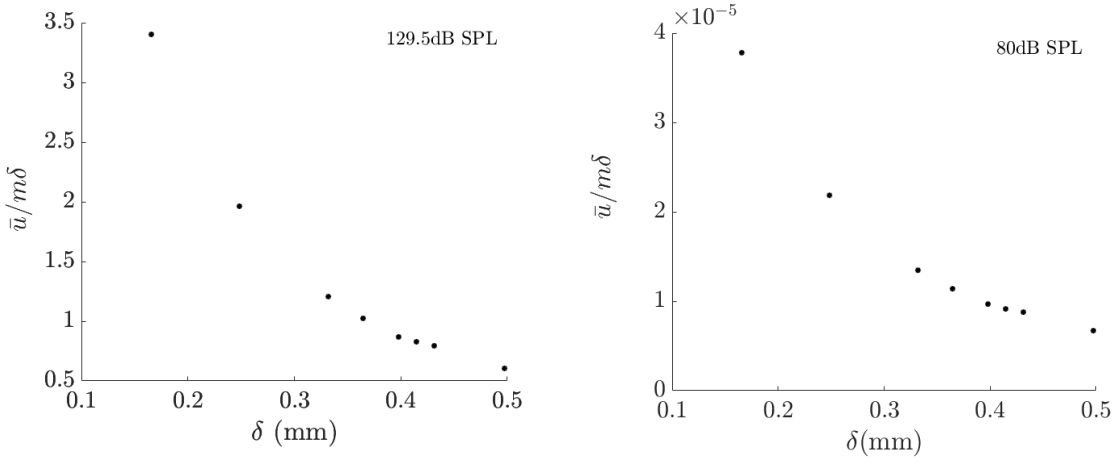

(a) (b)

Figure 6.11: $\bar{u}$ normalised by the ratio of the successive frequencies in the multi-frequency stimulation. If the steady streaming was proportional to the energy dissipated along a constant cochlear extent, then this normalized velocity would be constant. However, the normalized velocity increases strongly for smaller spatial separations, evidencing that the steady streaming becomes stronger when the multi-frequency stimulation uses many pure tones that successively differ only by a small amount.(a) the 129.5 dB SPL simulations and (b) scaled appropriately to give the expected speeds for stimulation at 80 dB SPL.

.

6.3.2 80 dB SPL

In order to show the vector field and therefore the combination of the circulation regions, the simulation was run over a longer timescale at the amplitude of the 80 dB SPL stimulus and the analysis of § 5 repeated using δ= 0.17 mm. Fig. 6.12 shows u_{ss} and v_{ss} over 20000 timesteps and it should be noted that the speeds present in the system are higher because of the superposition of wave envelopes causing a larger sound stimulus to be applied. The important result is the clear increase in longitudinal influence on the flow, with the field showing u_{SS} showing that in the streaming channel near the membrane, the particles experience a force purely in the positive x direction. In Fig. 6.13 the circulation region combination is apparent, with clear enhanced global rotation and the 10 individual circulation regions discernible the region close to the BM.

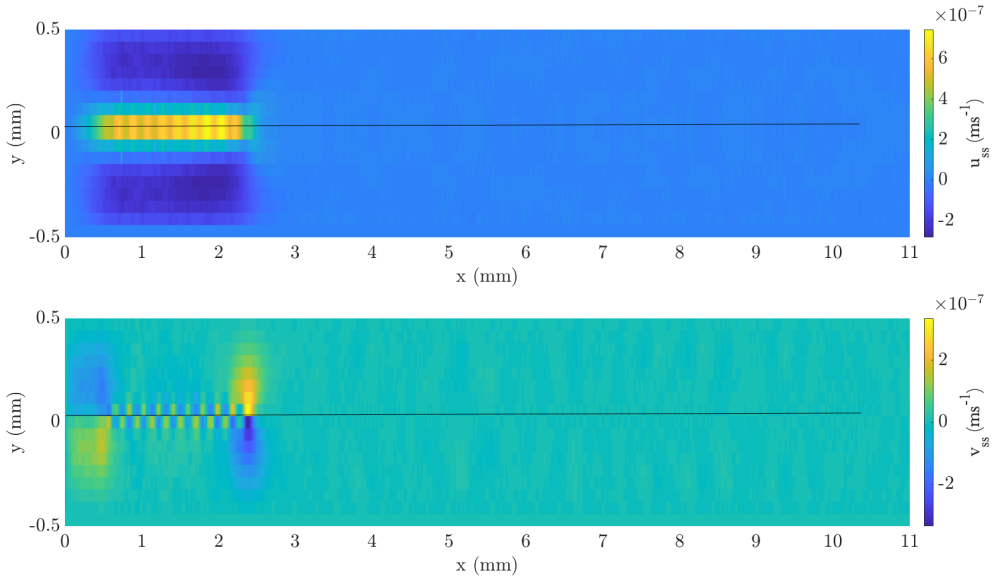

Figure 6.12: u_{SS} (top panel) and v_{SS} (bottom panel) for a linear superposition of 10 pure tones ranging from 24 kHz to 15.3 kHz (δ= 0.17 mm) at 80 dB SPL. The black line at $y = 0$ indicates the location of the basilar membrane.

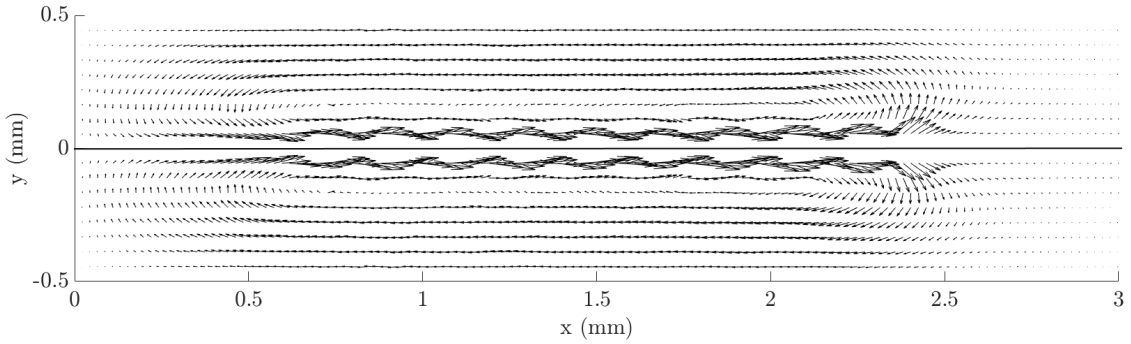

Figure 6.13: Vector field up to the characteristic place for a linear superposition of 10 pure tones ranging from 24 kHz to 15.3 kHz (δ= 0.17 mm) at 80 dB SPL. The black line at $y = 0$ indicates the location of the basilar membrane. The 10 individual regions of circulation can be seen clearly near the BM and the way in which they combine is also clear.

6.3.3 Recirculation Depth

The vertical distance from the membrane from which the particles are transported along the channel is important. At 129.5 dB SPL the entire depth of the channel is affected by the stimulus and even particles which lie very close to the bottom of the channel are transported to the BM and towards the apex of the cochlea. The simulations were run again, this time for decreasing SPL to monitor how this affected the circulation region depth. The motivation was to find the region within the cochlea that a drug must be injected in order for this procedure to work. Although the magnitudes of the average velocities decreased with SPL, the spatial size of the circulation regions were found to be constant. The normalised depth profiles for the $\bar{v}$ at the basal edge of the circulation region for δ= 0.17 mm are displayed in Fig. 6.14.

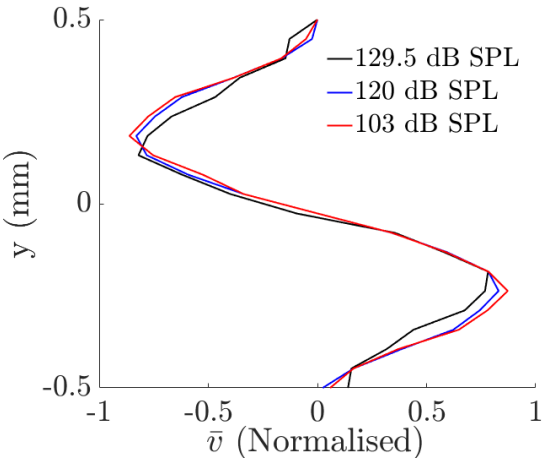

Figure 6.14: Depth profile of $\bar{v}$ for δ= 0.17 mm for a range of SPL to show that although the magnitude of the velocity decreases, the size of the circulation regions is almost constant. This means that a quieter sound will still induce a global circulation region although its strength will be diminished.

Chapter 7

Conclusion

7.1 Summary

The initial hypothesis of this work was that a sound stimulus of a descending frequency could be optimised such that the phenomenon of steady streaming could be used to transport an injected drug from the base of the cochlea towards its apex. Current research into drug therapies in the cochlea is constrained by the fact that not only is it difficult to apply a drug to the inside of the cochlea, it is even more difficult to control the location at which it is concentrated.

This work represents an early stage investigation into the phenomenon of steady streaming as a method for drug delivery. Whereas previous work has investigated the streaming fields in the cochlea [34][46] , the novel approach in this work was to track individual particles through the flow. Initially extensive efforts were focused on the creation of the CFD simulation of a simplified cochlear model. This simplification came from two factors: firstly the geometry was vastly simplified from a 3D spiralled tapering channel to a 2D straight one. The second simplification was due to the use of a passive cochlear model to generate the travelling waves along the basilar membrane surface. Linear theory was used to derive the waves and a compressive non-linearity around the peak was possible through the use of a damping parameter in the impedance of the membrane which was fixed according to experimental data. However, there was a trade-off at this point between the realistic wave amplitude and a realistic wave envelope. The envelope which have been used throughout this work are sharper than those which occur physiological. This behaviour was constrained by the use of a linear mathematical model. The CFD model was then used to determine the steady streaming velocities of individual particles placed into the cochlear fluid under a range of pure-tone frequency stimuli. The frequencies initially ranged from

5 to 20 kHz and the results of this portion of the investigation revealed that our wave model was only valid down to around 10 kHz: spanning a distance of around 1/4 of the cochlear length. This was more than enough to begin investigations into whether or not the frequency sweeps would be effective. The pure-tone results were used in order to compare the simulation output to the steady streaming theorised by Lighthill, and these were found to follow the same functional behaviour, up to a constant scaling factor. The scale factor was necessary in order to use Lighthill's equations to optimise the frequency so that the rate of change in frequency would match the streaming speed of particles at that location. Furthermore, Edom and Obrist have undertaken modelling of the cochlear channel in 2D, and found the maximum value of u_{SS} to be around $4.8 \times 10^{-6}\ ms^{-1}$. Their investigations were undertaken at 1kHz stimulation at 76dB SPL. In order to compare their speeds with those found here, scaling is necessary to account for both the difference in SPL, and the difference in frequency. Using the usual scaling for SPL and approximating the change in amplitude with frequency as liner, this leads to an equivalent result of $1.14 \times 10^{-6}\ ms^{-1}$ if we consider a stimulus of 10kz at 80dB SPL. This is around 10 times faster than we find here, which is to be expected due to their inclusion of a 2D stiffness tensor for the basilar membrane, instead of the one dimensional stiffness implemented here. They therefore have another contribution to the streaming, which forces the particles in a way which we cannot account for in this model. The depth profiles of both components of the streaming velocity were investigated and it was found that the size of the recirculation region around the characteristic place is constant through changes in SPL. This is important as it means that although for quieter sounds the streaming velocities are lower, the region of influence of the travelling waves on the particles in the flow is predictable.

Running preliminary cases with an optimised frequency sweep were then completed, and it became apparent very quickly that the frequency sweep had some downfalls which made it far less effective than hypothesised. Firstly, although the sweep of the resonance location along the basilar membrane did indeed drag particles along with it, the region of influence was very small, meaning that particles lying sufficiently far from the membrane were barely affected. Secondly, the set of particles nearest to the peak location and hence moving the quickest, were pulled into the back-flow of the streaming vortex generated by the BM wave. After attempting to use a second, simultaneous frequency sweep beginning at a lower frequency in order to try to translate the entire vortex of particles, it became clear that the combination of frequencies was instead resulting in a combined vortex and the creation of a "streaming channel" along which particles had a higher horizontal velocity.

From this point, the frequency sweeps were no longer pursued, and instead the focus changed to optimising the superposition of frequencies in order to maximise this horizontal steady streaming. It was found that not only were combined vortices more effective at transport, but that they are significantly more so. Although the increase in speed is mainly due to the increase in amplitude overall after frequency superposition, the main reason for the increase in horizontal displacement is the combination of the eddies. Use of an optimised frequency superposition therefore led to timescales of around 2 hours for particles injected near the base of the cochlea (through the round window for example) to be transported 1/4 of its length. Importantly, this work provides a method of generating a sound stimuli which can be tailored to transport a drug to a specific location along the cochlea, from prior knowledge of hair cell damage after undergoing an audiogram for example.

7.2 Model Limitations

There are certain limitations to the CFD model used in this work which should ideally be addressed in order to pursue this streaming further.

Firstly, the dimensions and experimental parameters used here all originate from small rodents. Including experimental results from a human cochlea into the model would be useful in order to ensure that the very promising timescales found in this work are still the case for humans.

Secondly, as mentioned above, is the issue of the active process. The relation between the membrane velocity and the pressure difference across it outlined in Eq. 3.15, leads to the wave equation for the pressure difference, which we solve using the WKB method. However, using a non-linear relation here leads to a new, nonlinear term in the wave equation and yields more realistic behaviour.

Thirdly, problems relating to the particle tracking implementation. The time frames over which the simulations could be run were limited because they would hang indefinitely once particles approached the BM too closely. It was not clear why this should happen. The conclusion was that the redefinition of the BM surface between timesteps could have led to some particles having their next set of coordinates on the other side of the membrane between time steps, leading to problems with the convergence of the solution. This problem was avoided by removing particles which came too close to the BM and by injecting particles sufficiently far from the membrane at the start of the simulation. This vertical distance from the membrane at which the initial injection was possible increased with SPL and so for

this reason, during the 129.5 dB SPL investigation, particles were injected at almost quarter of the total channel height away from the membrane. Another improvement to the particle tracking model would be to introduce a more complex interaction model for collisions. Currently the model allows almost elastic collisions with walls and no collisions with one another. Although this was a sufficient condition for the pure-tone investigations of § 5 where displacements were incredibly small, this may no longer have been adequate for the more complex flows encountered in § 6. The biggest problem as a result of the lack of proximity of particles to the BM was that it was difficult to resolve the boundary layer width and behaviour because no particles were injected there. Finally, the fact that the simulation required extremely small Courant numbers (typically $\mathcal{O}(10{-}5)$) was also assigned to issues regarding particle motion, because of the tiny displacements between time steps.

Finally, the sharpness of the tuning used in his work needs some improvement, ideally through inclusion of non linear terms in the initial equations. A direct result of broadening the envelopes will be that the choice of 100 μm as the width of the non-linear interaction region would also need to be increased. The width is already quite small, and once the improved BM wave model is implemented in order to capture more of the non-linear behaviours, this width would need to be reassessed according to the wave envelopes this model generates.

Although there are undeniably limitations to this model, these results are very encouraging. Most of the issues outlined above, once improved, will result in an increased value of u_{ss} to that seen here, ideally towards the values found by Edom and Obrist, which are around ten times higher than those seen here. This increase would be significant for drug delivery, where the efficacy of a therapy (due to re-absorption or drug deterioration for example) reduces with time meaning that any increase in the magnitude of the streaming is desirable for the application of drug delivery.

7.3 Further Investigation

As well as the improvements touched upon above, the next way to extend the work is to create a more realistic cochlear geometry, by tapering the channel firstly, and then potentially extending this by including the 3D nature of the flow and ultimately the spiral geometry. As has also been mentioned throughout this work, the sharpness of the tuning can be improved through inclusion of a non-linear wave model for the BM deflection. The stimuli can also be optimised further. For

example an initial frequency superposition could be played for some time, until a large proportion of the drug has been transported along the channel and then switched off. After this, either the drug is allowed to diffuse locally, resulting in a much improved dosage at that location compared to passive diffusion from the round window alone, or a pure-tone corresponding to the frequency at that location played, to locally recirculate the flow and attempt to keep it in the vicinity of the damaged hair cells until it has been absorbed. For drugs which rely on a time delayed liberation, this could be particularly powerful. Another route to explore is the use of varying SPL during the stimulus, something which has not been attempted here: perhaps changing the loudness of the sound with some modulation will have a significant effect on the streaming. By varying the SPL as a function of frequency (for example reducing the SPL with frequency), it could be possible to have a higher acceleration for the particles nearer the base of the cochlea than those which lie more apically along it. Such a stimulus would mean that the high frequency, lower amplitude (for the same SPL compared to lower frequencies) region of the cochlea could be traversed more quickly in order to efficiently transport the drug in a shorter time, but without the overall SPL of the stimulus being too high for a patient to listen to comfortably. Finally, a simplistic superposition method has been used here, merely adding the separate wave forms together for different frequencies and using this as an input to the simulation. It would be useful to superpose these waves such that the overall amplitude of the resulting wave is still at the SPL desired. This is important because increasing the SPL of the resulting signal could lead to further damage to, or at least discomfort for, a patient.

The conclusion of this work is therefore that one can in fact achieve drug delivery through steady streaming in the cochlea, and it is possible to specifically target locations along the cochlear channel by designing the appropriate frequency stimulus such that a streaming channel is set up, along which particles travel. We also show that the timescales over which these stimuli must be played to achieve this transport are reasonable for therapies: around 2 hours for a displacement of 1/4 of the cochlea. Now that it has been shown that for a passive cochlea at least steady streaming is a viable method of delivery, there is a rich landscape of sound stimuli to explore.

Bibliography

[1] G. Emadi, C.P Richter, and P. Dallos. Stiffness of the gerbil basilar membrane: Radial and longitudinal variations. *Journal of Neurophysiology*, 91(1):474–488, 2004.

[2] N. Cooper and W. Rhode. Mechanical responses to two-tone distortion products in the apical and basal turns of the mammalian cochlea. *Journal of Neurophysiology*, 78(1):261–270, 1997.

[3] J. Pickles. *An Introduction to the Physiology of Hearing. Third Ed.* Emerald House Publishing, 2008.

[4] C. Dai, M. Lehar, D. Sun, L. RVT, J. Carey, T. MacLachlan, D. Brough, H. Staecker, A. Della Santina, T. Hullar, and C. Della Santina. Rhesus cochlear and vestibular functions are preserved after inner ear injection of saline volume sufficient for gene therapy delivery. *Journal of the Association for Research in Otolaryngology*, 18(4):601–617, 2017.

[5] A.K Wise and L. Gillespie. Drug delivery to the inner ear. *Journal of neural engineering*, 9(6):065002, 2012.

[6] R.T Richardson and P.J Atkinson. Atoh1 gene therapy in the cochlea for hair cell regeneration. *Expert opinion on biological therapy*, 15(3):417–430, 2015.

[7] W. Chien, K. Isgrig, S. Roy, I.A Belyantseva, M.C Drummond, L.A May, T.S Fitzgerald, T.B Friedman, and L.L Cunningham. Gene therapy restores hair cell stereocilia morphology in inner ears of deaf whirler mice. *Molecular Therapy*, 24(1):17–25, 2016.

[8] J. Suzuki, K. Hashimoto, R. Xiao, L.H Vandenberghe, and M.C Liberman. Cochlear gene therapy with ancestral aav in adult mice: complete transduction of inner hair cells without cochlear dysfunction. *Scientific reports*, 7:45524, 2017.

[9] S.K Juhn, B.A Hunter, and R.M Odland. Blood-labyrinth barrier and fluid dynamics of the inner ear. *The international tinnitus journal*, 7(2):72–83, 2001.

[10] S.K Juhn and L.P Rybak. Labyrinthine barriers and cochlear homeostasis. *Acta oto-laryngologica*, 91(1-6):529–534, 1981.

[11] S.K Juhn, L.P Rybak, and W.L Fowlks. Transport characteristics of the blood—perilymph barrier. *American journal of otolaryngology*, 3(6):392–396, 1982.

[12] X. Liu, M. Li, H. Smyth, and F. Zhang. Otic drug delivery systems: Formulation principles and recent developments. *Drug Development and Industrial Pharmacy*, 0(0):1–14, 2018.

[13] A.A McCall, E.E Leary Swan, J.T Borenstein, W.F Sewell, S.G Kujawa, and M.J McKenna. Drug delivery for treatment of inner ear disease: current state of knowledge. *Ear and hearing*, 31(2):156, 2010.

[14] H. Watanabe, J.W Kysar, and A.K Lalwani. Round window membrane as a portal for inner ear therapy. *Recent Advances in Otolaryngology Head & Neck Surgery*, 6:39, 2017.

[15] N.B Abt, M. Lehar, C. Guajardo, R.T Penninger, B.K Ward, M.S Pearl, and J.P Carey. Intratympanic iodine contrast injection diffuses across the round window membrane allowing for perilymphatic ct volume acquisition imaging. *Otology & neurotology: official publication of the American Otological Society, American Neurotology Society [and] European Academy of Otology and Neurotology*, 37(4):403, 2016.

[16] A.N Salt and S.K Plontke. Principles of local drug delivery to the inner ear. *Audiology and Neurotology*, 14(6):350–360, 2009.

[17] N.J Creber, H.T Eastwood, A.J Hampson, J. Tan, and S.J O'leary. Adjuvant agents enhance round window membrane permeability to dexamethasone and modulate basal to apical cochlear gradients. *European Journal of Pharmaceutical Sciences*, 126:69–81, 2019.

[18] K. Mäder, E. Lehner, A. Liebau, and S. K. Plontke. Controlled drug release to the inner ear: Concepts, materials, mechanisms, and performance. *Hearing Research*, 2018.

[19] M. Peppi, A. Marie, C. Belline, and J.T Borenstein. Intracochlear drug delivery systems: a novel approach whose time has come. *Expert opinon on drug delivery*, 2018.

[20] S.K Plontke, J.J Hartsock, R.M Gill, and A.N Salt. Intracochlear drug injections through the round window membrane: Measures to improve drug retention. *Audiology and Neurotology*, 21(2):72–79, 2016.

[21] A.N Salt. Dexamethasone concentration gradients along scala tympani after application to the round window membrane. *Otology & neurotology: official publication of the American Otological Society, American Neurotology Society [and] European Academy of Otology and Neurotology*, 29(3):401, 2008.

[22] A.N Salt and S.K Plontke. Pharmacokinetic principles in the inner ear: Influence of drug properties on intratympanic applications. *Hearing research*, 2018.

[23] P. Wangemann. K+ cycling and the endocochlear potential. *Hearing research*, 165(1-2):1–9, 2002.

[24] T Gold and R.J Pumphrey. Hearing 1: The cochlea as a frequency analyzer. *Proceedings of the Royal Society of London B: Biological Sciences*, 135(881):462–491, 1948.

[25] T. Gold. Hearing 2 the physical basis of the action of the cochlea. *Proceedings of the Royal Society of London B: Biological Sciences*, 135(881):492–498, 1948.

[26] Georg Von Békésy and Ernest Glen Wever. *Experiments in hearing*, volume 8. McGraw-Hill New York, 1960.

[27] W.S Rhode. Observations of the vibration of the basilar membrane in squirrel monkeys using the mössbauer technique. *The Journal of the Acoustical Society of America*, 49(4B):1218–1231, 1971.

[28] M.A. Ruggero. Responses to sound of the basilar membrane of the mammalian cochlea. *Current Opinion in Neurobiology*, 2(2):449–456, 1992.

[29] A.J Hudspeth. Mechanical amplification of stimuli by hair cells. *Current opinion in neurobiology*, 7(4):480–486, 1997.

[30] S. Jia, J. Zuo, P. Dallos, and D. He. The cochlear amplifier: Is it hair bundle motion of outer hair cells? In *Auditory Mechanisms: Processes And Models: (With CD-ROM)*, pages 261–269. World Scientific, 2006.

[31] A.W Peng and A.J Ricci. Somatic motility and hair bundle mechanics, are both necessary for cochlear amplification? *Hearing research*, 273(1-2):109–122, 2011.

[32] N. Riley. Steady streaming. *Annual review of fluid mechanics*, 33(1):43–65, 2001.

[33] J. Lighthill. Acoustic streaming in the ear itself. *Journal of Fluid Mechanics*, 239:551–606, 1992.

[34] E. Edom, D. Obrist, and L. Kleiser. Steady streaming in a two-dimensional box model of a passive cochlea. *Journal of fluid mechanics*, 753:254–278, 2014.

[35] C.R Steele and D.H Jen. Analysis of streaming flow induced in the tectorial gap. In *Peripheral Auditory Mechanisms*, pages 169–176. Springer, 1986.

[36] M.B Lesser and D.A Berkley. Fluid mechanics of the cochlea. part 1. *Journal of Fluid Mechanics*, 51(3):497–512, 1972.

[37] G. Zweig. Finding the impedance of the organ of corti. *The Journal of the Acoustical Society of America*, 89(3):1229–1254, 1991.

[38] D. Manoussaki, R.S Chadwick, D.R Ketten, J. Arruda, E.K Dimitriadis, and J.T O'Malley. The influence of cochlear shape on low-frequency hearing. *Proceedings of the National Academy of Sciences*, 105(16):6162–6166, 2008.

[39] N. Gavara, D. Manoussaki, and R.S Chadwick. Auditory mechanics of the tectorial membrane and the cochlear spiral. *Current opinion in otolaryngology & head and neck surgery*, 19(5):382, 2011.

[40] T. Reichenbach and A.J Hudspeth. The physics of hearing: fluid mechanics and the active process of the inner ear. *Reports on Progress in Physics*, 77(7):076601, 2014.

[41] L. Robles and M.A Ruggero. Mechanics of the mammalian cochlea. *Physiological reviews*, 81(3):1305–1352, 2001.

[42] G. Zweig, R. Lipes, and J.R Pierce. The cochlear compromise. *The Journal of the Acoustical Society of America*, 59(4):975–982, 1976.

[43] C. R Steele and L.A Taber. Comparison of wkb and finite difference calculations for a two-dimensional cochlear model. *The Journal of the Acoustical Society of America*, 65(4):1001–1006, 1979.

[44] L.C Peterson and B.P Bogert. A dynamical theory of the cochlea. *The Journal of the Acoustical Society of America*, 22(3):369–381, 1950.

[45] Richard P Beyer Jr. A computational model of the cochlea using the immersed boundary method. *Journal of computational physics*, 98(1):145–162, 1992.

[46] E. Edom, D. Obrist, . Henniger, L. Kleiser, J. Sim, and A.M Huber. The effect of rocking stapes motions on the cochlear fluid flow and on the basilar membrane motion. *The Journal of the Acoustical Society of America*, 134(5):3749–3758, 2013.

[47] E. De Boer and M.A Viergever. Validity of the liouville-green (or wkb) method for cochlear mechanics. *Hearing research*, 8(2):131–155, 1982.

[48] J.J Zwislocki. Sharp vibration maximum in the cochlea without wave reflection. *Hearing research*, 9(1):103–111, 1983.

[49] J. Lighthill. Acoustic streaming. *Journal of sound and vibration*, 61(3):391–418, 1978.

[50] M.H Holmes. Low frequency asymptotics for a hydroelastic model of the cochlea. *SIAM Journal on Applied Mathematics*, 38(3):445–456, 1980.

[51] M. Andoh and H. Wada. Prediction of the characteristics of two types of pressure waves in the cochlea: theoretical considerations. *The Journal of the Acoustical Society of America*, 116(1):417–425, 2004.

[52] R Courant, K Friedrichs, and H Lewy. On the partial difference equations of mathematical physics. *Mathematische Annalen*, 100, 1928.

[53] Lei Cheng, Robert D White, and Karl Grosh. Three-dimensional viscous finite element formulation for acoustic fluid–structure interaction. *Computer methods in applied mechanics and engineering*, 197(49-50):4160–4172, 2008.

[54] L. Xu, X. Huang, N. Ta, Z. Rao, and J. Tian. Finite element modeling of the human cochlea using fluid–structure interaction method. *Journal of Mechanics in Medicine and Biology*, 15(03):1550039, 2015.

[55] K. Kamieniecki, J. Piechna, and P. Borkowski. Basilar membrane vibration in time domain predicted by fluid–structure interaction model in pre-and post-stapedotomy state. *Procedia IUTAM*, 24:48–63, 2017.

[56] T. Koike, C. Sakamoto, T. Sakashita, K. Hayashi, S. Kanzaki, and K. Ogawa. Effects of a perilymphatic fistula on the passive vibration response of the basilar membrane. *Hearing research*, 283(1-2):117–125, 2012.

[57] J. Rhoads. *OpenFOAM Workshop: Effects of grid quality on solution accuracy.* www.pointwise.com for OpenFOAM, 2014.

[58] A. Vallier. Coupling of vof with lpt in openfoam. *http://www.tfd.chalmers.se*, pages created in 2011, Accessed in 2015.

[59] J. Fisher, F. Nin, T. Reichenbach, R.C Uthaiah, and A.J Hudspeth. The spatial pattern of cochlear amplification. *Neuron*, 76(5):989–997, 2012.

Appendix A

The following figures display the variables which the OpenFOAM solver required in order to run all of the cases outlines in this thesis, including the schemes used in calculations in the finite volume scheme itself, as well as the solution.

```
/*--------------------------------*- C++ -*----------------------------------*\
| =========                 |                                                 |
| \\      /  F ield         | OpenFOAM: The Open Source CFD Toolbox           |
|  \\    /   O peration     | Version:  3.0.1                                 |
|   \\  /    A nd           | Web:      www.OpenFOAM.org                      |
|    \\/     M anipulation  |                                                 |
\*---------------------------------------------------------------------------*/
FoamFile
{
    version     2.0;
    format      ascii;
    class       dictionary;
    location    "system";
    object      fvSchemes;
}
// * * * * * * * * * * * * * * * * * * * * * * * * * * * * * * * * * * * * * //

ddtSchemes
{
    default         Euler;
}

gradSchemes
{
    default         Gauss linear;
    grad(p)         Gauss linear;
}

divSchemes
{
    default         none;
    div(phi,U)      Gauss linear;
        div((nuEff*dev2(T(grad(U))))) Gauss linear;
}

laplacianSchemes
{
    default         Gauss linear orthogonal;
}

interpolationSchemes
{
    default         linear;
}

snGradSchemes
{
    default         orthogonal;
}


// ************************************************************************* //
```

Figure A.1: fvSchemes (finite volume schemes) file from the OpenFOAM simulation solver BMicoFoam

```
/*--------------------------------*- C++ -*----------------------------------*\
| =========                 |                                                 |
| \\      /  F ield         | OpenFOAM: The Open Source CFD Toolbox           |
|  \\    /   O peration     | Version:  3.0.1                                 |
|   \\  /    A nd           | Web:      www.OpenFOAM.org                      |
|    \\/     M anipulation  |                                                 |
\*---------------------------------------------------------------------------*/
FoamFile
{
    version     2.0;
    format      ascii;
    class       dictionary;
    location    "system";
    object      fvSolution;
}
// * * * * * * * * * * * * * * * * * * * * * * * * * * * * * * * * * * * * * //

solvers
{
    p
    {
        solver          PCG;
        preconditioner  DIC;
        tolerance       1e-06;
        relTol          0;
    }
pFinal
    {
        $p;
        tolerance       1e-06;
        relTol          0;
    }

    pcorr
    {
        $p
        tolerance       0.02;
        relTol          0;
    }
    U
    {
        solver          smoothSolver;
        smoother        symGaussSeidel;
        tolerance       1e-05;
        relTol          0;
    }
 UFinal
    {
        $U;
        tolerance       1e-05;
        relTol          0;
    }
cellDisplacement
        {
                solver          PCG;
        preconditioner  DIC;
        tolerance       1e-08;
        relTol          0;
        }
}


 PISO
  {
      nCorrectors     2;
      nNonOrthogonalCorrectors 4;
      pRefCell        0;
      pRefValue       0;
  }
relaxationFactors
{
    equations
    {
        "U.*"           0.3;
                "p.*"           0.3;
    }
}


// ************************************************************************* //
```

Figure A.2: fvSolution (finite volume solution) file from the OpenFOAM simulation solver BMicoFoam